POLITECNICO
MILANO 1863

School of Industrial and Information Engineering

Master of science in Energy Engineering – Power Production

1D FLUID DYNAMIC MODELLING OF A NATURAL GAS LIGHT-DUTY IC ENGINE: PREDICTED RESULTS vs MEASURED DATA

Supervisor:

Prof. Ing. Angelo ONORATI

Master graduation thesis of:

Luca CASTELLI

Registration number 863557

Academic year 2017-2018

Quando qualcuno ti chiede: “Chi sei?”
e tu rispondi: “Sono un ingegnere”,
dal punto di vista esistenziale la tua risposta è errata.
Come potresti mai essere un ingegnere?
L’ingegnere è ciò che fai, non è ciò che sei.
Non chiuderti troppo nell’idea della funzione che svolgi
perché vorrebbe dire chiudersi in una prigione.
Osho

Ringraziamenti

Sommario

Lo scopo di questa tesi è stata la creazione e la validazione di un modello termo fluido dinamico per un motore a quattro cilindri in linea alimentato a Gas Naturale, SI, turbocompresso, per veicoli leggeri dedicati al settore dei trasporti. Il motore in analisi, ancora in fase di sviluppo, è l'F1C CNG realizzato da FPT (Fiat Power Train) e testato su un banco prova dedicato presso EMPA – Swiss Federal Laboratories for Materials Science and Technology, che ci fornisce i dati sperimentali necessari per un confronto completo con i risultati delle simulazioni. Inoltre, è stato creato un modello, da parte di EMPA, che utilizza un software commerciale già affermato ed utilizzato di nome GT-Power e da esso è stato possibile estrarre alcune importanti informazioni relative al sistema motore e in particolar modo tutte le dimensioni di ogni componente che deve essere utilizzato durante il processo di costruzione del nostro modello. Altri dati fondamentali per il modello sono stati forniti, in seguito ad alcune richieste di chiarimento, attraverso dei file Excel dedicati.
Il software utilizzato per le simulazioni numeriche è Gasdyn, un codice di calcolo scritto dal gruppo "Internal Combustion Engine" (ICE) del Politecnico di Milano con la collaborazione di Exothermia SA. Esso è accoppiato con una interfaccia grafica (GUI), che, nella sua ultima versione, è chiamata GASDYNPRE3. Attraverso essa lo schema del motore può essere disegnato in tutti i suoi componenti al fine di creare dei file di input necessari per svolgere le simulazioni termo-fluido dinamiche. Alcuni problemi di vario genere sono stati messi in luce durante il periodo di tesi, così da rendere possibile un continuo miglioramento del software.
L'analisi dei risultati delle simulazioni è svolta utilizzando alcuni file Excel creati, gradualmente, durante il periodo di tesi, appositamente per permettere una rapida comprensione degli output ed un confronto esaustivo tra i valori simulati e quelli misurati.

Parole chiavi: *1D CFD, Gasdyn, Motore SI Sovralimentato, Gas Naturale, Modellazione.*

Abstract

The aim of this thesis has been the creation and validation of a thermo-fluid dynamic model dedicated to a four cylinder in line, turbocharged, light-duty, Spark Ignition, Natural Gas engine dedicated to the truck transportation. The analysed engine, still in the developing phase, is the F1C CNG. It is built by FPT (Fiat Power Train) and it is tested on a dedicated test bench at EMPA – Swiss Federal Laboratories for Materials Science and Technology, which provides the experimental data necessary for a complete comparison procedure with respect to the simulated results. Moreover, this engine is also modelled, by EMPA, using a more affirmed and tested commercial software named GT-Power and from that scheme it is possible to obtain some important informations relative to the engine system and in particular way all the geometric dimensions which have to be used during the building process of our model. Other fundamentals data are provided, after some request of clarifications, through dedicated excel files.

The software used for the calculations is Gasdyn, a computational research code made by the "Internal Combustion Engine" (ICE) group of the "Politecnico di Milano" in cooperation with Exothermia SA. It is coupled with a Graphical User Interface (GUI), that, in its last version, is called GASDYNPRE3. Through it the scheme of the engine is drawn in all its main components to create the input files necessary to perform the thermo-fluid dynamic simulations. Some problems of various kind have been highlighted during the thesis work period and in this way has been possible to continuously adjust and improve the software.

The post processing analysis of the simulation results is carried out with some excel files created, step by step, during the thesis period, specifically to allow a quick comprehension of the outputs and a good and exhaustive comparison between the simulated and measured values.

Keywords: *1D CFD, Gasdyn, Turbocharged SI engine, Natural Gas, Engine modelling.*

Index

Introduction

Nowadays the world of the transportations is searching to new types of sources for the automotive vehicle and in particular for heavy and light-duty trucks. Over the traditional engines, Gasoline and Diesel, and electric vehicles (full electric, hybrid), the natural gas engine are more and more adopted in these years, due to the big availability of the fuel, good pollutants emissions and presence of a wide and consolidated distribution grid already built.

The internal combustion engine operates in very different conditions and so it is important to analyze the engine performances in a lot of rotational speeds and at different loads, to simulate a lot of real operating points. The study of the fluid-dynamic processes in internal combustion engines is particularly challenging due to cyclic substitution of the charge inside the cylinders, which makes the phenomenon strongly unstable both in the intake and exhaust systems. In the past, research activities were based only on experimentation in laboratories through test bench, even if this methodology was onerous in terms of costs and time. Thanks to the numerical codes, it is now possible to create models that are able to simulate the behaviour of an engine, thus reducing the use of experimental campaigns. The 1D and multi-D approaches allow to predict different quantities that are not easily measurable through the experiments and to understand which variables have a greater influence on the different phenomena. Also the pollutants emissions can be predicted by using Gasdyn, and this is a key point nowadays, due to the environmental limits imposed by different countries on the new engines. A big distinction has to be made between 1D and 3D simulation approaches. At the beginning has to be clarified the purpose of the simulation, because if we are interested to study in depth a single process or a certain engine zone it is preferable to use a complex and onerous, but precise 3D model. On the other hand, if the target is to model the entire engine to evaluate performances and global parameters, a 1D model is adopted. Obviously, it is not possible to pretend a high accuracy level in certain complex processes due time and cost reason. In relation to our target we use a 1D computational code (Gasdyn).

The thesis work is divided into 5 chapters:

1st In the first chapter, a review of the governing equations of the fluid motion in a duct is provided under some assumptions, which make faster and easier the computational processes. Conservations equations are obtained and then a vectorization process produce a system written in a matrix form which in required by the numerical methods explained in the next chapter.

2nd In the second chapter, the numerical methods and models implemented in Gasdyn are explained. Starting from the Method of Characteristics subsequently two second order, space centered, finite differences methods are introduced: Lax-Wendroff and MacCormack methods. They are shock capturing methods which can find discontinuities in spatial and temporal domain, but obviously being second order accurate generates spurious oscillations according to the Godunov theorem, that can be eliminated with soma techniques. Then the Heat transfer models are presented.

3rd In the third chapter the engine, all its parts and the equipments used, are introduced and analyzed one by one in order to obtain the values required by Gasdyn as input. Starting from the real engine characteristics and using the GT-Power engine scheme as guide line has been possible to create a reliable model which faithfully represent the real operating points. A complete engine Gasdyn model is presented and so the simulations can start.

4th In the fourth chapter an initial study of the available measured data, provided by the EMPA test bench, is made and subsequently the transducers positions are decided, in order to obtain comparable simulated results. The simulation outputs are analyzed and collated with the experimental data in order to validate the engine Gasdyn model. In addition to the performances also other parameters and phenomena are analyzed such as: turbocharger functioning, air mass flow rate and fuel injection, cylinder pressure, ram and waves effects.

5th In the last one the conclusions are summarized and some possible improvements both on the engine model and also on the real motor are proposed and illustrated. Moreover, the future Gasdyn model developments have been briefly introduced for the next student which will be interested by this type of thesis work.

1 Governing equations

1.1 Introduction

Internal combustion engine is classified as reciprocating fluid-dynamic machine, characterized by a non-stationary fluid motion due to the engine cyclic behaviour (steady-state hypothesis is not valid). In the intake and exhaust engine ducts the moving gas can be defined as:

- Unsteady
- Compressible
- Viscous
- 3-Dimensional
- Heat fluxes across wall
- High temperatures and pressure gradients
- High Reynold's numbers

Numerical simulation of this kind of machine has to be done with appropriate numerical codes that take in to account the complexity of the system and can correctly reconstruct pressure waves in the engine ducts. Using a DNS methods which study Navier-Stokes equations in the 3D domain, it is possible to achieve quite precise outcomes, but the computational complexity and the time expenditure is too much in relation to the accuracy obtainable using faster approaches.

1.2 Governing equations

To study an internal combustion engine is more adequate to rewrite the N-S equations under a 1 D point of view and introducing some approximations, obtaining others governing equations which define in a good way the gas motion in the ducts. In this way we are able to simplify the system and use faster computational approaches, keep accuracy above a certain reasonable limit and drastically reduce the necessary amount of time.

The simplified hypothesis are:

- Unsteady gas flow
- 1-D motion inside the engine ducts. The directions different from the curvilinear abscissa are negligible
- Compressible flow
- Non-adiabatic process
- Non-isentropic process (Inviscid fluid)
- Heat fluxes and friction exist only at the wall
- Negligible variation of the duct section

Applying an Eulerian approach and considering the previous assumptions I can consider this control volume and analyze these quantities:

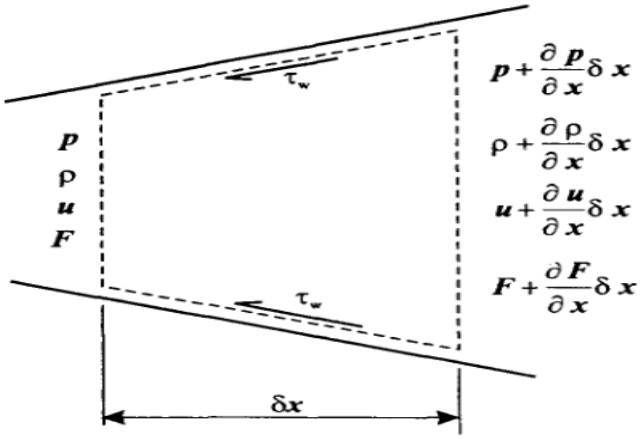

Figure 1: Duct control volume for balance equations

1.2.1 Mass conservation equations

The net rate of change of mass within the control volume, has to be equal to the mass flow rate variation between the inlet and the outlet. Considering F, the variable cross-sectional area, it is possible to write the continuity equation:

$$\left(\rho+\frac{\delta\rho}{\partial x}dx\right)\left(u+\frac{\delta u}{\delta x}dx\right)\left(F+\frac{\partial F}{\partial x}dx\right)-\rho uF=-\frac{\delta}{\partial t}(\rho F\,dx) \qquad \textbf{1.1}$$

Making some reasonable simplifications and neglecting the infinitesimals of the second and higher order we can rewrite the continuity equations as:

$$\frac{\partial\rho}{\partial t}+\frac{\partial}{\partial x}(\rho u)+\frac{\rho u}{F}\frac{dF}{dx}=0 \qquad \frac{\partial\rho}{\partial t}+\rho\frac{\partial u}{\partial x}+u\frac{\partial\rho}{\partial x}+\frac{\rho u}{F}\frac{dF}{dx}=0 \qquad \textbf{1.2}$$

1.2.2 Momentum conservation equation

The variation, during the time unit, of the momentum of the mass contained into the volume to which we add its net flow, must coincide with the sum of the pressure and shear forces acting on the surface of the control volume. The resulting force on the control volume is given by the pressure differential between the terminal sections and components along x of the pressure acting on the lateral surface of the volume.

The various components can be divided into:

- the contribution of pressure field in x-direction is represented by:

$$pF - \left(\rho + \frac{\partial p}{\partial x}dx\right)\left(F + \frac{\partial F}{\partial x}dx\right) + p\frac{dF}{dx} = -\frac{\partial(pF)}{\partial x} + p\frac{\partial F}{\partial x}dx \qquad \textbf{1.3}$$

  The first two terms take into account the whole pressure on the boundary sections, since the curvilinear abscissa of pipe parallel to the normal versor of pressure. The third term represent force in x-direction produces by the pressure on the sides of control volume.
- The shear force on the control volume is due to the friction between moving fluid and the surface of the duct. Starting from shear stress definition it is possible to write the equation for the friction force on the lateral surfaces:

$$F_f = \tau_w \cdot (\pi D\, dx) \qquad with \qquad \tau_w = f \cdot \frac{1}{2}\rho u^2 \qquad \textbf{1.4}$$

  Usually in 1-D model of internal combustion engine this term is the only that include the fluid viscosity and the character of the governing equation remains essentially inviscid.

The rate of change of momentum within the volume is expressed as follows:

$$\frac{\partial(\mathrm{u\rho F\,dx})}{\partial \mathrm{t}} \qquad \textbf{1.5}$$

The net flux of momentum through the control volume, is:

$$\frac{\partial(\rho F u^2)}{\partial x}dx \approx \left(\rho + \frac{\partial \rho}{\partial x}dx\right)\left(u + \frac{\partial u}{\partial x}dx\right)^2\left(F + \frac{\partial F}{\partial x}dx\right) - \rho u^2 F \qquad \textbf{1.6}$$

So, the whole momentum conservation equation becomes:

$$\frac{\partial(u\rho F)}{\partial t} + \frac{\partial(\rho u^2 + p)F}{\partial x} - p\frac{dF}{dx} + \frac{1}{2}f\,\rho u^2 \cdot (\pi D) = 0 \qquad \textbf{1.7}$$

It is possible to introduce a new term G, which consider the viscosity:

$$G = f\frac{u^2}{2}\frac{u}{|u|}\frac{4}{D} \quad \textbf{1.8}$$

The equation can be rewritten as:

$$\frac{\partial u}{\partial t} + u\frac{\partial u}{\partial x} + \frac{1}{\rho}\frac{\partial p}{\partial x} + G = 0 \quad \textbf{1.9}$$

1.2.3 Energy conservation equation

The energy equation can be derived by applying the First Law of Thermodynamics to the control volume:

$$\frac{\partial E_0}{\partial t} + \frac{\partial H_O}{\partial x}dx = \dot{Q} - \dot{W}_s \quad \textbf{1.10}$$

The first term represents the variation in time of the total stagnation internal energy, while the second term represents the net flux of enthalpy through the control surface. The summation of these two contributes is equal to the difference of heat entering the system and mechanical work exiting the system.

The two terms at the left-hand side can be rewritten using the specific stagnation quantity:

$$\frac{\partial(e_0\,\rho\,F\;dx)}{\partial t} \qquad with \qquad e_0 = e + \frac{1}{2}u^2 \quad \textbf{1.11}$$

$$\frac{\partial(h_0\,\rho\,F\,u)}{\partial x}dx \qquad with \qquad h_0 = e_0 + \frac{p}{\rho} \quad \textbf{1.12}$$

The work exchanged in the intake and exhaust ducts is null and the energy equation can be rewritten:

$$\frac{\partial(e_0\,\rho\,F\,dx)}{\partial t} + \frac{\partial(h_0\,\rho\,F\,u)}{\partial x}dx = \dot{q}\,\rho\,F\,dx + \Delta H_{reaction}\,F\,dx \quad \textbf{1.13}$$

The conservation equations written above are three hyperbolic non-linear partial differential equations. The system is composed of 3 equations and 4 unknowns (ρ, p, u, e), and so cannot be solved. It is required an additional equation and we use a relationship on the gas behaviour.

For the gases, in an internal combustion engine manifolds and cylinders, it is usually sufficiently accurate a perfect gas with constant specific heat state equation; this refers to a gas that respects the ideal gas state equation and has an internal energy defined as the product of the specific heat at constant volume and the actual temperature. These properties are translated in these relationships:

$$\frac{p}{\rho} = R^* T \qquad equation\ of\ state\ for\ ideal\ gas \tag{1.14}$$

$$e = c_v T \qquad internal\ energy\ for\ a\ perfect\ gas\ with\ cv, cp\ =\ const \tag{1.15}$$

The energy equation can be written eliminating the specific internal energy:

$$\frac{\partial}{\partial t}\left[(\rho\ F\ dx)\left(c_v\ T + \frac{u^2}{2}\right)\right] + \frac{d}{\partial x}\left[(\rho\ F\ dx)\left(C_v\ T + \frac{p}{\rho} + \frac{u^2}{2}\right)\right] =\ q\ \rho\ F\ dx + \Delta H_r\ F\ dx \tag{1.16}$$

From the expansion of equation, combined with the conservation of mass equation and with momentum equation the non-conservative formulation of the equation of energy is reached:

$$\left(\frac{\delta\rho}{\partial t} + u\frac{\delta\rho}{\partial x}\right) - a^2\left(\frac{\delta\rho}{\partial t} + u\frac{\delta\rho}{\partial x}\right) - \rho\ (k-1)\left(q - \frac{\Delta H_r}{\rho} + u\ G\right) = 0 \tag{1.17}$$

$$where \qquad k = \frac{c_p}{c_v} \qquad and \qquad a = \sqrt{K R^* T}$$

The hyperbolic system of governing equations is in the non-conservative form and it is:

$$\begin{cases} \dfrac{\partial\rho}{\partial t} + \dfrac{\partial}{\partial x}(\rho\ u) + \dfrac{\rho\ u}{F}\dfrac{dF}{dx} = 0 \\ \dfrac{\partial u}{\partial t} + u\ \dfrac{\partial u}{\partial x} - \dfrac{1}{\rho}\dfrac{\partial p}{\partial x} + G = 0 \\ \left(\dfrac{\delta\rho}{\partial t} + u\dfrac{\delta\rho}{\partial x}\right) - a^2\left(\dfrac{\delta\rho}{\partial t} + u\dfrac{\delta\rho}{\partial x}\right) - \rho(k-1)\left(q - \dfrac{\Delta H_r}{\rho} + uG\right) = 0 \\ \dfrac{p}{\rho} = R^* T \\ e = c_v T \end{cases} \tag{1.18}$$

The system is now written in a form suitable for the resolution with the Method of Characteristics.

The evolution of CFD and the need to capture in a accurate way all the phenomena that characterise the fluid flow has led to a conservative formulation of the non-linear hyperbolic system. This formulation, solved with Shock-Capturing numerical methods, allows to take into account and describe in a correct way possible discontinuity in the studied flow. The system written in strong conservative form is:

$$\begin{cases} \dfrac{\partial(\rho\ F)}{\partial t} + \dfrac{\partial(\rho\ u\ F)}{\partial x} = 0 & mass\ conservatiom\ equation \\ \dfrac{\partial(\rho\ u\ F)}{\partial t} + \dfrac{\partial(\rho\ u^2 F + p\ F)}{\partial x} - p\dfrac{dF}{dx} + \rho\ G\ F = 0 & impulse\ equation \\ \dfrac{\partial(\rho\ e_0\ F)}{\partial t} + \dfrac{\partial(\rho\ h_0\ u\ F)}{\partial x} - q\ \rho\ F - \Delta H_r\ F = 0 & energy\ equation \end{cases} \tag{1.19}$$

To apply the Shock Capturing numerical method, the system is rewritten as a matrix, identifying four vectors:

- Vector of conserved independent variables, whose fluxes remain unchanged through the shockwaves:

$$\bar{W}(x,t) = \begin{pmatrix} \rho F \\ \rho u F \\ \rho e_0 F \end{pmatrix} \quad \textbf{1.20}$$

- Vector of conserved variables fluxes:

$$\bar{F}(\bar{W}) = \begin{pmatrix} \rho u F \\ (\rho u^2 + p) F \\ \rho u h_0 F \end{pmatrix} \quad \textbf{1.21}$$

- Vector of the source terms due to pressure force derived from the pipe cross sectional change:

$$\bar{B}(\bar{W}) = \begin{pmatrix} 0 \\ -p\dfrac{dF}{dx} \\ 0 \end{pmatrix} \quad \textbf{1.22}$$

- Vector of source terms related to the fluid friction and heat transfer:

$$\bar{C}(\bar{W}) = \begin{pmatrix} 0 \\ \rho G F \\ (q\rho + \Delta H_r) F \end{pmatrix} \quad \textbf{1.23}$$

The system, rewritten in the matrix form, will look as follows:

$$\frac{\partial \bar{W}(x,t)}{\partial t} + \frac{\partial \bar{F}(\bar{W})}{\partial x} + \bar{B}(\bar{W}) + \bar{C}(\bar{W}) = 0 \quad \textbf{1.24}$$

The problem has still three equations and four unknowns; so, to be solved, it is necessary to introduce a relationship that describes the gas behaviour. As done above, it is possible to apply the simplifying hypothesis of perfect gas at specific constant temperatures or adopt a more generic model describing a mix of ideal gasses.

2 Numerical methods and models

It is not usually possible to determine an analytical solution of the partial differential hyperbolic system described above. It is necessary to discretize the governing equations to form an algebraic set of relationships that can be solved with the use of a computer. Historically, the first step to find the solution of similar problems was made by Riemann when he developed the Methodology of Characteristics, introducing new computational perspectives, that brought to new numerical methods. The approach is quasi-linear in determining fundamentals between two nodes of the mesh. The main limitations of this method are substantially three:

- Assumption of the perfect gas at specific constant temperatures
- Linear approximation: the space-time domain has been meshed by a calculation grid on the plain (x, t) and the solution is determined between subsequent nodes with accuracy to the first order
- Discontinuity in the solution: the method is not capable to properly detect possible discontinuities in the resolution, as the typical case of shock waves, distributing the phenomenon over the several nodes of the calculation grid.

Hence, besides the Method of Characteristics, that remains the most diffused one (because of its simplicity and its physical approach to solve the hyperbolic problem), there are other computational techniques: the shock-capturing finite difference methods. The ability of these techniques is to get the possible shock waves automatically, without the knowledge of the discontinuity position.

There are two groups of these methods. In the first one, “upwind” methods are classified, or “characteristic based”, that give the best results in terms of discontinuity resolution, with high computational burden, since they solve the Riemann problem in each mesh. In the second group, there are the “non-upwinded” methods, also called symmetrical or centered, that apply in each node the same scheme of finite difference, to express partial derivative terms. The Lax-Wendroff, MacCormack and Conservation Element - Solution Element methods enter this class.

2.1 Shock-Capturing Methods

The main advantage of the Shock capturing methods is to correctly perceive possible discontinuities in the solution, such as: shock waves, contact discontinuity due to temperature or chemical composition. Within this family the symmetrical finite differentials methods resulted as the most efficient, representing a good compromise between: accuracy, validity of solution, simplicity and length of calculation. The symmetry of the method consists in applying at each node of the grid the same finite differentials scheme to express the terms of the space derivatives, independently from the type of the flow field. The following methods are explicit and have a 2nd order accuracy in the space-time domain. Unfortunately, as it is known from Godunov's Theorem, accuracy of a higher order than the first leads to spurious oscillations problems in the solution; so, it is necessary the use of particular algorithms in order to mitigate this effect.

Previously, we have seen all the passages bringing to the definition of the vector *W(x,t)*, that allows us to characterize completely the motion of the compressible fluid. Now this vector is considered under the hypothesis of constant cross-sectional area and becomes:

$$\bar{W}(x,t) = \begin{pmatrix} \rho \\ \rho u \\ \rho e_0 \end{pmatrix} \qquad \textbf{2.1}$$

In order to proceed in the numerical modelling, we have to substitute the vector *W(x, t)* with the equivalent W_i^n, approximation to W $(i\Delta x;\ n\Delta t)$, where the subscript i defines the spatial coordinate, while the apex n indicates the considered instant of time. In this way, we obtain a computational grid, characterized by the steps Δx and Δt.

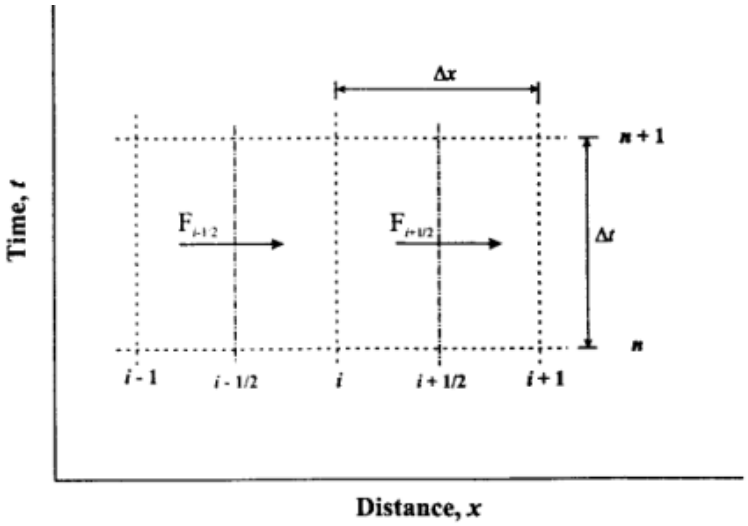

Figure 2: Spatial and temporal discretization

Shock-Capturing methods are applied to the hyperbolic system written in conservative and matrix form, with the additional hypothesis about the evolving gas model. Referring to equation 1.24 and deleting the source term vectors, it is possible to obtain Euler Equations, which describe a homentropic flow:

$$\frac{\partial \bar{W}(x,t)}{\partial t} + \frac{\partial \bar{F}(\bar{W})}{\partial x} = 0 \qquad \textbf{2.2}$$

Integrating and applying the Gauss Divergence theorem:

$$\int_t^{t+\Delta t} \int_x^{x+\Delta x} \left(\frac{\partial \bar{W}(x,t)}{\partial t} + \frac{\partial \bar{F}(\bar{W})}{\partial x} \right) dx\, dt = 0 \qquad \textbf{2.3}$$

A discretization process of the space-time domain is necessary to apply the finite differences methods. The vector $\bar{W}(x,t)$ becomes:

$$\bar{W}(x,t) \cong \bar{W}_i^n(i\Delta x; n\Delta t) \qquad \textbf{2.4}$$

Introducing that in the integral:

$$(\bar{W}_i^{n+1} - \bar{W}_i^n)\Delta x + \left(\bar{F}^n_{i+1/2} - \bar{F}^n_{i-1/2}\right)\Delta t = 0 \qquad \textbf{2.5}$$

Where the terms *W* and *F* are obtained by making the average in the space and time of the relative vectors:

$$W_i = \frac{1}{\Delta x}\int_{x_i-1/2}^{x_i+1/2} \bar{W}\, dx \qquad\qquad F_{i\pm 1/2} = \frac{1}{\Delta t}\int_{i^n}^{i^{n+1}} \bar{F}\, dt \qquad \textbf{2.6}$$

Equation 2.3 permits to disengage from the condition of derivability, requested by the Euler Equations, even in the presence of discontinuity, furthermore integral formulation has the advantage of treating discontinuities even without prior knowledge of their location. Rearranging properly the terms of equation 2.4 we can write:

$$\bar{W}_i^{n+1} = \bar{W}_i^n - \Delta t \frac{\left(\bar{F}^n_{i+1/2} - \bar{F}^n_{i-1/2}\right)}{\Delta x} \qquad \textbf{2.7}$$

By summing the differences along x is obtained:

$$\Delta x \sum_i \bar{W}_i^{n+1} = \Delta x \sum_i \bar{W}_i^n + \Delta t \left(\bar{F}^n_{imin+1/2} - \bar{F}^n_{imax-1/2}\right) \qquad \textbf{2.8}$$

In detail:

- the first term on the left-hand side represents the total mass, momentum and energy at time level n + 1.
- the first term on the right-hand side represents the total mass, momentum and energy at time level n
- the second term on the right-hand side represents the flux of conserved quantities through the pipe ends.

The equations so defined, represent a conservative discretization scheme, which guarantees the preservation of integral property of the governing equations.

In the following steps, the Lax Wendroff and MacCormack Shock-Capturing methods will be introduced, both used in Gasdyn and belonging to the finite differentials methods, non-upwind, explicit and with an accuracy of the II° order.

2.2 Lax-Wendroff Scheme

This scheme is based on Taylor series expansions of solution vector ***W(x,t)*** and it is developed in two variants: one-step scheme, two step scheme. The version one-step effort requires the calculation of a Jacobian matrix A in each node for all time steps of the simulation, so requires a high computational. The two-step scheme instead removed the need to calculate the Jacobian matrix, while retaining second-order accuracy, by solving the equations in a two-step procedure, inserting an intermediate step in the calculation of the solution vector in the node and at the desired time.

1 Step Scheme

Let's now consider Taylor's series expansion of the state vector $\bar{W}$ in the discretized domain at time *n+1* and at node *i*:

$$\bar{W}^{n+1} = \bar{W}^{n} + \frac{\partial \bar{W}}{\partial t}\Delta t + \frac{\partial^2 \bar{W}}{\partial t^2}\frac{(\Delta t)^2}{2!} + o(\Delta t^3) \qquad \textbf{2.9}$$

Knowing that:

$$\frac{\partial \bar{W}}{\partial t} = -\frac{\partial \bar{F}}{\partial x} \qquad \& \qquad \frac{\partial^2 \bar{W}}{\partial t^2} = -\frac{\partial}{\partial x}\left(\frac{\partial \bar{F}}{\partial t}\right) \qquad \textbf{2.10}$$

$$\frac{\partial \bar{F}}{\partial t} = \frac{\partial \bar{F}}{\partial \bar{W}}\frac{\partial \bar{W}}{\partial t} = \frac{\partial \bar{F}}{\partial \bar{W}}\left(-\frac{\partial \bar{F}}{\partial x}\right) = -A\frac{\partial \bar{F}}{\partial x} \qquad \textbf{2.11}$$

The Jacobian Matrix A [3x3] is composed of elements defined by:

$$a_{i,j} = \frac{\partial F_i}{\partial \overline{W}_j} \quad \textbf{2.12}$$

The equation 2.2 becomes:

$$\frac{\partial \overline{W}(x,t)}{\partial t} + \boldsymbol{A}\frac{\partial \overline{W}}{\partial x} = \bar{0} \quad \textbf{2.13}$$

The spatial differences can be approximated by central differences and the series is truncated at second-order terms, giving:

$$\frac{\overline{W}_i^{n+1} - \overline{W}_i^n}{\Delta t} = + \frac{\bar{F}_{i+1}^n - \bar{F}_{i-1}^n}{2\Delta x} + \frac{\left[\left(\boldsymbol{A}\frac{\partial \bar{F}}{\partial x}\right)_{i+1/2}^n - \left(\boldsymbol{A}\frac{\partial \bar{F}}{\partial x}\right)_{i-1/2}^n\right]}{\Delta x}\frac{(\Delta t)^2}{2!} \quad \textbf{2.14}$$

Terms in the square brackets can be discretized as:

$$\left.\frac{\partial F}{\partial x}\right|_i = \frac{\bar{F}_{i+1} - \bar{F}_{i-1}}{2\Delta x} \quad \textbf{2.15}$$

So, the Lax-Wendroff equation becomes:

$$\overline{W}_i^{n+1} = \overline{W}_i^n - \frac{\Delta t}{2\Delta x}(\bar{F}_{i+1} - \bar{F}_{i-1}) - \frac{(\Delta t)^2}{2(\Delta x)^2}\left[\boldsymbol{A}_{i+\frac{1}{2}}^n(\bar{F}_{i+1}^n - \bar{F}_i^n) - \boldsymbol{A}_{i-\frac{1}{2}}^n(\bar{F}_i^n - \bar{F}_{i-1}^n)\right] \quad \textbf{2.16}$$

The Jacobian matrix can be evaluated as:

$$A_{i\pm\frac{1}{2}} = \frac{1}{2}(A_i - A_{i\pm1}) \quad \textbf{2.17}$$

Due to the necessity of calculating the Jacobian Matrix at each step, the single step Lax Wendroff method ends up being very resource intensive.

2 Step Scheme

Such method avoids calculating the Jacobian matrix, introducing an intermediate step into the calculation of the solution vector, and therefore it is particularly suited for implementing the calculation codes.

- The 1st step is based on space-centered differences. Knowing vectors *W* and *F* at nodes *i-1*, *i+1* and at time *n*, we obtain solution vector *W*, using a Taylor's series expansion halted at the first order, at intermediate time *n+1/2* in intermediate nodes *i+1/2*. Introducing the approximation at the finite centred differentials, we obtain:

$$\bar{W}_{i+1/2}^{n+1/2} = \frac{\bar{W}_{i+1}^{n} - \bar{W}_{i}^{n}}{2} - \frac{\bar{F}_{i+1}^{n} - \bar{F}_{i}^{n}}{2\Delta x}\Delta t \qquad \textbf{2.18}$$

$$\bar{W}_{i-1/2}^{n+1/2} = \frac{\bar{W}_{i}^{n} - \bar{W}_{i-1}^{n}}{2} - \frac{\bar{F}_{i}^{n} - \bar{F}_{i-1}^{n}}{2\Delta x}\Delta t \qquad \textbf{2.19}$$

- 2nd step: calculate flow vector *F* at intermediate time *n+1/2* in intermediate nodes *i+1/2* and *i-1/2*, after which it is possible to determine solution vector *W* at time *n* in node *i*:

$$\bar{W}_{i}^{n+1} = \bar{W}_{i}^{n} - \frac{\bar{F}_{i+1/2}^{n+1/2} - \bar{F}_{i-1/2}^{n+1/2}}{\Delta x}\Delta t \qquad \textbf{2.20}$$

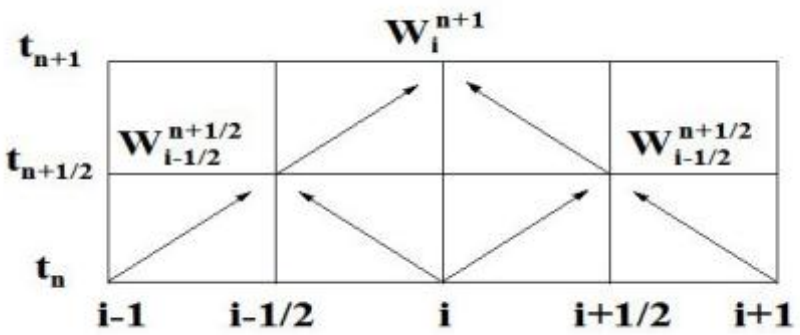

Figure 3: Computational stencil for 2 step Lax-Wendroff scheme

The general case of non homentropic flow is expressed by introducing the appropriate discretized source terms:

$$\begin{cases} \begin{cases} \bar{W}_{i+\frac{1}{2}}^{n+\frac{1}{2}} = \frac{1}{2}(\bar{W}_{i+1}^{n} + \bar{W}_{i}^{n}) - \frac{\Delta t}{2\,\Delta x}(\bar{F}_{i+1}^{n} + \bar{F}_{i}^{n}) - \frac{\Delta t}{4}(\bar{C}_{i+1}^{n} + \bar{C}_{i}^{n}) \\ \bar{W}_{i-\frac{1}{2}}^{n+\frac{1}{2}} = \frac{1}{2}(\bar{W}_{i}^{n} + \bar{W}_{i-1}^{n}) - \frac{\Delta t}{2\,\Delta x}(\bar{F}_{i}^{n} + \bar{F}_{i-1}^{n}) - \frac{\Delta t}{4}(\bar{C}_{i}^{n} + \bar{C}_{i-1}^{n}) \end{cases} & 1°\ Step \\ \bar{W}_{i}^{n+1} = \bar{W}_{i}^{n} - \frac{\Delta t}{\Delta x}\left(\bar{F}_{i+\frac{1}{2}}^{n+\frac{1}{2}} + \bar{F}_{i-\frac{1}{2}}^{n+\frac{1}{2}}\right) - \frac{\Delta t}{4}\left(\bar{C}_{i+\frac{1}{2}}^{n+\frac{1}{2}} + \bar{C}_{i-\frac{1}{2}}^{n+\frac{1}{2}}\right) & 2°\ Step \end{cases} \qquad \textbf{2.21}$$

We remind that, in order to establish the dimension of the temporal step, it is used the Courant-Friedrichs-Lewy stability criterion, according to which the max temporal step is equal to:

$$\Delta t = \upsilon\left(\frac{\Delta x}{|u| + a}\right) \qquad \textbf{2.22}$$

with $\upsilon \leq 1$, u and a taken from the node, where their sum is maximum.

2.3 MacCormack Method

The MacCormack method is another second-order accurate scheme that becomes identical to the Lax-Wendroff scheme for the linear case. The scheme uses alternative forward and backward spatial differences for the two steps in space. Consider the system of equations in conservative and matricial form, with the hypothesis of homentropic flux and constant cross-section duct.

$$\frac{\partial \bar{W}(x,t)}{\partial t} + \frac{\partial \bar{F}(\bar{W})}{\partial x} = \bar{0} \qquad \textbf{2.23}$$

- *Predictor step*: once the vectors $\bar{W}$ and $\bar{F}$ are known in each node at time *n*, applying forward differencing, the value of the solution vector $\bar{W}^*$ is evaluated at time t^*:

$$\frac{\bar{W}_i^* - \bar{W}_i^n}{\Delta t} - \frac{\bar{F}_{i+1}^n - \bar{F}_i^n}{\Delta x} = \bar{0} \qquad \textbf{2.24}$$

$$\bar{W}_i^* = \bar{W}_i^n - \frac{\Delta t}{\Delta x}(\bar{F}_{i+1}^n - \bar{F}_i^n) \qquad \textbf{2.25}$$

- *Corrector step:* it uses backward spatial differencing while advancing over a time interval of $\Delta t/2$:

$$\frac{\bar{W}_i^{n+1} - \bar{W}_i^{n+1/2}}{\frac{1}{2}\Delta t} - \frac{\bar{F}_i^* - \bar{F}_{i-1}^n}{\Delta x} = \bar{0} \qquad \textbf{2.26}$$

  Where:

$$\bar{W}_i^{n+1/2} = \frac{1}{2}(\bar{W}_i^n + \bar{W}_i^*) \qquad \textbf{2.27}$$

Forward discretization in space used in the first step is unstable when all the eigenvalues of the Jacobian matrix, **A**, are positive, and this indicates that the flow is supersonic. The backward discretization in space is unstable for negative eigenvalues, but the overall scheme is stable and has second-order accuracy because the truncation errors for each step cancel out. The following scheme represents the two phases of the MacCormack method:

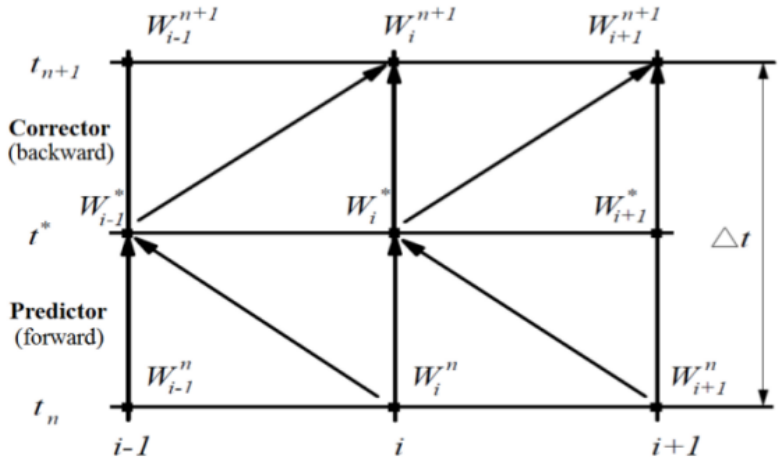

Figure 4: MacCormack method Graphical representation

The stability of the scheme in the case of discontinuities is influenced by the direction of the spatial differencing used in each of the steps. The "forward predictor/backward corrector" arrangement is best suited for discontinuities traveling from left to right, while the opposite is true for the "backward predictor/forward" corrector scheme. Since the propagation of discontinuities is usually not known at any instant, it is usual to reverse the order of spatial differencing at each time step.

Also for this method, the stability condition derives from the application of the CFL criterion:

$$CFL = (a + |u|)\frac{\Delta t}{\Delta x} \leq 1 \qquad \textbf{2.28}$$

2.4 Spurious Oscillations

The two methods exposed above are affected by spurious oscillations when the solution is close to a discontinuity (like shock waves and contact discontinuity). This is related to the Godunov's theorem, which demonstrate that if a numerical solution method is higher than first order of accuracy introduces not-physic oscillations in the solution. Some criterion is required to establish if schemes suffer or not from spurious oscillation. A very tested criterion is the total variation diminishing (TVD) principle. The total variation of solution $\bar{W}(x,t)$ at the time n is defined by:

$$TV(\bar{W}_i^n) = \sum_i |\bar{W}_{i+1}^n - \bar{W}_{i+1}^n| \qquad \textbf{2.29}$$

If the total variation of the solution doesn't increase from one-time step to the next one the data are said to be total variation diminishing and so the considered numerical scheme will not produce spurious oscillations at discontinuities.

There are essentially two classes of numerical methods for achieving the total variation diminishing condition with high order accuracy:

- Pre-processing schemes: characterized by the fact that the totality of data is modified before updating the solution.
- Post-processing schemes: the solution is updated each time using the chosen numerical scheme and subsequently modified to fulfil the prerequisites of TVD schemes. In this group we find FCT techniques and the flux limiters, which are implemented in the Gasdyn code.

2.4.1 FCT techniques

It uses a high order difference scheme for the initial stage, allowing spurious oscillations to appear, and subsequently applies a global diffusion process to eliminate them. A limited anti-diffusive flux is then applied in order to restore the accuracy of the initial high order stage.

Thus, the general approach consists of three distinct stages:

- **Transport stage:** first attempt solution is obtained by two-step Lax-Wendroff or MacCormack methods.
- **Diffusion stage:** The purpose is to eliminate any spurious oscillation introduced by the linear second-order transport scheme. A diffusive flux Φ, is calculated as:

$$\bar{\Phi}\left(\bar{W}_{i+\frac{1}{2}}\right) = \frac{1}{8}(\bar{W}_{i+1} - \bar{W}_i) \quad \textbf{2.30}$$

$$\bar{\Phi}\left(\bar{W}_{i-\frac{1}{2}}\right) = \frac{1}{8}(\bar{W}_i - \bar{W}_{i-1}) \quad \textbf{2.31}$$

For which can be defined the diffusion operator:

$$D = \bar{\Phi}\left(\bar{W}_{i+\frac{1}{2}}\right) - \bar{\Phi}\left(\bar{W}_{i-\frac{1}{2}}\right) \quad \textbf{2.32}$$

There are two possibilities for the diffusion operation:

- Diffusion via damping: $\bar{W}_D^{n+1} = \bar{W}_i^{n+1} + \boldsymbol{D}(\bar{W}_i^n)$ **2.33**
- Diffusion via smoothing: $\bar{W}_D^{n+1} = \bar{W}_i^{n+1} + \boldsymbol{D}(\bar{W}_i^{n+1})$ **2.34**

Where $\bar{W}_D$ represents the solution after the application of the diffusion operator.

- **Counter-diffusion stage:** we introduce the non-linear counter-diffusion agent A which removes, where not necessary, the diffusion introduced in a uniform way during the preceding phase. A is given by:

$$A(\bar{W}_i^{n+1}) = -\bar{\psi}\left(\bar{W}_{i+1/2}^{n+1}\right) - \bar{\psi}\left(\bar{W}_{i-1/2}^{n+1}\right) \quad \textbf{2.35}$$

Where ψ, called flux limiter, is defined as by Ikeda and Nakagawa.
The final solution can be calculated by:

(a) Damping case: $\bar{W}_{DA}^{n+1} = \bar{W}_D^{n+1} + \boldsymbol{A}(\bar{W}_i^n)$ **2.36**

(b) Smoothing case: $\bar{W}_{DA}^{n+1} = \bar{W}_D^{n+1} + \boldsymbol{A}(\bar{W}_i^{n+1})$ **2.37**

Damping algorithm is able to delete almost entirely spurious oscillations but make the method instable, is possible to avoid instabilities by imposing a CFL number minus-equal to 0.866.
The Smoothing algorithm though is stable but is not able to delete all the spurious oscillations.

2.4.2 Flux limiters

The general philosophy behind Flux Limiters is into the application of an anti-diffusive flow, only in the areas interested by discontinuities, this way we can prevent possible non-physical numeric oscillations. It can be shown that the Lax-Wendroff scheme for the linear advection equation, with $a > 0$, can be rewritten in the form:

$$\bar{W}_i^{n+1} = \bar{W}_i^n + \nu \bar{W}^n_{i-\frac{1}{2}} - \frac{1}{2\nu(1-\nu)\Delta_-\left(\Delta \bar{W}^n_{i+\frac{1}{2}}\right)} \quad \textbf{2.38}$$

Where:

$$\Delta_-\left(\Delta \bar{W}^n_{i+\frac{1}{2}}\right) = (\bar{W}^n{}_{i+1} - \bar{W}^n{}_i) - (\bar{W}^n{}_i - \bar{W}^n{}_{i-1}) \quad \textbf{2.39}$$

$$\nu = a\frac{\Delta t}{\Delta x} \quad \textbf{2.40}$$

Van Leer introduced parameter ϕ, called flux limiter, able to control the numeric oscillations of the solution. This parameter monitors the smoothness of the data and it is a function of the ratio of consecutive solutions gradients and it is defined as:

$$\phi_i = \phi(r_i) \quad \textbf{2.41}$$

Where:

$$r_i = \frac{\Delta W^n_{i-1/2}}{\Delta W^n_{i+1/2}} \qquad \textbf{2.42}$$

So, the scheme becomes:

$$\bar{W}^{n+1}_i = \bar{W}^n_i + \nu\, \bar{W}^n_{i-1/2} - \frac{1}{2}\nu\,(1-\nu)\,\Delta_-(\overline{\phi_i W}^n_{i+\frac{1}{2}}) \qquad \textbf{2.43}$$

The functionality principle of the algorithms for the application of the flux limiters is based on the following concept: when solutions of adjacent points are similar we maintain the accuracy of the II° order in the numeric method used, whereas in the presence of a discontinuity the accuracy of the method is degraded to the I° order to avoid the spurious oscillations problem.

2.5 Heat exchange models

In the Gasdyn code are present two heat exchange models which compute the net power exchanged between gases and walls. Numerical models that are used to study the evolution of the fluid in the cylinder needs a thermal sub-model able to calculate the instantaneous heat flux between the fluid in the chamber and the walls. The main processes that occurs during the heat transfer are:

- Thermal convection: It represent the main contribute of the total amount exchanged, and it is computed as:

$$\dot{q}_c = h_i\left(T_g - T_w\right) \qquad \textbf{2.44}$$

- Thermal radiation: This amount is described by the Stefan Boltzmann law:

$$\dot{q}_r = \varepsilon\,\sigma_0\left({T_g}^4 - {T_w}^4\right) \qquad \textbf{2.45}$$

  where σ_0 is the Black-body radiation coefficient, ε is emissivity factor, T_g and T_w are the temperatures of the hot gas and the walls. In the cylinder exhaust gas mixture, after combustion completion, only water and carbon dioxide molecules are able to radiate a significant amount of energy, their radiated energy is estimated in a 1% - 2% of total radiated energy on an entire cycle, exhaust product gas radiation is consequently negligible.

2.5.1 Annand model

Both the convective and the radiative contributes are taken into account using experimental coefficients. The instantaneous and space averaged exchanged heat flux results:

$$\dot{q} = h_i \left(T_g - T_w\right) + C_2\, \sigma_0 \left({T_g}^4 - {T_w}^4\right) \qquad \textbf{2.46}$$

The convective coefficient is related to physic characteristic and cinematic conditions of the gas:

$$h_i = C_1 \frac{\lambda}{D}\, Re^n = C_1 \frac{\lambda}{D} \left(\frac{\rho \overline{u_p} D}{\mu}\right)^n \qquad \textbf{2.47}$$

With: - $\overline{u_p}$ is the averaged piston velocity

- D is the cylinder bore

- $C_1 = 0.35 \div 0.8$

- $C_{2\,,combustion} = 0.6 \div 1.6$ & $C_{2\,,int-comp-disch} = 0$

- $n = 0.7 \div 0.8$

2.5.2 Woschini model

This model neglects the radiative heat flux component, which is considered by overestimating convective contribution. The governing equation of this model is:

$$\dot{q} = h_i\left(T_g - T_w\right) \qquad \textbf{2.48}$$

Where h_i represent the convective and radiative contributes, and is defined according the following physic relation:

$$Nu = C\, Re^{0.8} \qquad \rightarrow \qquad \frac{h\, D}{\lambda} = C \left(\frac{\rho\, u\, D}{\mu}\right)^{0.8} \qquad \textbf{2.49}$$

All variables used in the Woschini model are assumed as functions of the gas temperature:

$$\lambda \simeq T_g^{0.75} \qquad \mu \simeq T_g^{0.6} \qquad \rho \simeq T_g^{-1} \qquad \textbf{2.50}$$

Consequently, the heat transfer coefficient h_i is defined as:

$$h_i = C_1\, p^{0.8}\, D^{-0.2}\, T_g^{-0.53}\, u^{0.8} \qquad \textbf{2.51}$$

An important parameter, which has to be well defined and calculated, is the reference velocity which includes a contribute related to the density variation during combustion and to the gas exchange process:

$$u = C_2\,\bar{u}_p + C_3\left(\frac{V\,T_0}{p_0\,V_0}\right)(p - p_{tr}) \qquad \textbf{2.52}$$

With:

$$p_{tr} = p_0\left(\frac{V_0}{V}\right)^n \qquad \textbf{2.53}$$

3 1D Gasdyn Model

In the present chapter, with particular attention, we will describe the procedure followed for the modelling of the engine developed in Gasdyn, a simulation software internally developed at Energy department of "Politecnico di Milano", and more in detail by ICE Group and Exothermia SA. It is a 1D computational thermo-fluid dynamics code, able to simulate the operating conditions of an internal combustion engines, providing an important aid in the setting procedure of each part in order to optimize the interest's parameters such as torque, power, fuel consumption, noise and emissions, providing also the possibility to predict the gas pressure and temperature in each point of the system.

An internal combustion engine is a complex cyclical machine characterized by an important non-stationariness. Starting from the piston movements until pressure and mass flow variations, a relevant oscillation around an average value is present. Moreover, some gas behaviours are quite difficult to analyse and simulate due to the strong turbulence or complex reactions which occur. Some examples are combustion and gas exchange processes. In these cases, an accurate 3D model would be necessary to simulate with precision how the gas (air, fuel and their mixture) properties evolve in time and space. Obviously, the time expenditure and computational power required by the software to analyse one of these processes, in a certain fixed condition, is largely more onerous with respect to that one necessary for a 1D simulation.

Gasdyn works with a simplified computational code which analyse the situations mentioned above exploiting some models based on reasonable assumptions and approximations, obtaining reliable results quite closed to the experimental results and also to the 3D simulation outputs.

This type of analysis is a key point during the engine design procedure, because allow to study the intake and exhaust processes, which strongly influence the overall efficiency, but also to dimension all the other mechanicals parts which constitute the engine system. The waves and ram effects can be estimated with good accuracy and

continuously improved step by step, exploiting an easy 1D approach, saving time and money. Another advantage is the knowledge of the operating condition (temperature and pressure) of each pipe, which facilitate the material choice and dimensioning. In the past decades these analyses were carried out through a lot of tests at some significant rotating speeds and loads, made on the real engine, with the purpose to try as better as possible the real conditions in which the engine works.

3.1 Real engine data

The engine under investigation is the F1C CNG, produced by FPT, and it is intended to equip a light duty vehicle, which need to achieve high values of torque, rather than high peaks of power, for drivability reasons. The version fed with natural gas is obviously derived from its precursor, the Diesel engine, from which the analyzed engine get the main structure and a lot of mechanical parts. An exclusive design would be too expensive, without having a relevant improvement of performances and costs.

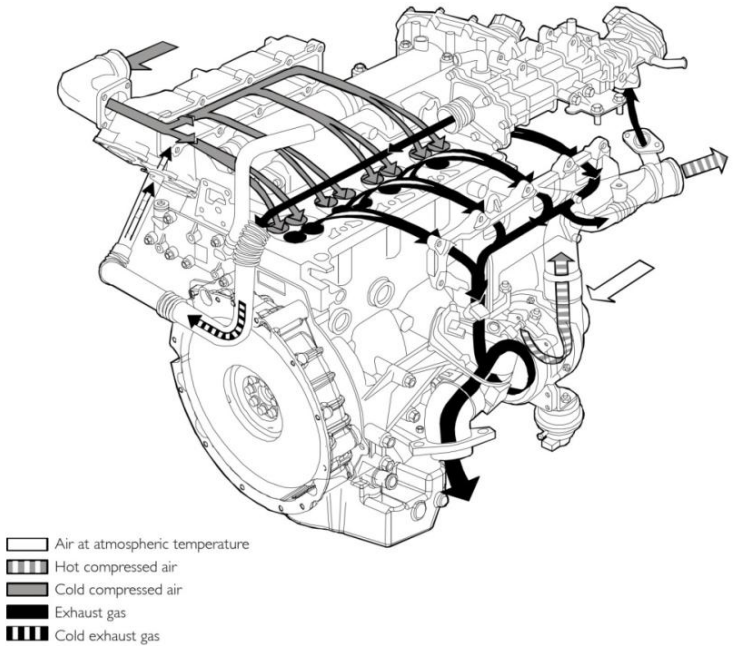

Figure 5: Engine representation

Some technical data:

Engine name	F1C CNG
Cycle	Otto cycle – 4 Stroke
	Turbocharged with Intercooler
Fuel	Methane gas
Injection	Multiple point – Port Fuel Injection
Structure	4 Cylinders in line
	4 Valves per cylinder
Combustion chamber shape	Cylindrical
Total displacement	2998 cm^3

Table 1: Engine's technical data

3.2 GT-Power scheme from EMPA

The F1C CNG Engine is actually studied and tested at EMPA – Swiss Federal Laboratories for Materials Science and Technology, with which "Politecnico di Milano" cooperate since few years. It provides the engine scheme used in GT-Power simulations, a validated software used for the modelling process and also experimental data measured from own test bench, useful during our validation process. All data related to the engine structure and setting of others mechanical parts are provided through a big text file, which contain the main part of the necessary values referred to all engine's component, and where necessary it is explained in deep with some additional excel files. Others necessary data, initially missing or encrypted, have been provided after a request of clarification to EMPA on some values which GT-Power sees as default and so cannot be extracted by the text file. In some rare particular situations, no data was available and so some realistic values which produce the attended results has been found through a trial and error procedure.

In the Figure 6 the engine scheme used by EMPA into the GT-Power for the simulations is printed.

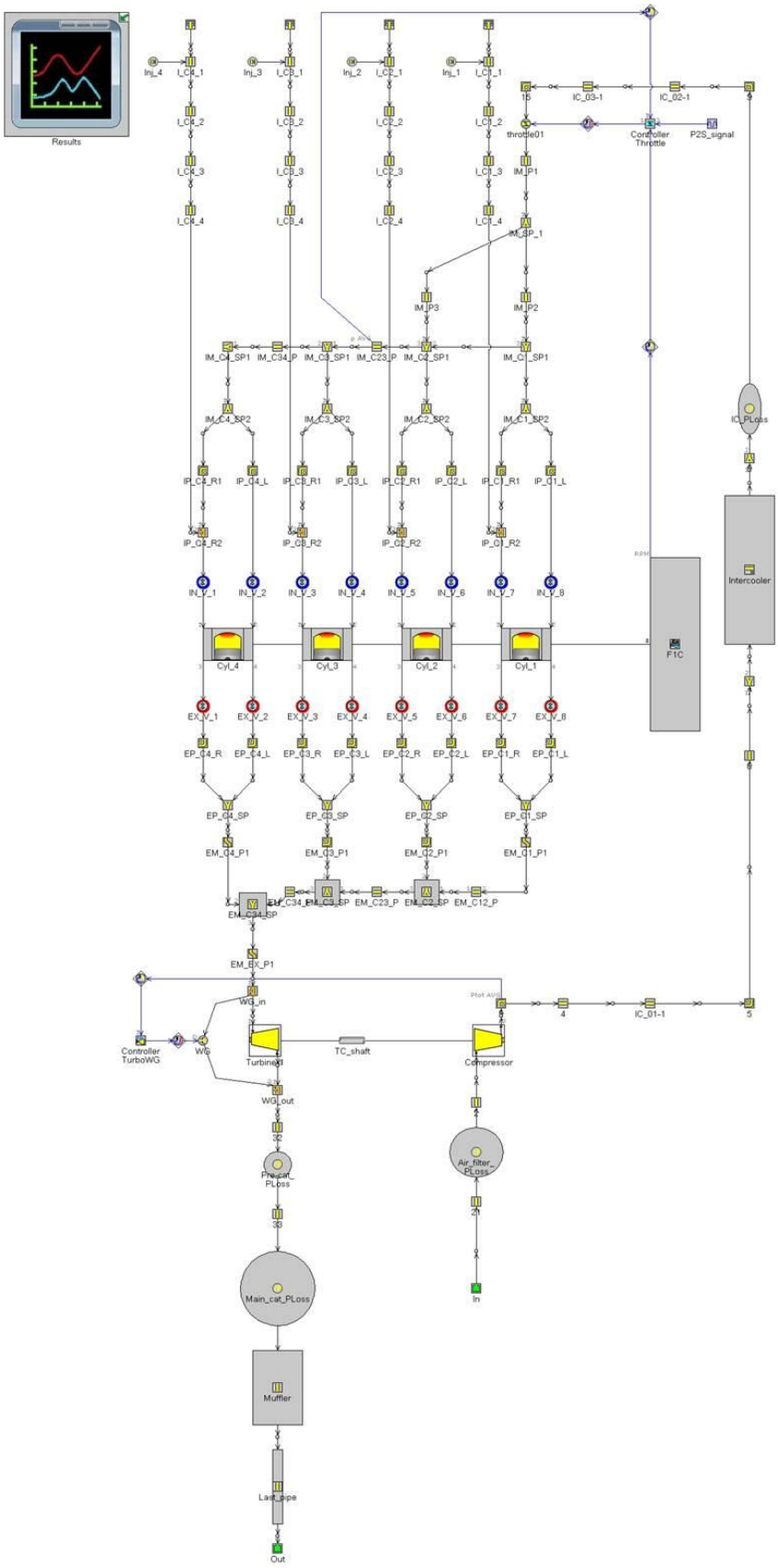

Figure 6: GT-Power engine scheme from EMPA

3.3 Cylinders

Dimensioning of the combustion chamber and definition of the combustion process parameters has a fundamental importance into the model building procedure. They are responsible for the conversion of the chemical energy into thermal one and finally into mechanical power. The reactions which occur, heavily influence pressure and temperature both in the cylinder and in the exhaust manifold, and so obviously also the performances can be modified. Geometry and combustion have effects on the entire engine operating point and, indirectly, also on the intake side, by changing the rotational speed of the turbocharger shaft, and consequently changing the delivery pressure.

Unfortunately, the combustion process cannot be detailed studied using a 1D approach, but a more complex 3D model is required. This because chemical reactions, air-fuel mixing process and turbulence flow are very difficult to simulate, and the time and computational power required are quite heavy in comparison to our logic. Gasdyn has the purpose to predict pressure, heat release and some pollutants concentration exploiting an easy and fast engine model and so an simplified combustion model is chosen (usually zero-dimensional).

The cylinder geometry has already been defined few pages above during the real engine characteristic presentation and the values used into the simulations are obviously the same. Regarding to the combustion parameters assumed, the combination reported in the **Errore. L'origine riferimento non è stata trovata.** is chosen at the beginning with the purpose to fit better as possible the measured cylinder pressure curve with respect to the crank angle for the whole engine speed range.

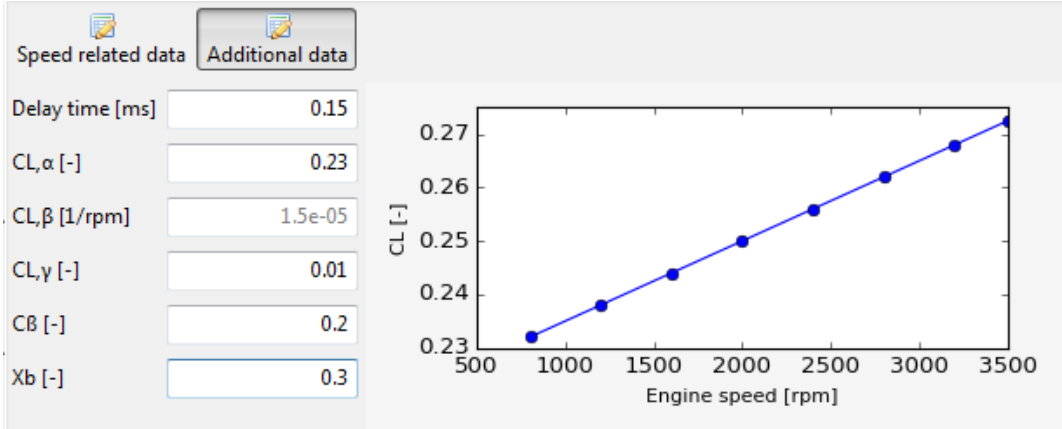

Figure 7: Combustion parameters

During the thesis work has been necessary to vary these values, keeping the starting point as reference, otherwise could not be possible to reach a good combustion process using a unique set of parameters for the whole engine speed range. The first step is represented by the research of the parameters which mainly influence the in-cylinder pressure and temperature. After that a dedicated setting procedure for each regime is necessary to find the final combination of combustion parameters.

3.4 Valves

A right representation of the valve train is a key point of the model building process, because they play an important role in the engine performances which are strongly affected by the gas exchange process. It influences both the combustion, through a more or less efficient scavenging process, and the turbocharger functioning. Intake and exhaust valves are complex equipments which moves unsteadily and so must be well designed, taking into account also the strong accelerations that they have to support. Dimensioning and motion control are key concepts to promote the cylinder gas exchange process and so also the global engine performance. It is necessary to examine both direct and reverse gas flow, in order to calculate the discharge coefficients and consequently the effective flow areas.

In the ideal cycles, valves open and close instantaneously at piston dead center. In practice, they open and close in finite time (to maintain acceptable accelerations and velocities) and often quite far from the piston dead center, for fluid and/or thermo-dynamic reasons.

Each cylinder uses 2 valves to introduce fresh charge and others 2 to discharge the exhaust gases. The valves constitutive parameters as diameter, EVO, IVO, clearance and others cannot be written due to confidentiality reasons.

Flow discharge coefficients are calculated experimentally both for the intake and exhaust valves, and obviously the worst flow condition coincide with the second one. The available data coming from EMPA are expressed in a different scale with respect to the format required as input for Gasdyn and so they have to be rearranged. The measured values start from 0,9 when the lift is null and decrease during the valve opening period and are referred to the valve seat area $\left(\pi\, D_{valve}^2/4\right)$ which is always constant. On the other hand, the values required as input by Gasdyn have to be expressed starting from 0 when the valve is closed and increasing with the lift during the opening period; In this case the reference area is the curtain one $(\pi\, D_{valve}\, L)$ which clearly vary. So, to pass from the first to the second reference system, it is necessary to divide by the valve seat area and multiply for the curtain area.

The rearranged discharge coefficients are plotted in the Figure 8.

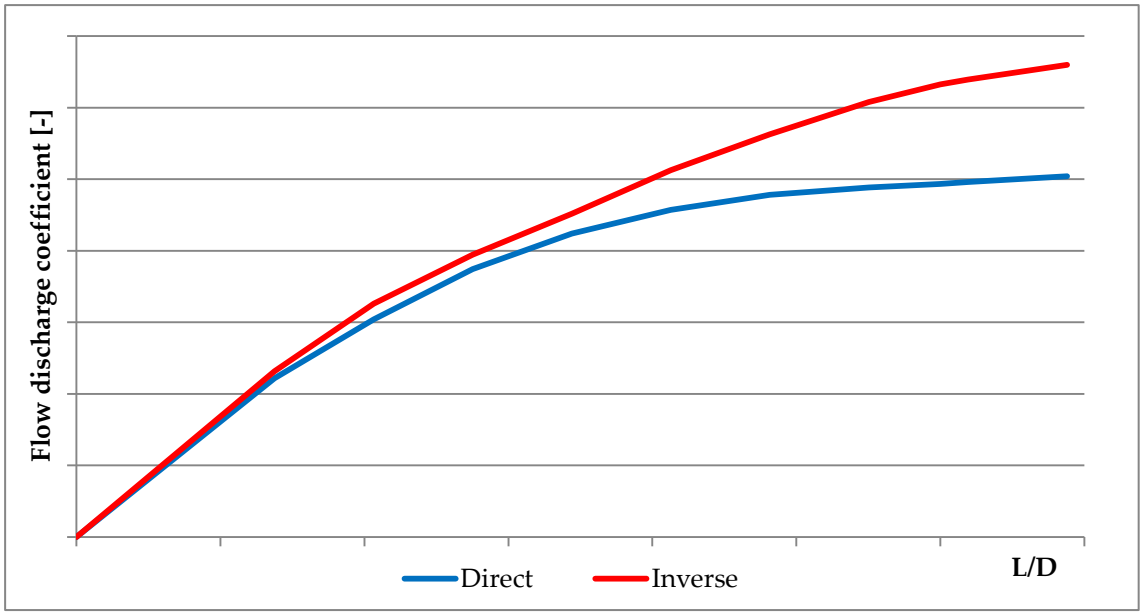

Figure 8: Direct and Inverse flow discharge coefficient

Valve lifts are provided by EMPA, and looking at the Figure 9 it is possible to note that the lower flow discharge coefficient and seat area of the exhaust valve is partially compensated by a greater lift.

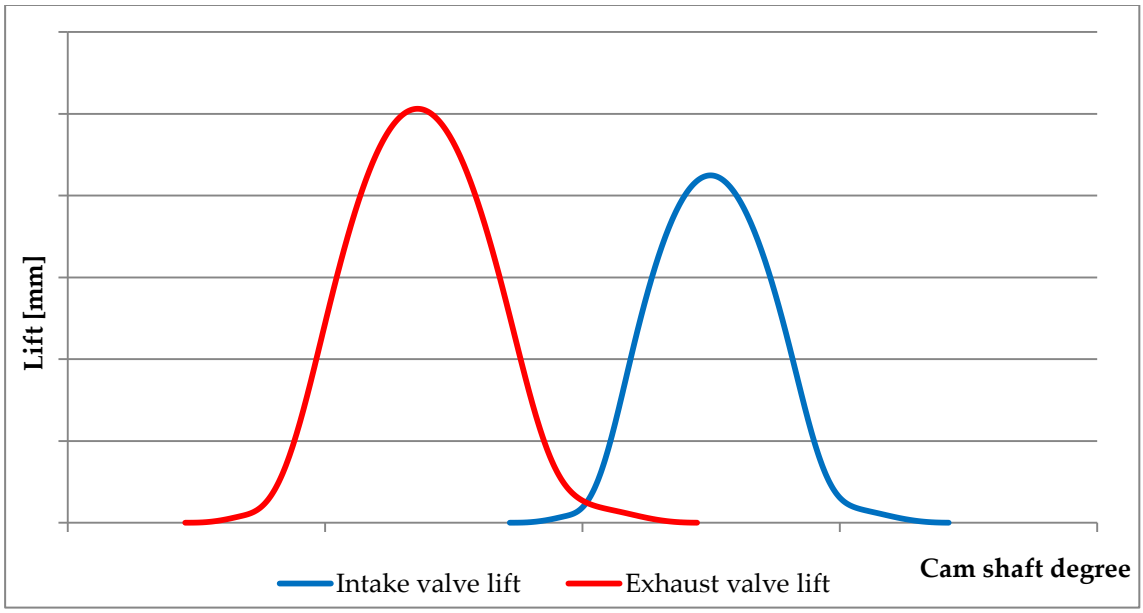

Figure 9: Intake and Exhaust valve lift

So, combining valve lifts and discharge coefficients, the effective flow area for exhaust (inverse) and intake (direct) valves can be computed and plotted in Figure 10.

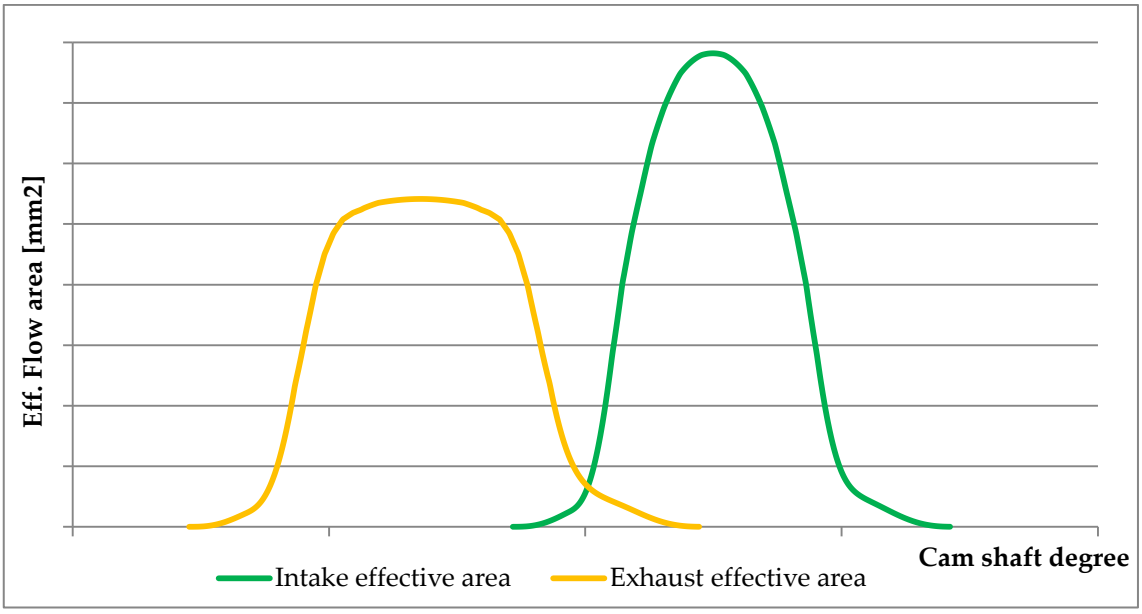

Figure 10: Intake and Exhaust effective flow area

Since the data shown above, the overlap period is obviously present and can be plotted both for cams and valves. The significant difference between the 2 overlap periods is due to the clearance which is not null due to space present between the cam and the head valve.

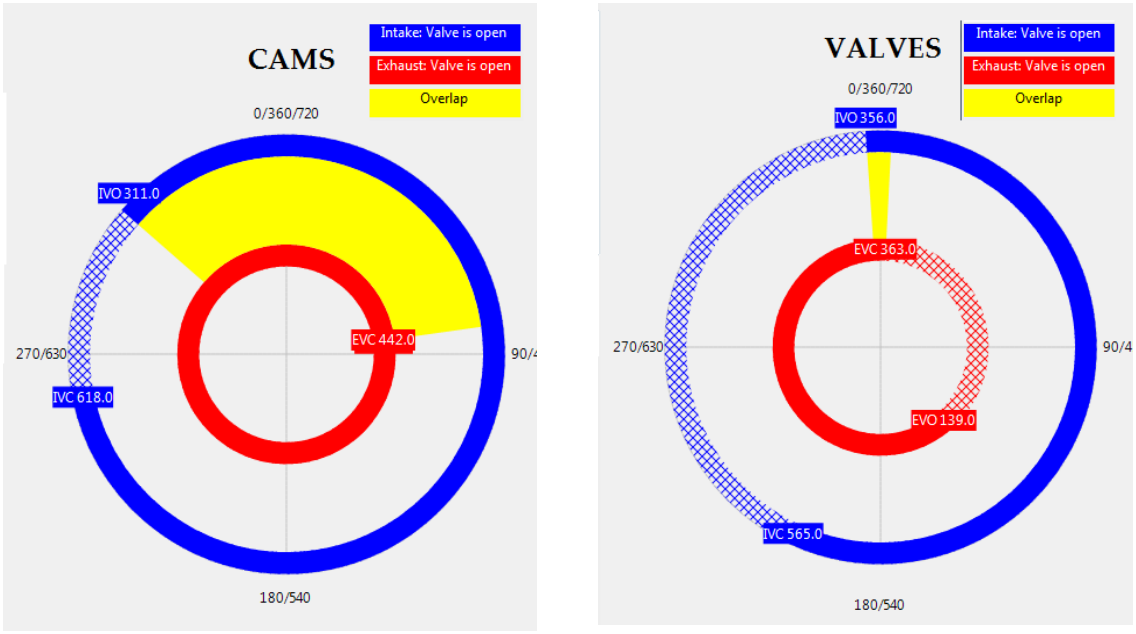

Figure 11: Cams and Valves timing

This phenomenon is fundamental to have a good gas exchange process exploiting the ram and waves effects which make the gas motions possible, also at crank angle degrees characterized by an opposite motion between piston and gas motion direction. The overlap period allows also to promote the scavenging process: the introduced fresh charge push out the burned exhaust gases.

At the moment a fixed valve timing system is used, but also the variable timing techniques might be applied, with the purpose of optimize the ram and waves effects at different engine speed.

3.5 Turbocharger

During the past decade, turbocharging has become the dominant trend in the automotive engine design, due to the large number of advantages with respect to the negligible drawbacks. It has been thought initially to boost up engine performances (Torque and Power) keeping unchanged all the other parts, but the global engine size reduction which includes lower costs, weight, space required and a fuel consumption reduction are the main reasons that have promoted the turbocharger use in the last years. Obviously, the required torque and power levels are achieved to guarantee a good drivability, but with a general saving in terms of pollution and costs. This goal can be reached by an increasing of the fresh charge density, exploiting a compression and a usual following cooling processes.

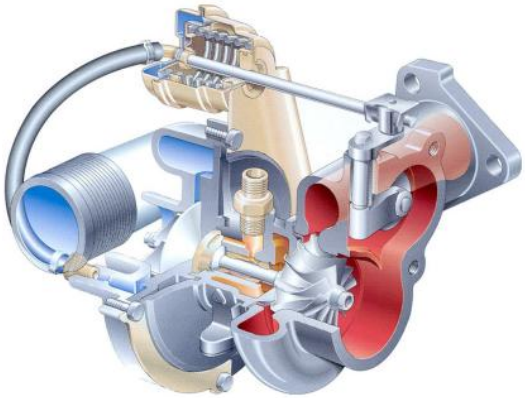

Figure 12: Example of turbocharger

The F1C CNG uses a Mitsubishi TD04HL-F6.0 turbocharger group, composed of a fixed geometry radial turbine and compressor splined on the same shaft, characterized by a pulse system arrangement. Pulse system turbochargers are an evolution of the constant pressure systems, that tries to exploit the high kinetic energy contained in the exhaust gases without transform it in pressure energy. It is possible using narrow pipes which directly connect the exhaust port with the turbine enter section. In this way turbine works with lower efficiency due to the wide flow oscillations, but with an increased available enthalpy drop which produce a greater amount of energy recovered and transmitted to the compressor shaft.

With careful choice of cylinders exhaust ducts grouping in a common duct, combined with a good exhaust pipes design, it is possible to obtain reasonably high turbine

operating efficiencies (although rarely as high as values of the constant pressure system). This is particularly critical in a 4-cylinder engine like the F1C where the distance between pressure peaks is 180 CAD. It is inevitable the presence of a certain degree of interference between cylinder exhaust phases, but a multiple turbine entry could be even worse due to the too wide period between consecutive pressure peaks (360 CAD).

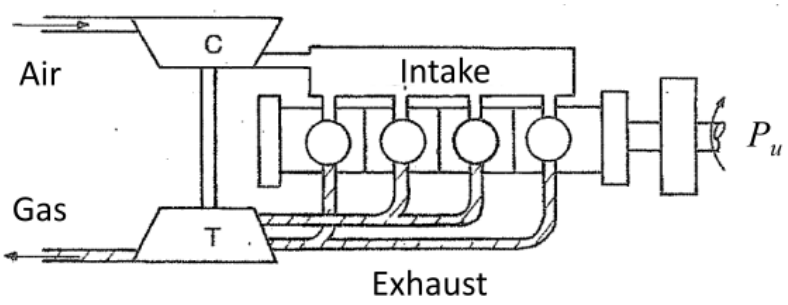

Figure 13: Example of multiple entry pulse turbocharger

To describe the turbocharger behaviour, it is necessary to define characteristics curves both for the compressor and for the turbine, functions of parameters which can be calculated depending on the real operating condition. In this way, it is possible to handle turbocharger with different sizes, using the same process exploiting the similarity theory. All calculations use values expressed in the S.I. system.

3.5.1 Compressor map

The compressor characteristic curve can be drawn with the following parameters defined as:

- *Mass flow parameter* $\dot{m}\frac{\sqrt{T_{1,tot}}}{p_{1,tot}}$ **3.1**
- *Compression ratio* $\frac{p_{2,tot}}{p_{1,tot}}$ **3.2**
- *Compressor efficency (total to static)* $\frac{h_{2,iso}-h_{1,tot}}{h_2-h_{1,tot}}$ **3.3**

All these values are calculated at each speed parameter value, defined as:

Speed parameter $\frac{n}{\sqrt{T_{1,tot}}}$ **3.4**

The turbocharger manufacturer provides the compressor map curves function of these parameters, expressed in a reference system which is different from that one necessary as Gasdyn input and so some calculations are required. Each curve is referred to a speed parameter and can be used, with the others, to predict the shaft behaviour, and as consequence the engine operating points.

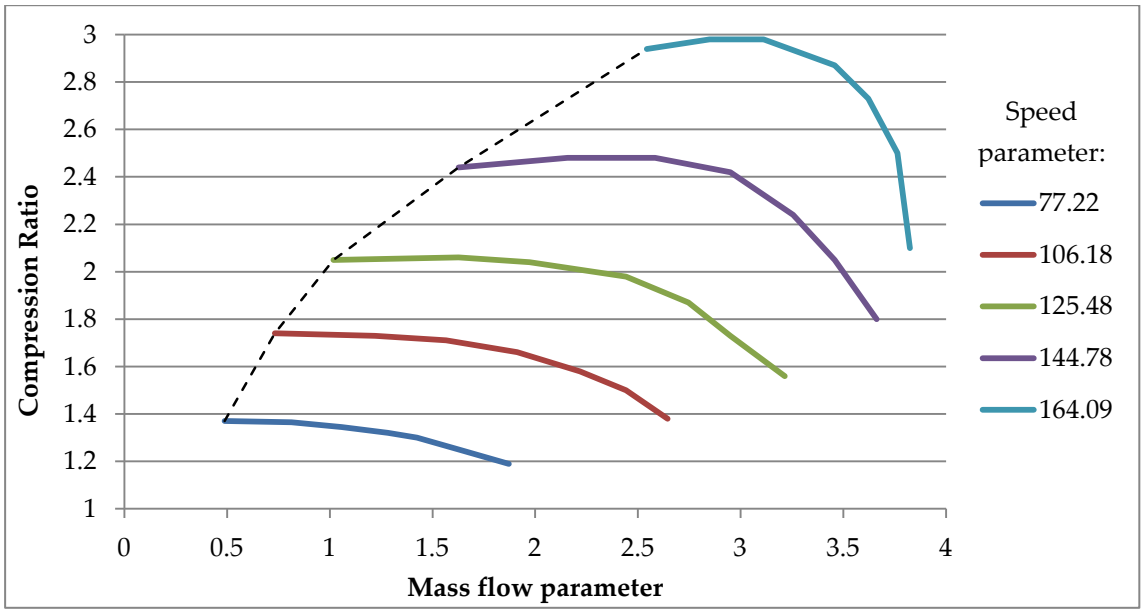

Figure 14: Compressor map (characteristic curves)

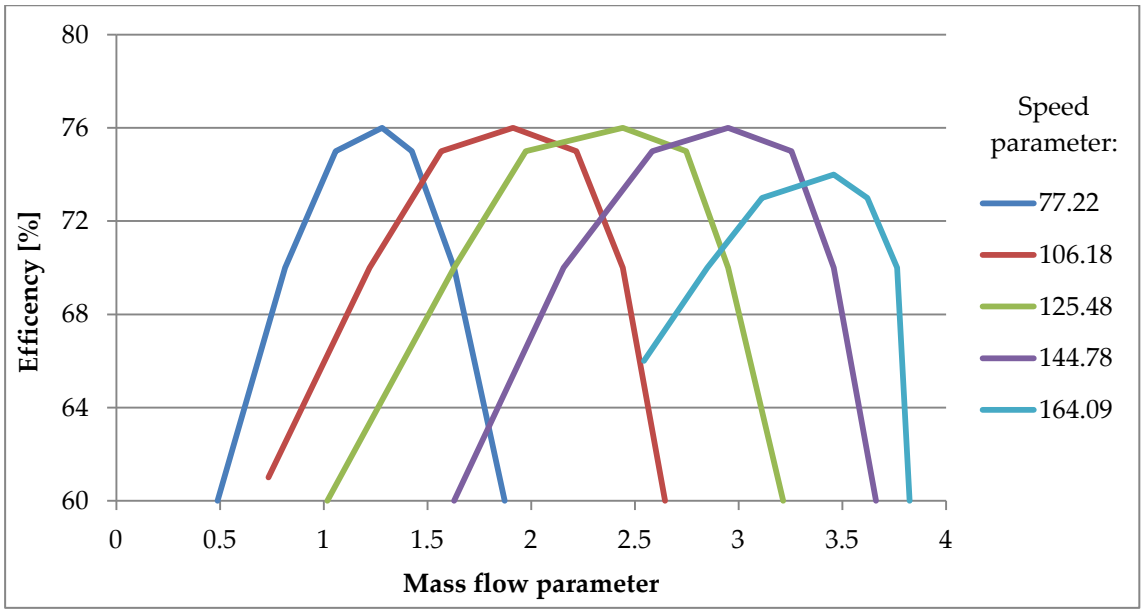

Figure 15: Compressor efficiency map

During simulation we have note that at 800 rpm and 1200 rpm, turbocharger works in non-real conditions because the curves arrives until efficiency of 60% as lowest value and also the compression ratio cannot be decrease below 1,4 for low mass flow parameters. At these engine speeds the compressor stabilises in an operating condition which doesn't represent the reality both for the efficiency and for the compression ratio, and indeed in the simulation the target boost pressure is not achieved.

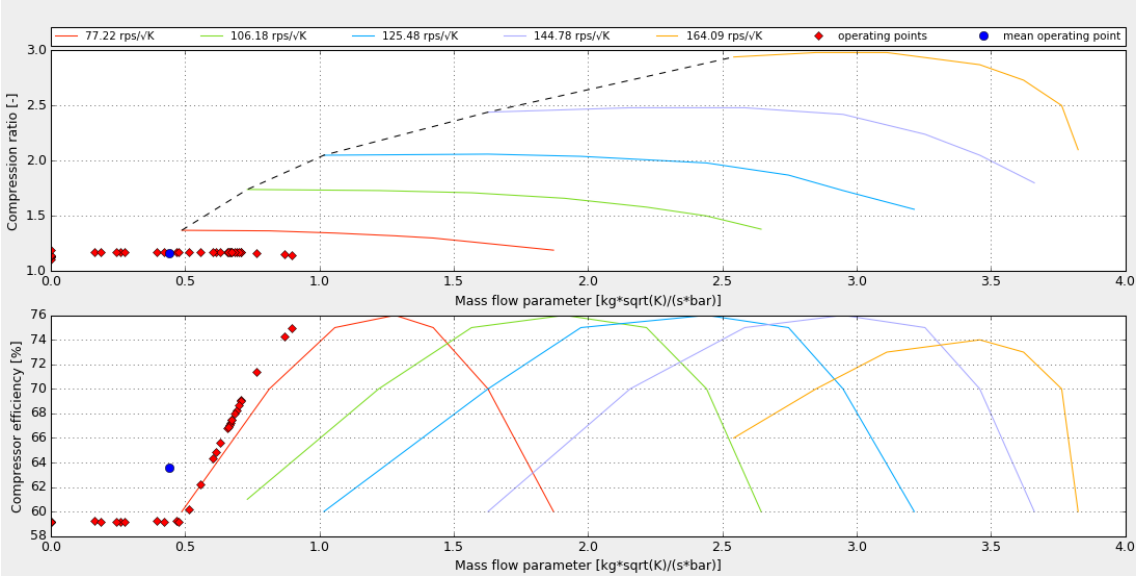

Figure 16: Initial compressor operating point

At these regimes the efficiency decreases also below the bottom values, and so the characteristics curves are manually extended, keeping as much as possible a reasonable trend similar to the original ones. The same is made also for the compression ratio graph, introducing a new curve below the others with a lower speed parameter which represent those points with compression ratio closed to 1. In this way the turbocharger can works in a more realistic way, with a lower efficiency and a more correct compression ratio.

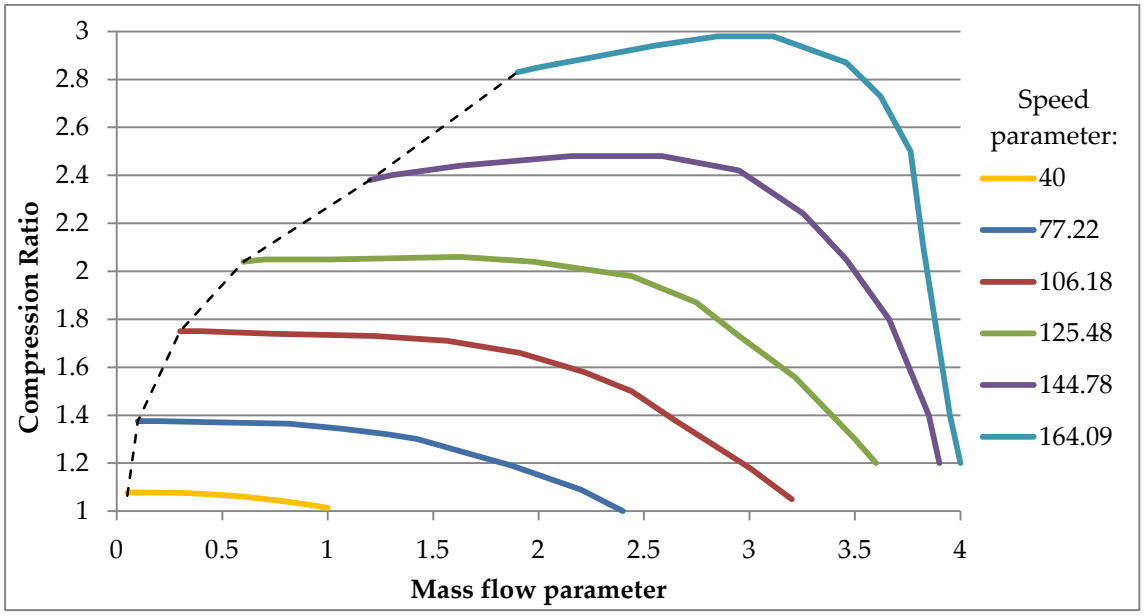

Figure 17: Extended compressor map

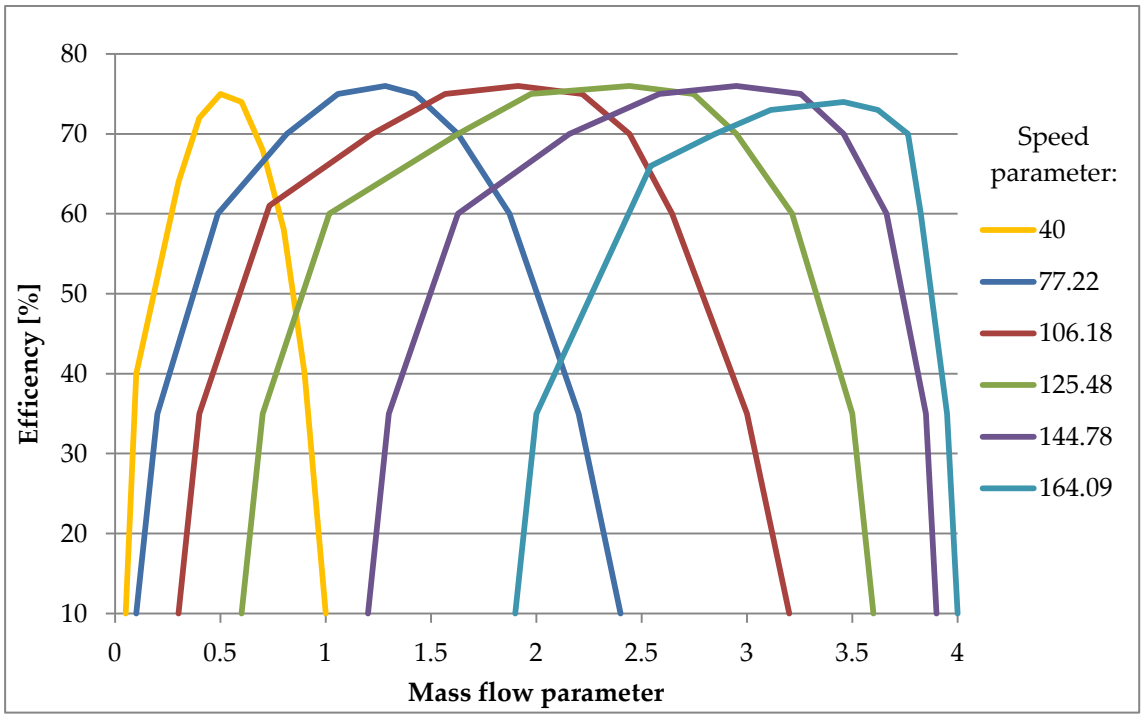

Figure 18: Extended compressor efficiency map

The extended compressor characteristic curves contribute significantly only at 800 rpm and 1200 rpm solving the non-real functioning problem. At higher regimes the compressor operating points remain in the zone defined by the standard curves and so using only manufacturer certified data.

3.5.2 Turbine map

Also turbine can be treated in the same way of the compressor using a little bit different parameters, but with the same meaning, defined in the following way:

- *Mass flow parameter* $\dot{m}\frac{\sqrt{T_{0,tot}}}{p_{0,tot}}$ **3.5**
- *Expantion ratio* $\frac{p_{1,tot}}{p_2}$ **3.6**
- *Blade speed ratio* $\frac{U}{C_{is}}$ **3.7**

  Where C_{is} is the isentropic velocity, that is the velocity of an ideal gas during an isentropic expansion process given by:

$$h_{0,tot} - h_2 = \frac{C_{is}^2}{2} \quad \textbf{3.8}$$

- *Turbine efficency (total to static)* $\frac{h_{0,tot} - h_2}{h_{0,tot} - h_{2,iso}}$ **3.9**

All these values are calculated at each speed parameter value, defined as:

Speed parameter $\frac{n}{\sqrt{T_{1,tot}}}$ **3.10**

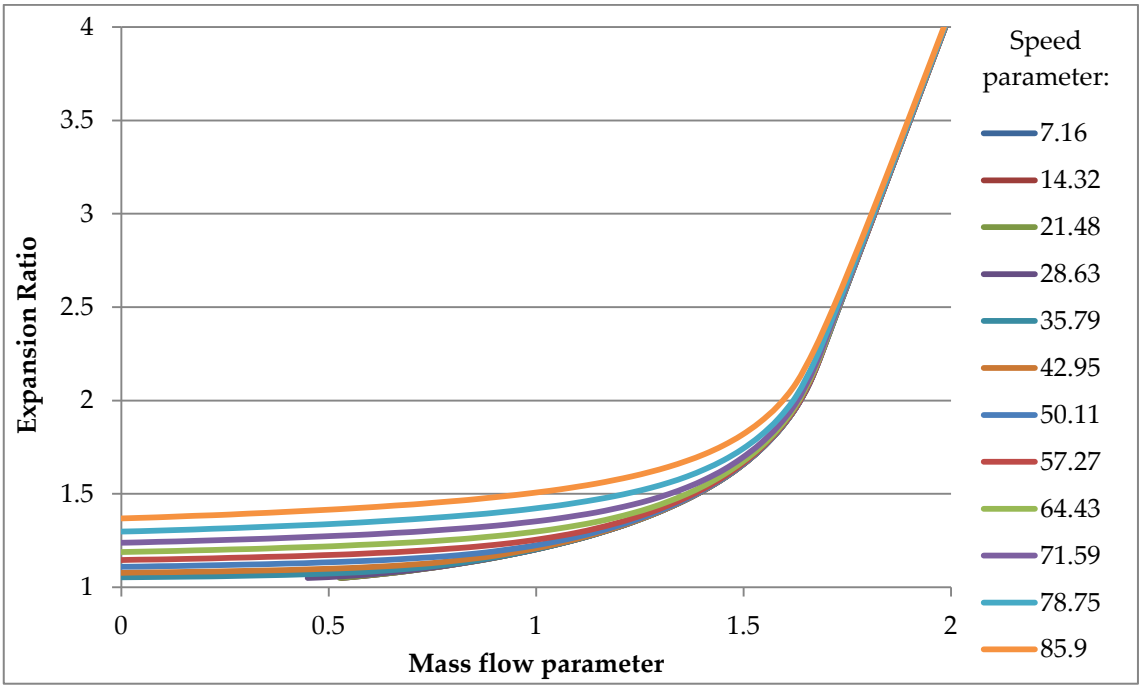

Figure 19: Turbine map

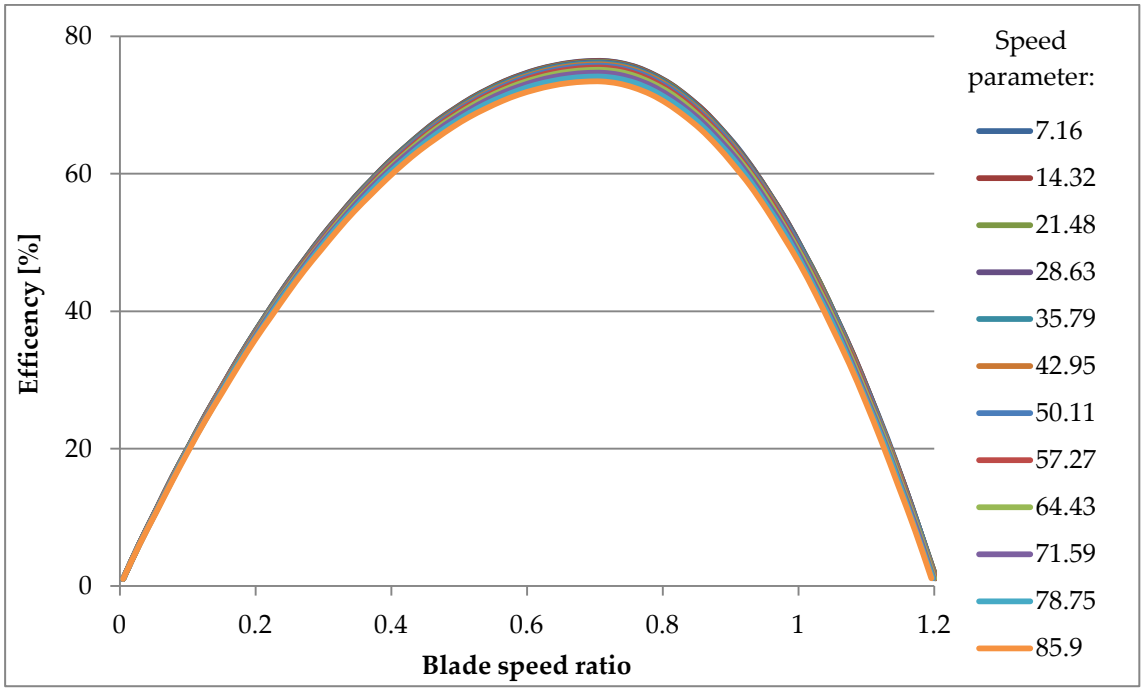

Figure 20: Turbine efficency map

In this case it is not necessary to modify or extend the characteristic curves, because the operating points remain, at each regime, in a defined zone and the simulation well represent the reality.

3.5.3 Turbocharger matching

In steady state condition the power produced by the turbine has to coincide with the power absorbed by the compressor, and the shaft reach the equilibrium condition. This phenomenon is called turbo-matching, and if it doesn't occur there is a shaft velocity variation until reaching a new equilibrium velocity. The scheme is:

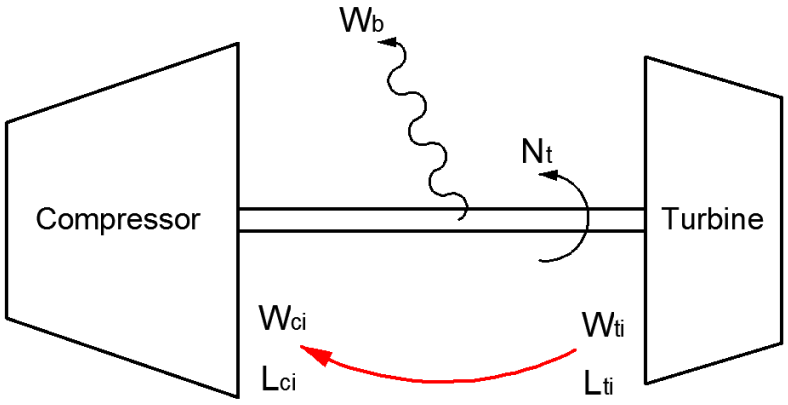

Figure 21: Turbocharger power diagram

Gasdyn consider also the frictional losses generated on the bearings and compute the right rotational speed to reach the imposed boost pressure, keeping, if it is possible, the shaft in equilibrium from the power point of view. The torques drawn in the previous diagram which characterized the system are:

$$L_{ti} = \frac{W_{ti}}{2\pi N} \quad \textbf{3.11}$$

$$L_{ci} = \frac{W_{ci}}{2\pi N} \quad \textbf{3.12}$$

$$L_B = \frac{W_B}{2\pi N} = (1-\eta_M)\frac{W_{ti}}{2\pi N} = (1-\eta_M)L_{ti} \qquad with \qquad \eta_M = \frac{W_{ti}-W_B}{W_{ti}} \quad \textbf{3.13}$$

Therefore, we can express the torque balance as:

$$L_{ti} - L_{ci} - L_B = 2\pi J\frac{dN}{dt} \quad \textbf{3.14}$$

$$\frac{dN}{dt} = \frac{1}{2\pi J}(\eta_M L_{ti} - L_{ci}) \quad \textbf{3.15}$$

Where ***J*** represent the polar moment of inertia of the rotating parts.

Note that the turbocharger acceleration is proportional to the instantaneous net torque and inversely proportional to the polar moment of inertia of the moving parts.

Now, recalling the definitions of instantaneous turbine work W_{ti} and hence the instantaneous torque L_{ti}:

$$L_{ti} = \frac{\dot{W}_t}{2\pi N} = \frac{\eta_T}{2\pi N}\dot{m}\frac{C_{is}^2}{2} \quad \textbf{3.16}$$

and the same for the compressor through the equation:

$$L_{c_i} = \frac{p_1}{\eta_c}\left(\frac{\dot{m}\sqrt{T_1}}{p_1}\right)\left(\frac{\sqrt{T_1}}{N}\right)\frac{c_p}{2\pi}\left[\left(\frac{p_2}{p_1}\right)^{\frac{k-1}{k}} - 1\right] \quad \textbf{3.17}$$

Where:

- $\dot{W}_t$ = turbine power
- C_{is} = turbine isentropic speed
- η_c, η_T = adiabatic compressor and turbine efficiencies

At the following time step, the turbocharger speed can be calculated as:

$$N_{i+1} = N_i + \frac{1}{2\pi J}(\eta_m L_{ti} - Lc_i)\,dt \quad \textbf{3.18}$$

The power balance at the turbocharger shaft is solved for every crank angle and it is therefore fluctuating through the engine cycle, due to the unsteady characteristics of the flow. This is obviously linked with the design choice of the impulse turbocharging system, rather than use a wide exhaust manifold which would lead to a steady flow with the drawback of lower available enthalpy drop. For this reason, it is required the adoption of a convergence criteria that considers the average speed of the turbocharger throughout the engine cycle.

It is also adopted an automatically controlled wastegate valve, which opens in case of too high pressure levels reached after the compressor, reducing the power produced by the turbine and wasting a part of the available exhaust mass flow rate. Indirectly, also the rotational shaft speed is reduced and the pressure in the intake manifold too, until reaching the target boost pressure. It is regulated using a PID control procedure. It is a strong, but necessary, dissipative process due to the fact that it is not possible to have a turbine with the optimal dimension for each engine speed and load. In the Figure 22 is reported a mechanical scheme representing the wastegate valve system structure and its working method.

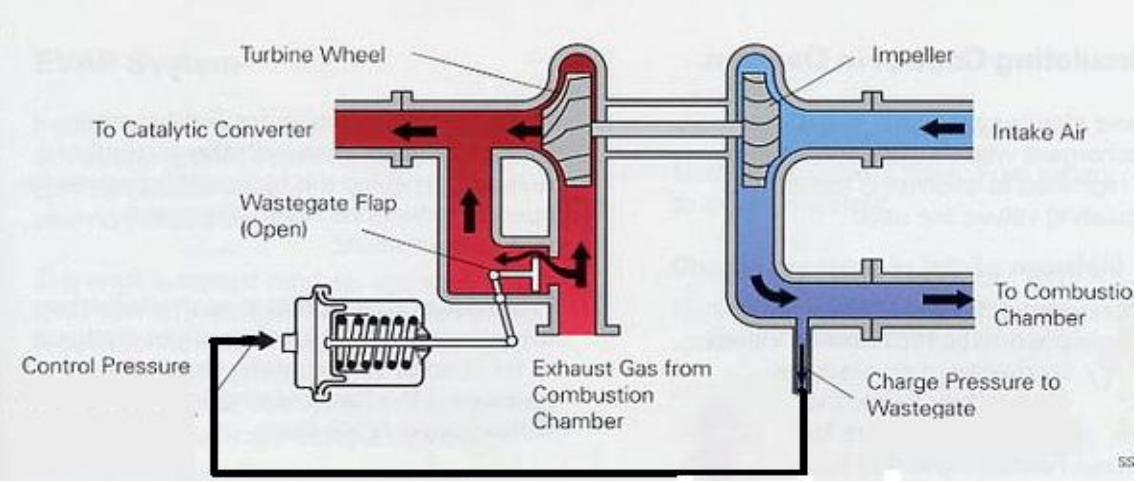

Figure 22: Wastegate valve scheme

A possible improvement is to use a VGT (Variable Geometry Turbine), able to fit better all the real operating points. It is possible to regulate the load without using a dissipative valve, and so recovery a bigger amount of energy from the exhaust flow. With a rotation of the statoric blades a change in the shape of the velocity triangles and also on the magnitude of the vectors occur and consequently there is a variation of the flow area which modify the mass flow rate. In this process there is no waste of the available enthalpy contained in the hot exhaust gases and no pressure drops occur. A schematic draft is represented in the Figure 23.

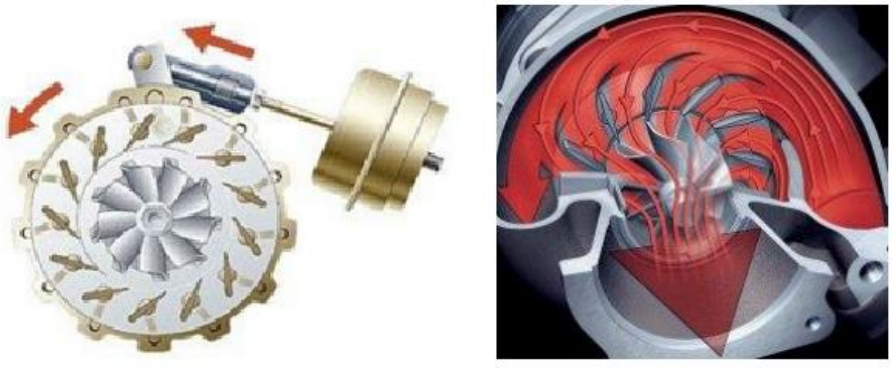

Figure 23: Representation of a variable inlet section position of a VGT turbine

3.6 Intercooler

As said previously, a turbocharger is chosen in this engine to reducing the structure size, increase performances and reduce the fuel consumption. Its target is to increase the density of the fresh charge drawn into the engine at each cycle and this can be reach increasing pressure and reducing the temperature. During the compression process some losses occur, due to the non isentropicity of the process, and it is followed by an increase of temperature which obviously reduce the air density. This increment can be computed according:

$$\Delta T = \frac{T_{in} \cdot \left[\left(\frac{P_{out}}{P_{in}}\right)^{\gamma-1/\gamma} - 1\right]}{\eta_c} \qquad \textbf{3.19}$$

The density ratio is obviously linked with the compression ratio, but strongly depends also on the final gas temperature. This relation is represented in the Figure 24.

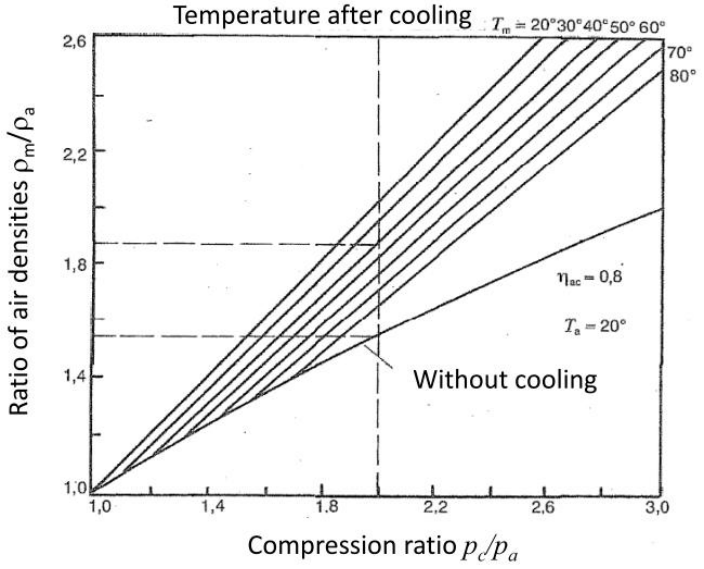

Figure 24: Relation between density and compression ratio as function of cooling process

So, an intercooler is always adopted to cool down the flow, even if some pressure losses are generated by the high number of tiny ducts necessary to have an efficient heat exchange process.

For the F1C CNG engine an air-water heat exchanger is adopted, to enhance the overall efficiency and reduce the size. The achieved fresh charge density is obviously higher than the initial one and this carry to a have an enhanced breathed air mass, volumetric efficiency and all performances. We don't know the real characteristics dimensions of intercooler adopted in the engine under analysis, but the measured temperature after the cooling process are available. So, it is necessary to find a group of values which allow to cool enough the air and the combination present in the Table 2 is only one possibility among the endless whole existents.Table 2: Intercooler dimensioning

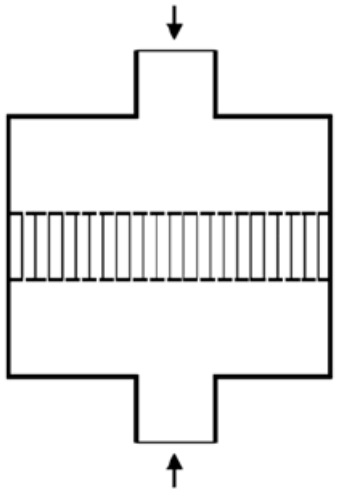

Figure 25: Intercooler scheme

Matrix diameter	200 mm
Length	500 mm
N of ducts	200
Duct diameter	13 mm
Friction coefficient	2

Table 2: Intercooler dimensioning

These intercooler measures, as previously said, doesn't represent the real dimensions, but allow to achieve the target temperature after the intercooler. It is important to highlight that this is only one combination of values, but there are infinite other possibilities which can be used in the simulation without changing the results. The unique sensible parameters which assume different values using a different dimension is the refrigerant mass flow rate and the temperature increase of the coolant through the heat exchanger, but we are not interested to it in this thesis. The whole thermal power exchanged remain always the same.

The outlet temperature is fixed in order to reach a compromise between air temperature difference and coolant flow rate, which take into account also intercooler size and coolant pump energy consumption. Moreover, it is not convenient to cooling down the air below a certain temperature, because one always great percentage of the water contained as humidity would condense with a consequent problem related to the water stagnation inside the heat exchanger channels. Fixed gas outlet temperature can

be plotted to have a better idea also of the ΔT, and so also of the cooling power, that the intercooler has to subtract to the air flow. In the Figure 26 are represented the parameters cited above, but due to the great confidentiality of the data has not been possible to write the absolute values, which would have introduced a more realistic point of view.

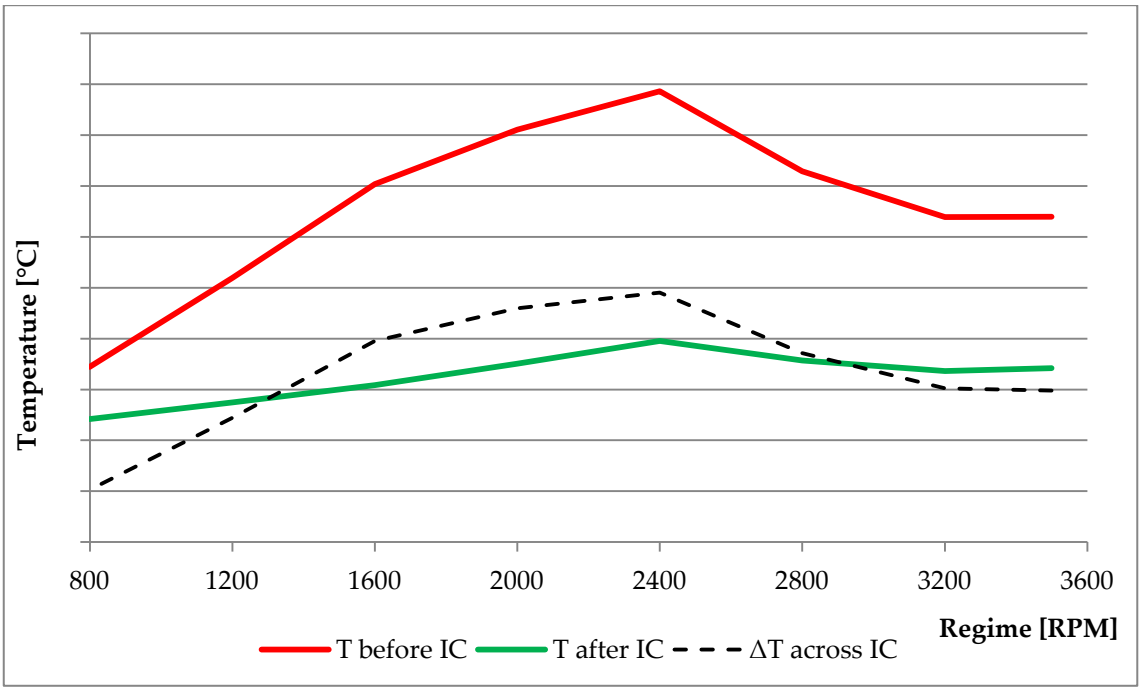

Figure 26: Temperature profile across Intercooler

3.7 Throttle valve

In relation to the fluid type, also at full load the throttle valve position is not totally open, in order to reduce a little bit the amount of breathed air and allow a good injection of fuel. Due to gaseous state of the natural gas, the fuel occupies a bigger amount of volumetric flow rate with respect to the traditional liquid fuels, and keeping the same engine structure and mechanical parts, a partial closure of the throttle valve is necessary.

EMPA provides us a percentage measure of the geometrical flow area, with respect to that attainable with a maximum opening of the valve ψ_{max}, which correspond to an angle of 85°. Using the relation written in the equation 3.20, it possible to compute the valve rotation angles, one for each regime, which are used as input data in the Gasdyn pre-processor.

$$\frac{4\,A_{TH}}{\pi\,D^2} = \left(1 - \frac{\cos\psi}{\cos\psi_0}\right) + \frac{2}{\pi}\left[\begin{array}{c} \frac{a}{\cos\psi}\sqrt{(\cos^2\psi - a^2\cos^2\psi_0)} + \\ -\frac{\cos\psi}{\cos\psi_0}\arcsin\left(\frac{a\,\cos\psi_0}{\cos\psi}\right) - a\sqrt{(1-a^2)} + \arcsin(a) \end{array}\right] \quad \textbf{3.20}$$

With:

- A_{TH} is the geometrical throttle area.
- $a = {}^{d}/_{D}$ with d is the shaft diameter and D the throttle body diameter.
- $\psi_0 = 5°$ is the throttle opening angle.
- ψ is the throttle opening angle.

The numerical terms introduced above as ψ_{max} and ψ_0 don't represent a real measure of the angles which the throttle valve is subject but are only a reference values necessary to allow the conversion process.

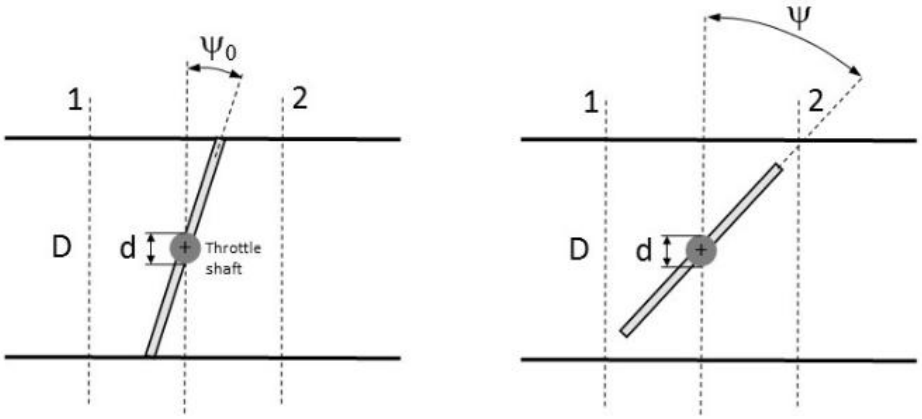

Figure 27: Throttle valve position

After some calculations the opening angles at full load, for each regime, are obtained, but in this thesis work cannot be plotted or written due to confidentiality reasons. It is possible to confirm that also the calculated values regarding the full load condition is significantly far from the maximum opening angle.

3.8 Injection

The fuel injection in this type of engines is a key process which require an accurate analysis due to its gaseous physical state. It implies that the fuel fills a significant percentage of the total volume, subtracting a part of it at the fresh air, in comparison to the liquid types. The PFI (Port Fuel Injection) techniques is applied, and preferred to the direct one, due to the big volume flow rate required to have a certain injected mass of fuel, in particular way at high regimes at which the injector opening period reach 440 crank angle degrees.

For this reason, the amount of air introduced in the combustion chamber is reduced in relation to the standard liquid fuel engine, due to the relevant amount fuel injected volume. The throttle valve has to work with a lower opening angle as previously explained.

The Table 3 collect the injectors data introduced as input in the Gasdyn pre-processor.

RPM	Temp. [K]	Press. [bar]	Mass flow [kg/s]	Start [deg.]	End [deg.]
800	320	1	3 e-04	0	720
1200	317	1.2	5 e-04	0	720
1600	311	1.45	7 e-04	0	720
2000	309	1.6	9 e-04	0	720
2400	304	1.7	11 e-04	0	720
2800	303	1.5	12 e-04	0	720
3200	302	1.4	12.5 e-04	0	720
3500	300	1.4	12.5 e-04	0	720

Table 3: Injectors Gasdyn input data

It is important to remember that these values are not measured or taken from official data, but are random values used only to have an initial condition. During simulations the computational code calculate the right injected mass of fuel to reach the A/F ratio value, fixed as target. In this way we don't introduce a limit on the injector opening and closing angles, but we inject the right amount of fuel, allowing to the engine to work at the required load. Also the injected gas pressure and temperature fixed as input for Gasdyn don't represent the real values and moreover their values cannot significantly modify the injected mass of fuel.

The injector opening period is set as always open even if the right values are available. This because Gasdyn, working in the closed loop mode, search the mass of fuel to inject to reach the target A/F ratio independently from the opening period.

3.9 Gasdyn scheme

Starting from the text file which contains all the interesting and necessary data relating to the engine structure and operating points, and also using other data provided by constructor, we have built step by step an engine scheme on Gasdyn. It is important to keep in mind that, the scheme used in the software, don't represent mandatorily the real ducts and manifolds geometric characteristic, because it would be too challenging,

in relation to the relevant presence of complex shapes. In particular way the intake manifold is characterized by a very complex shape, represented in Figure 28, and it is modelled using only circular ducts.

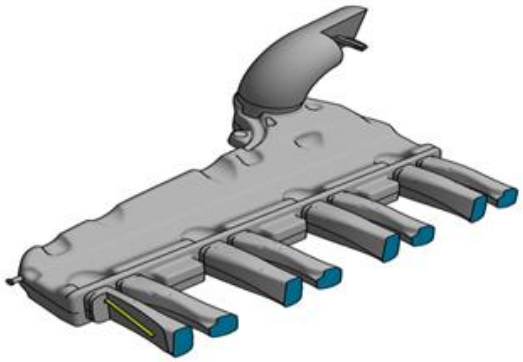

Figure 28: Intake manifold

With respect to the real engine and the GT-Power simulated one, our scheme doesn't take into consideration pre-treatment and after-treatment processes such as: air filtering, pollutant removal from exhaust gases and silencer. Their contributes are introduced by modifying the boundary conditions (temperatures and pressures) at the inlet and outlet sections.

During the thesis work period, this scheme has been modified and improved step by step, with the purpose of fit always better the experimental data, keeping at the same time a realistic guide line.

The Gasdyn scheme is represented in the

Figure 29.

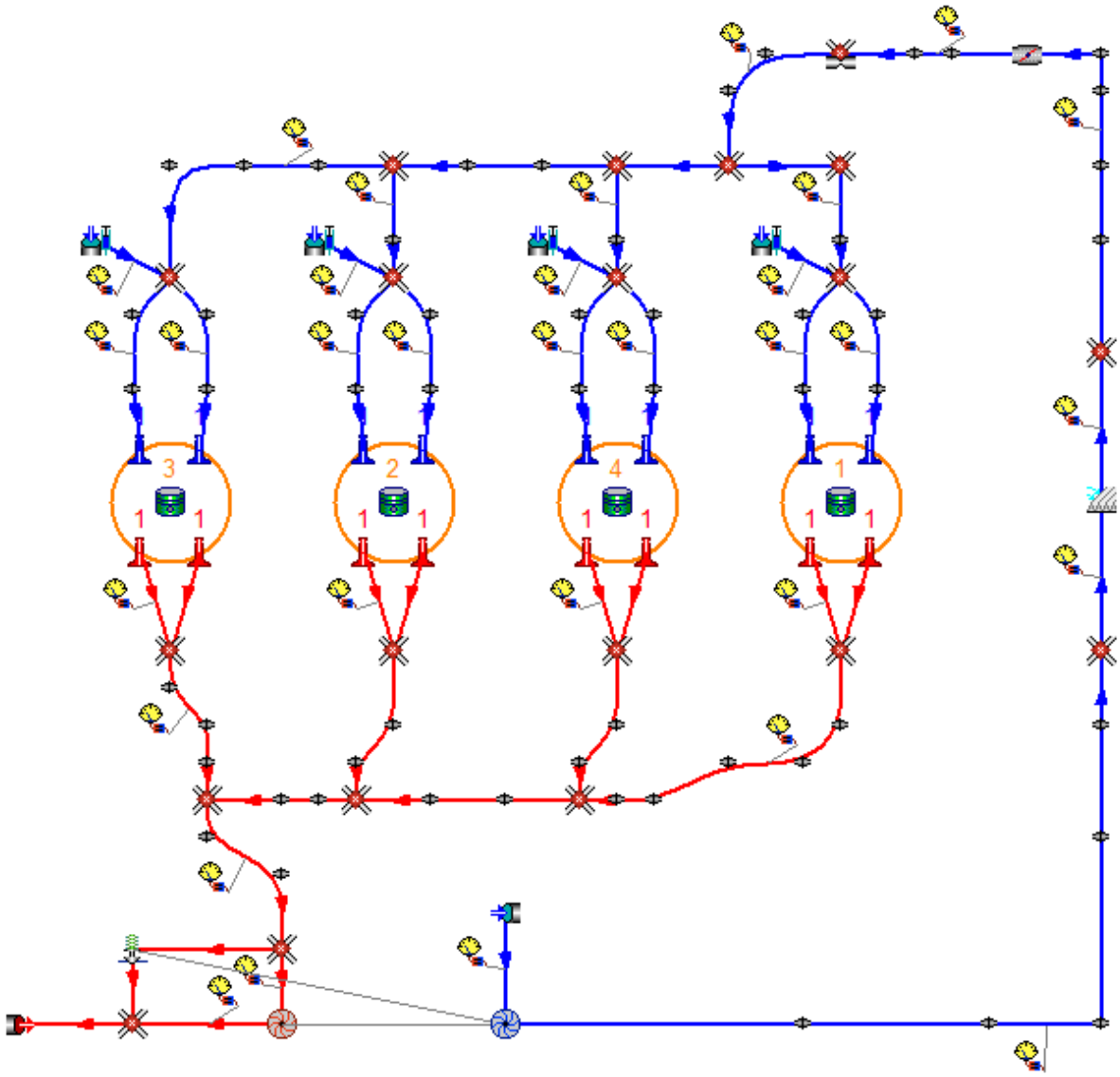

Figure 29: Gasdyn Engine scheme

3.9.1 Processing of the results

Once the model is completed, the simulation can start, and the required amount of time depends on the model's complexity, on the number of tested engine regimes, on the number of elements and on the computer performances. Each engine speed requires a variable number of calculation cycles before reach the convergence condition.

All the numerical results produced by the software are saved in the same folder of the input ones, under the shape of various text files, divided according to their argument and reference area. Some files are automatically produced during the simulation, while others are obtained by inserting virtual transducers in the scheme. For example, it is possible to calculate both mean and instantaneous characteristic values in different cross-sections of the ducts (pressure, temperature, velocity, mass flow and species concentration), as a function of the crank angle. Also the evolution of the cylinder pressure with the crank angle and the pressure waves effects into the ducts can be predicted and analysed.

These data are post-processed with a proper Excel file, created and continuously improved during the thesis work, and compared with the experimental measurements in order to validate the Gasdyn simulation model.

4 Full load engine results

As mentioned in the introduction, in this chapter we will compare the experimental data measured on the test bench, with those obtained by numerical simulations computed using Gasdyn. This is a key step during the construction and the development of the model, to verify if the adopted parameters are reliable or not and test the software's ability to correctly simulates all the thermo and fluid dynamics processes, that occur in the engine.

It is important to remember that these types of studies (1D modelling) are based on some system's approximations, experimental parameters and empirical laws, which cannot perfectly represent the real behaviour of the fluid due to the complex cyclic nature of the machine and also to the great pressure, temperature and velocity gradients which the fluid has to support during an engine revolution. So, some little discrepancies between measured data on the real engine and simulated results are possible.

4.1 Experimental data

A lot of data are measured on the test bench, using transducers placed in strategic positions, in order to obtain reliable and meaningful results. They are able to measure pressure, temperature and others important variables. The engine load is provided by using an electric generator, splined at the crank shaft, which can be easily regulate to reach a certain operating point, and remain in this condition for a certain period, sufficient to bring all the parts to a stationary working condition, and allow to the instruments to conclude the transient processes and detect a stable measure. It is also used to measure the torque and power produced by the engine at various regimes and different loads.

The Figure 30 represent the test bench equipped with the all measuring instruments.

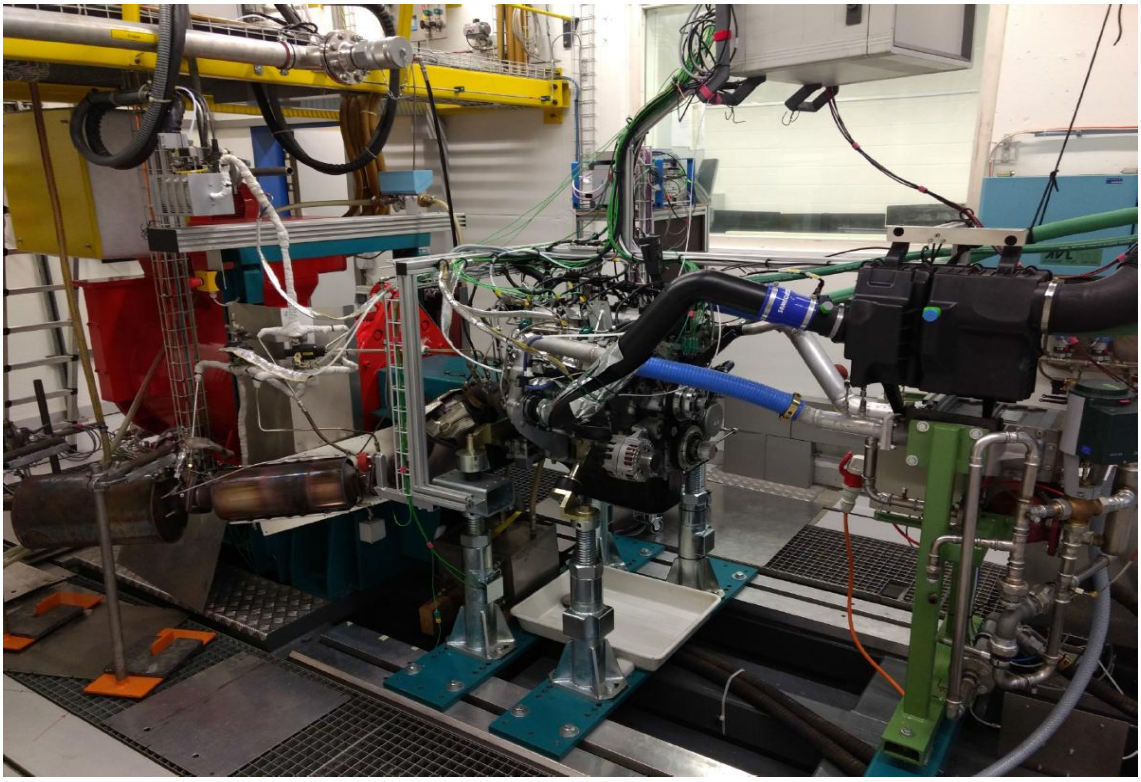

Figure 30: F1C CNG test bench

To study the waves effect and its comparison with the experimental data, it is fundamental to well identify the place where the pressure transducer, in the intake and exhaust manifold, are applied. From Figure 31, provided by EMPA, it is possible to localize they in the real engine and find a corresponding position in the model.

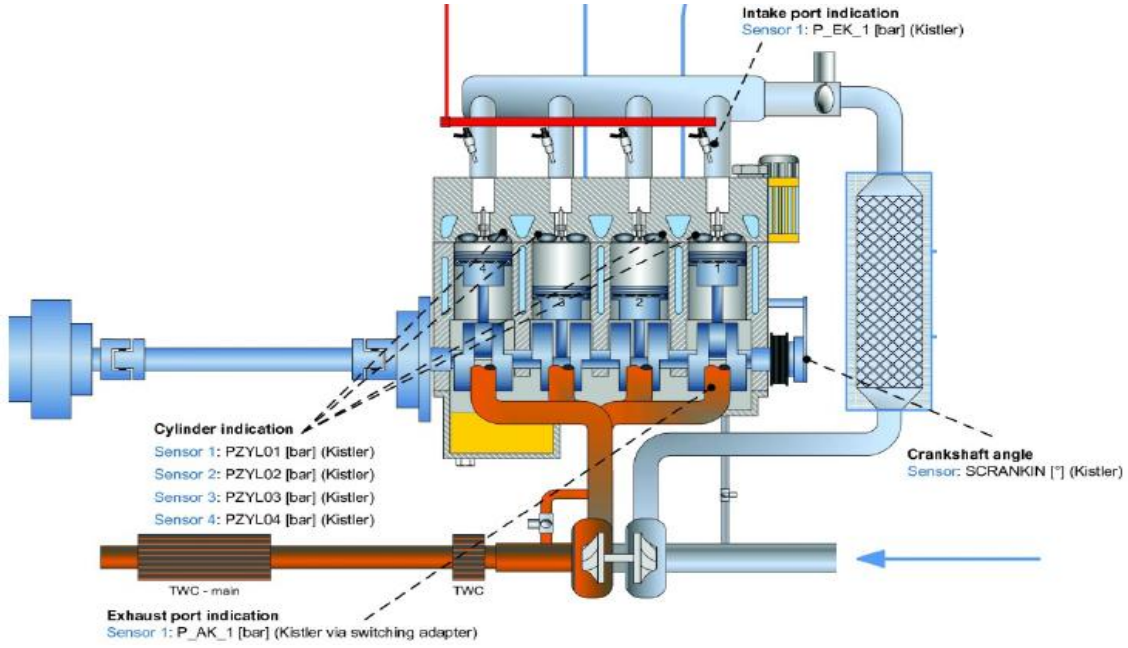

Figure 31: Tranducers position

The engine has been tested in a lot of operating points, represented in the Figure 32, where the measured brake torque values are expressed with respect to the engine speed, at different loads.

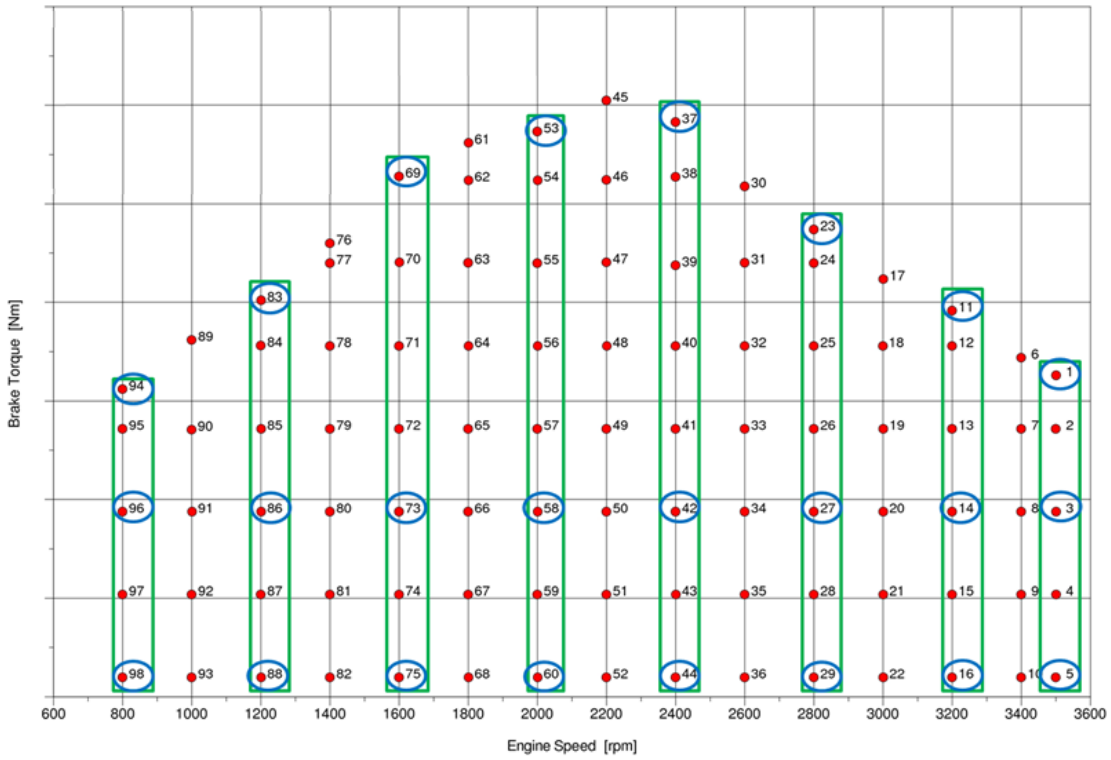

Figure 32: Experimental brake torque curve

Others measured data, for each operating point, are provided into an additional excel files.

4.2 Transducer position

It is quite important to well define the position in which place transducers, because the measured variables can change, also in significant way, at few centimetres of distance. This is true, in particular way, for the pressure sensors installed in the intake and exhaust manifold, which have to analyze the waves timing with respect to the valves opening, and so can detect an unreal phase displacement.

Other transducers are introduced into the engine Gasdyn model in order to evaluate other variables such as pressure drop, temperature and mass flow rates, of which the average value on the cycle is a more relevant data.

The engine scheme, with all the transducers positions, is represented in the

Figure 33.

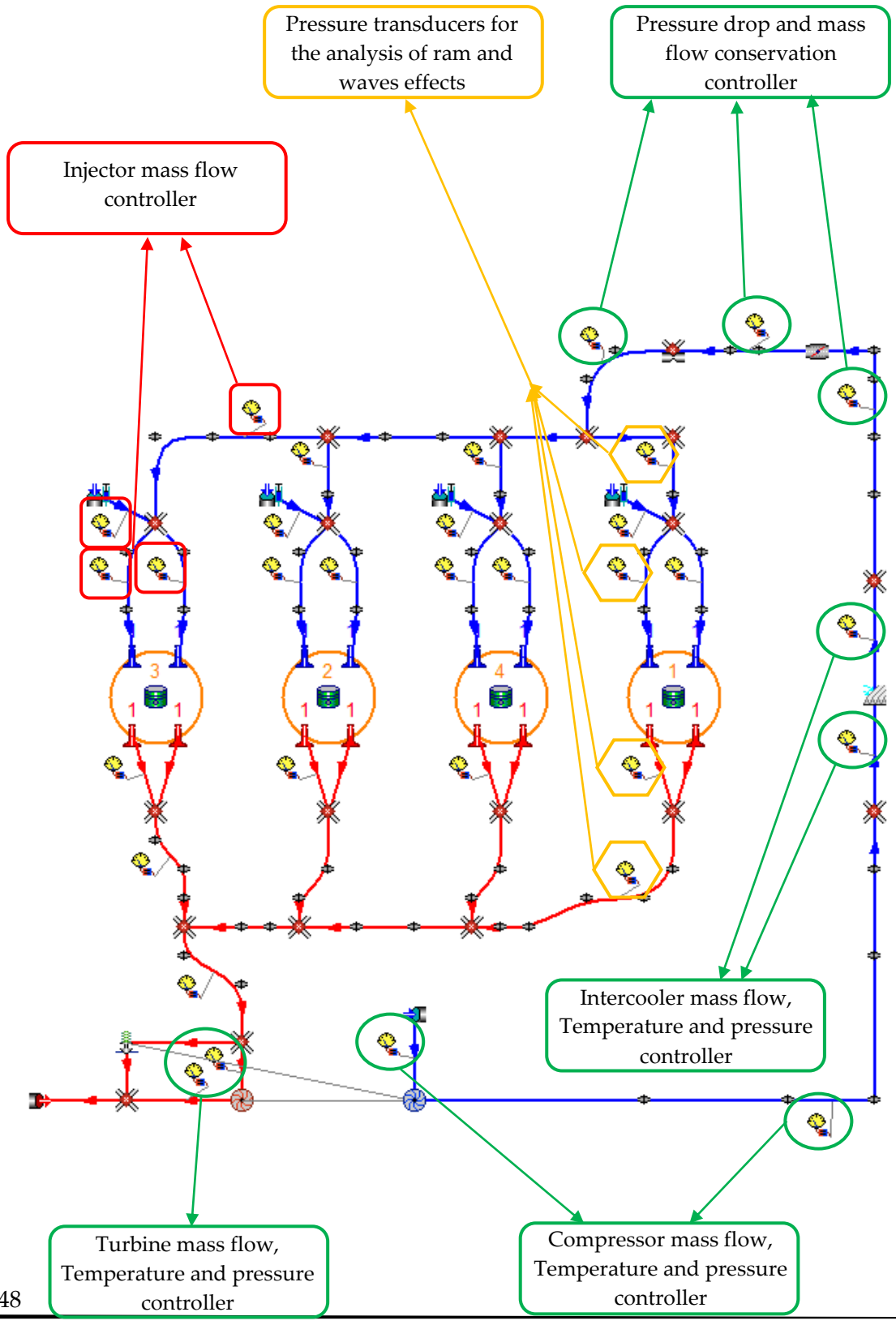
Pressure transducers for the analysis of ram and waves effects
Pressure drop and mass flow conservation controller
Injector mass flow controller
Intercooler mass flow, Temperature and pressure controller
Turbine mass flow, Temperature and pressure controller
Compressor mass flow, Temperature and pressure controller

Figure 33: Transducers position into the Gasdyn engine scheme

4.3 Model validation

In this part of the chapter, some relevant parameters are compared with the experimental data, in order to check if the Gasdyn model output faithfully represent the real engine behaviour at the same operating conditions. As already mentioned previously, some discrepancies are possible, due to the assumption made and models used which cannot perfectly represent the real gas process. This is a compromise between the accuracy level required as target and the computational power available in terms of money and time.

4.3.1 Performances

With performances means those quantities which identify the engine capability to do works and in particular are: Torque, Power and Specific fuel consumption. These quantities identify the engine size, its category and its range of use. In our situation we are considering a light-duty vehicle and so the final engine utilisation will be characterized by a good torque level already available at the low speeds, to increase the drivability, without the necessity of reach elevated levels of power. Furthermore, it is important to keep the fuel consumption as low as possible saving money and reducing the pollutants emitted quantity.

First of all, it is important to introduce and define the Brake Mean Effective Pressure (*bmep*), a fundamental parameter for the internal combustion engine, that is the effective work per unit cycle and unit volume displaced by the engine. It indicates how good the engine design has been done in exploiting the available volume displaced by the piston and the degree of success of handling high pressure gases with relevant thermal load. It is included in the definition of many relevant quantities and so strongly influences the performances. It is defined in the equation 4.1.

$$bmep = \eta_b \cdot \lambda_v \cdot \frac{\rho_a}{\alpha} \cdot Q_{HV} \qquad \textbf{4.1}$$

Where:

- η_b represent the engine brake efficiency.

- λ_v is the volumetric efficiency and represent the capability of the engine to fill the cylinder with fresh charge. So, it is a sort of efficiency.
- ρ_a is the inlet air density affected by ambient pressure and temperature.
- α is the air fuel ratio.
- Q_{HV} is the fuel heating value.

This parameter is a key quantity which allow to compare the performances of an engine of a given type to another of the same type. It is computed into the numerical simulations on the engine Gasdyn model, and so it is possible to plot the obtained *bmep* values and compare they with the measured ones on the test bench. This comparison is represented in the Figure 34. We expect to have an average level, for the majority of the regimes under exam, between 1 and 3 MPa in relation to the turbocharged nature of the engine under analysis. In case of naturally aspirated motor the *bmep* value is usually lower than 1 due to the fact that the reference condition usually coincide with the ambient ones and some pressure drop is always present.

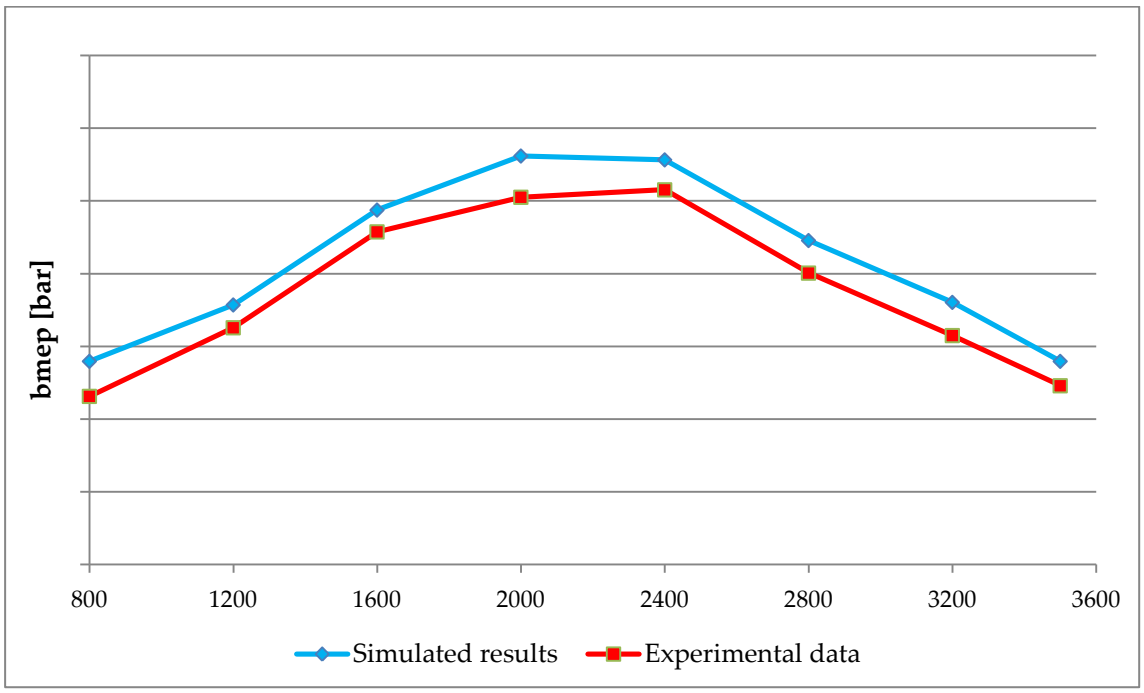

Figure 34: Measured vs Simulated *bmep*

This discrepancy between measured and calculated *bmep* could be attributed to an error into the estimation of the frictional mean effective pressure (*fmep*). It should be remembered that the brake mean effective pressure is defined and calculated as the difference between the indicated and the frictional ones. It represents a sort of engine efficiency under the mechanical point of view, considering all the frictional losses generated by the movement of the mechanical parts. An example could be the creeping

between the piston and the inner cylinder wall or the losses generated by the fast rotation of the crank shaft bearings. In the Gasdyn code the *fmep* calculation is carried out exploiting the modified Chen-Flynn model, defined according the equation 4.2.

$$fmep = a + b \cdot p_{max\ cyl} + c \cdot V_{piston} + d \cdot V_{piston}^2 \qquad \textbf{4.2}$$

Where *a*, *b*, *c*, *d* are parameters which are not given by EMPA, but have been chosen by us with a trial and error procedure, and so could be affected by errors. Factors are varied one by one and the simulation are repeated with the purpose to understand their behaviour and find the values which produce a frictional mean effective pressure curve as close as possible to the measured ones. The final parameters are reported in the Table 1 and the predicted *fmep* curve is plotted in comparison to the experimental one in the Figure 35.

$a\ [bar]$	$b\ [-]$	$c\ \left[{}^{bar}/_{m/s}\right]$	$d\ \left[{}^{bar}/_{(m/s)^2}\right]$
0.85	**0.005**	**0.03**	**0.001**

Table 1: Friction Mean Effective Pressure parameters

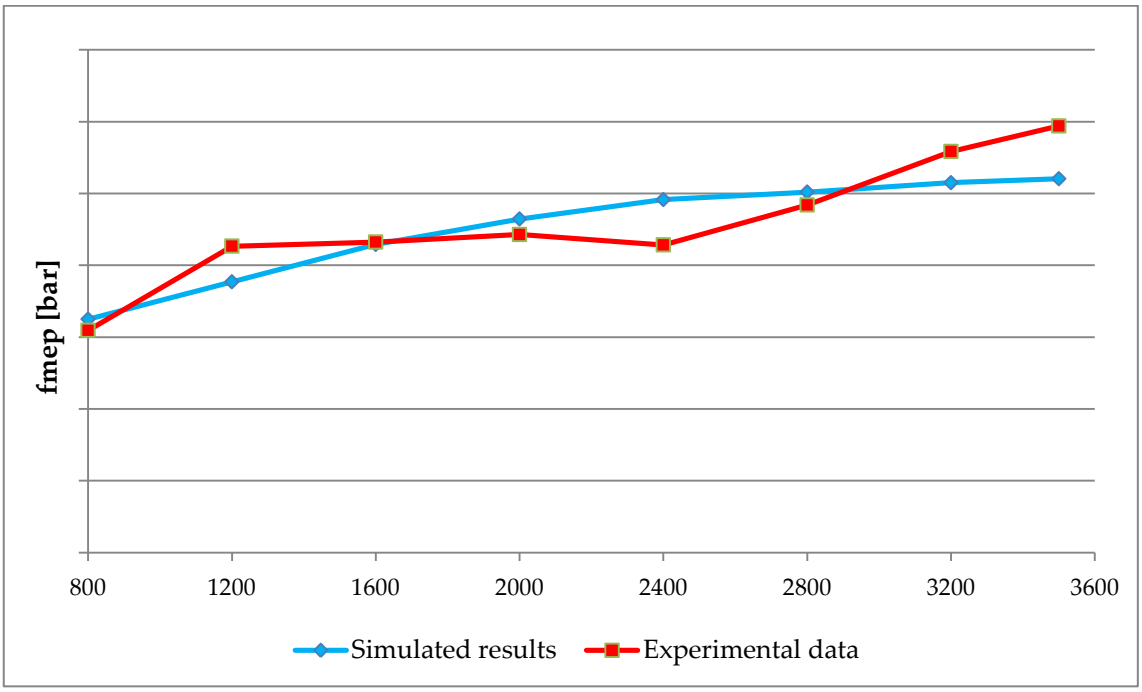

Figure 35: Measured vs Simulated *fmep*

A general good fitting of the experimental curve is achieved, even if at some regimes it would be feasible to make further improvements with the adoption of dedicated Chen-Flynn coefficients.

Now the concept of the volumetric efficiency is introduced to complete the definition of the previous one. It identifies the amount of air trapped in the cylinder per cycle with respect to the maximum theoretical one which can fill the engine displacement at the reference condition. Its definition can be written as in the equation 4.3.

$$\lambda_v = \frac{m_a}{m_t} = \frac{\dot{m}_a \cdot \varepsilon_{cycle}/n}{\rho_a \cdot V} \quad \textbf{4.3}$$

Obviously in case of NA engines this value is usually lower than 1 (0,8 ÷ 1), but with the adoption of the compressor this quantity grows up to enhance performances and improved the combustion process.

Knowing this quantities, the definitions of brake torque (Eq 4.4), brake power (Eq 4.5) and brake specific fuel consumption (Eq 4.6) can be introduced:

$$T_b = bmep \cdot \frac{V}{2\pi \cdot \varepsilon_{cycle}} \quad \textbf{4.4}$$

$$P_b = bmep \cdot \frac{V \cdot n}{\varepsilon_{cycle}} \quad \textbf{4.5}$$

Where:

- V is the total engine displacement
- n is the engine rotational speed
- ε_{cycle} is the number of crankshaft revolution for each power cycle. In our case (four-stroke engine) is equal to 2, while with a two-stroke engine is 1.

The engine under examination is intended to light-duty vehicles, due to their total displacement and structural characteristics, and so an excellent value of brake torque is required at low regimes yet, to enhance the drivability features. In fact, these types of vehicles work at low engine speeds for the main part of their life. On the other hand, the achievement of elevated levels of power at high revolution speed is not necessary, because it would lead to have greater stresses on the engine structure without a significant improvement of the drivability. This aspect would be interesting in case of sporting cars and not for light-duty vehicles as in our case. In the Figure 36 and Figure 37 are plotted the values of brake torque and brake power obtained from the numerical simulations, in comparison to the experimental ones.

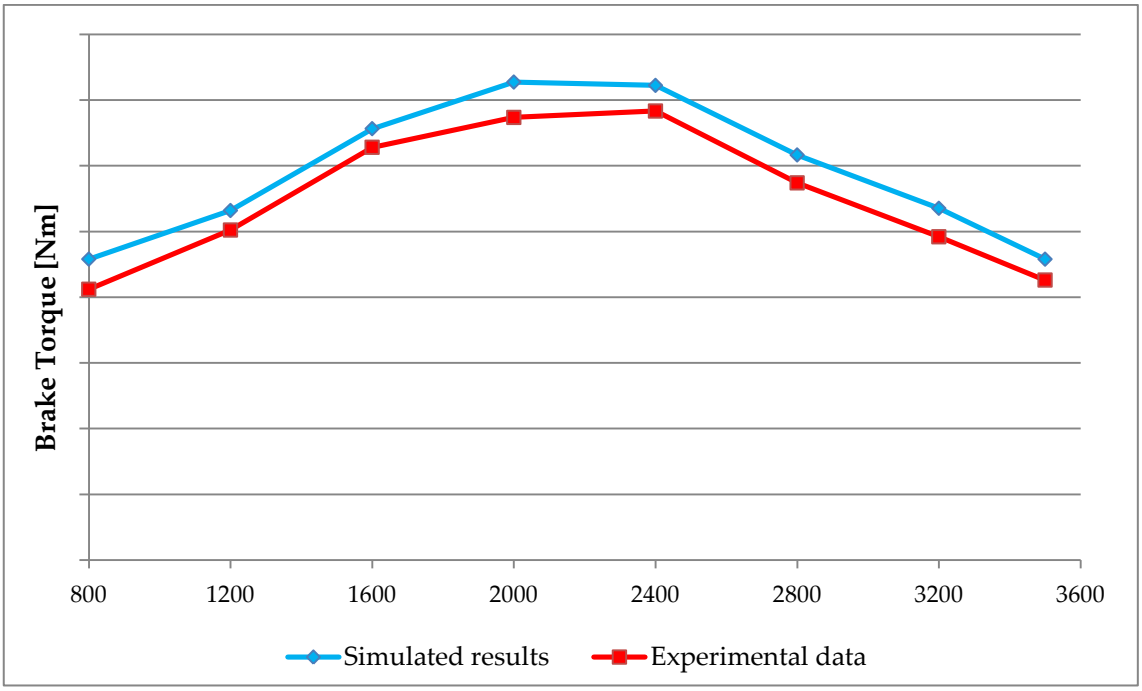

Figure 36: Measured vs Simulated Brake Torque

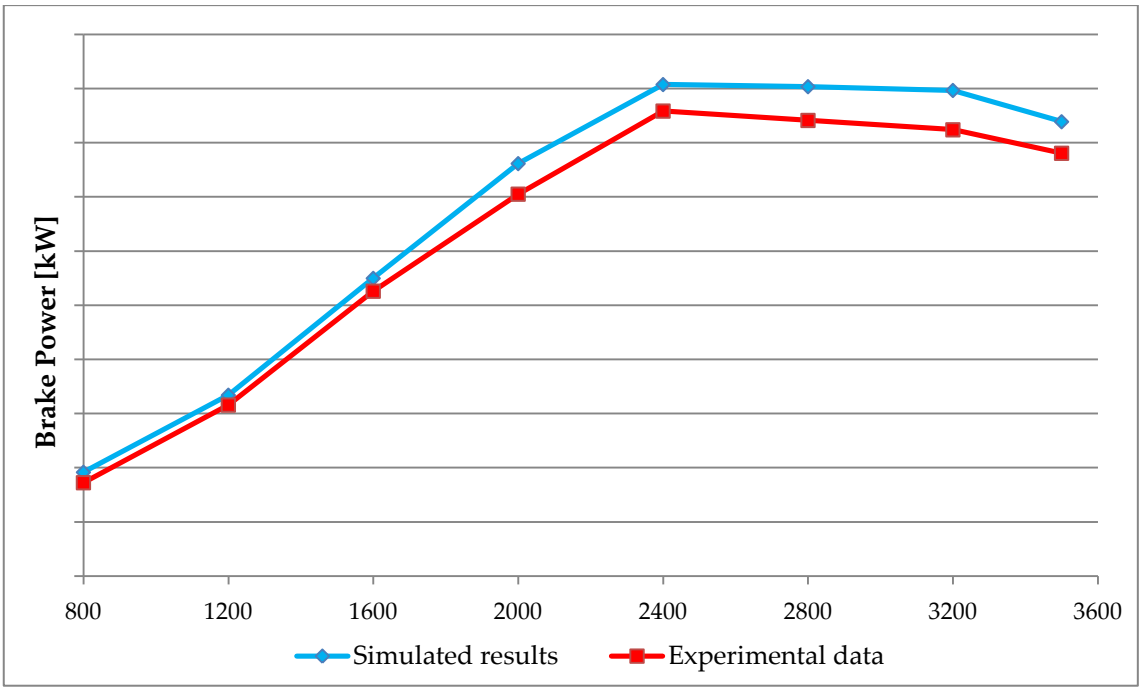

Figure 37: Measured vs Simulated Brake Power

A constant difference, in the order of about 4 ÷ 5%, between simulated and measured values is highlighted in the whole engine map. Among the potential causes there is the possible errors in the combustion process. With a different combustion parameters, the energy generated during the expansion stroke can be significantly different with

respect to the real one and it influences all the performances. It can be occurs also with a little variation into the cylinder pressure curves which ha already achieved a very good accuracy level.

Another important parameter is the BSFC (Brake Specific Fuel Consumption). It is a sort of efficiency, because it measures the quantity of fuel necessary to produce a certain amount of energy and so how efficiently the chemical energy contained in the fuel is transformed into work. It can be defined with the equation 4.6.

$$BSCF\ \left[{}^{g}/_{MJ}\right] = \frac{\dot{m}_f}{P_b} \qquad \textbf{4.6}$$

It is plotted with respect to the engine speed (at fixed load) and compared to the experimental data in the Figure 38.

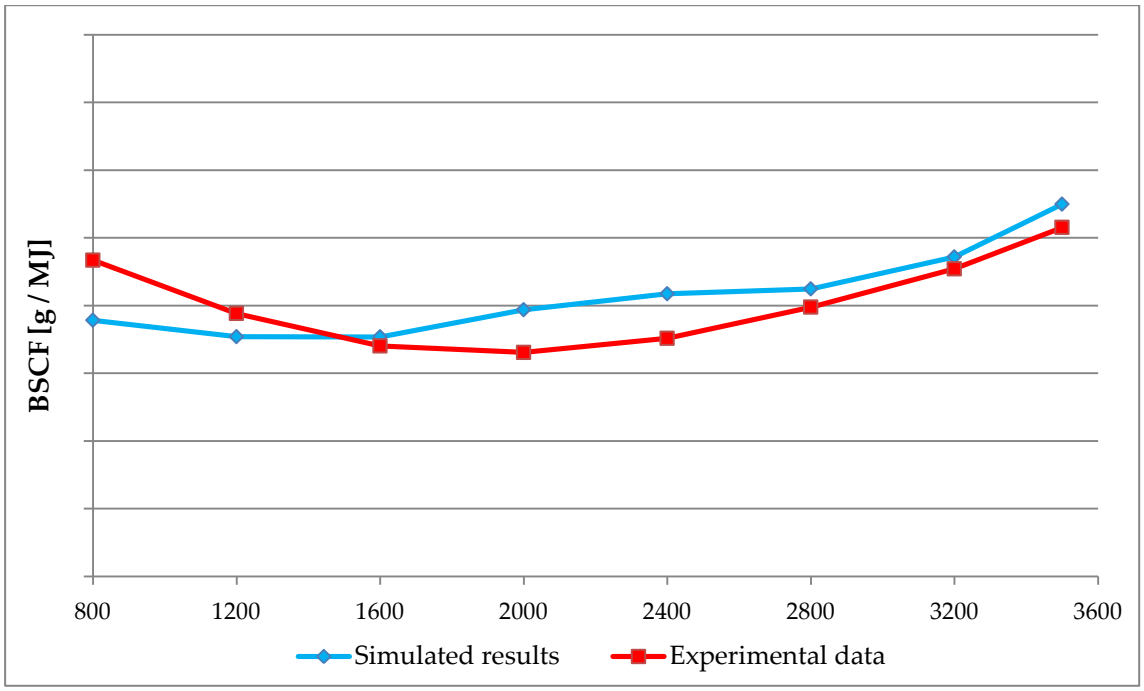

Figure 38: Measured vs Simulated BSFC

Looking the curves, it is possible to note that at high revs the gap is almost constant, but at low speeds the situation changes. This means that in certain conditions the simulated combustion process is more efficient than the real one and a more amount of energy is generated. On the other hand, in other operating points the opposite situation occurs.

As we can see, for low engine speeds specific fuel consumption increase, since thermal losses become more important, due to the proportionality with the resident time into

the combustion chamber, and combustion less stable. For higher rotational speeds the BSCF rises mainly in relation to higher friction losses, proportional to the piston speed.

Another coefficient adopted to evaluate the overall goodness of the engine design is the total efficiency. It considers all the losses generated during a complete cycle listed below:

- Mechanical and frictional losses due to the movement and creeping of the mechanical parts.
- Thermal losses through the engine structure and related to the water jacket cooling effect necessary for strength reasons.
- Energy loss due to non-perfect combustion process.
- Other minor losses.

The total efficiency is defined as the ratio between the mechanical power available at the engine shaft and the chemical energy contained into the fuel mass flow rate. So, it represents the overall system quality.

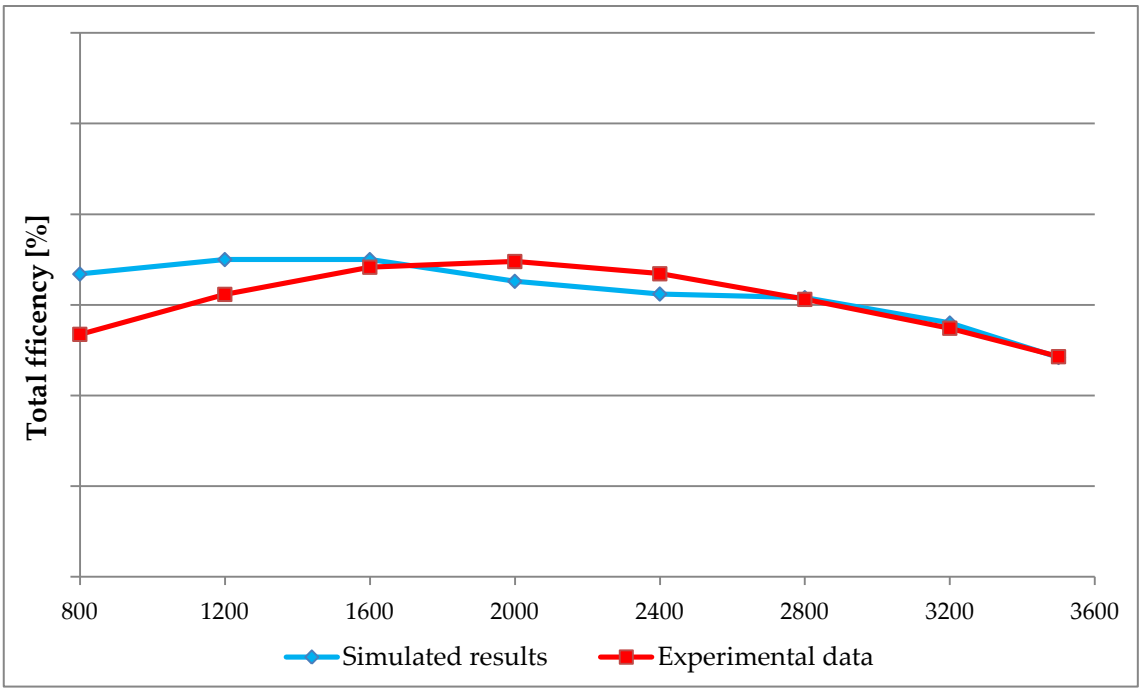

Figure 39: Measured vs Simulated engine total efficiency

Looking the simulated results in relation to the measured ones, it is possible to note that there is a good concordance, except for low regimes. It could be caused by a numerical error in the turbocharger calculation procedure, in fact, as explained in the following dedicated chapter (4.3.4), the simulated turbocharger shaft doesn't work at

the same rotational speed of the real one and in a situation there is also an issue in the mass conservation astride the compressor.

4.3.2 Cylinder pressure

The cylinder pressure is an important variable, because it is affected by many other parameters. The simulated values have to be considered during all the 4 periods of the power cycle (720 CAD), because in the expansion stroke the power is produced, but in the others three an energy consumption occurs. The first key parameter to understand the combustion model goodness and the accuracy is the pressure peak value and its behaviour can be observed in the Figure 40.

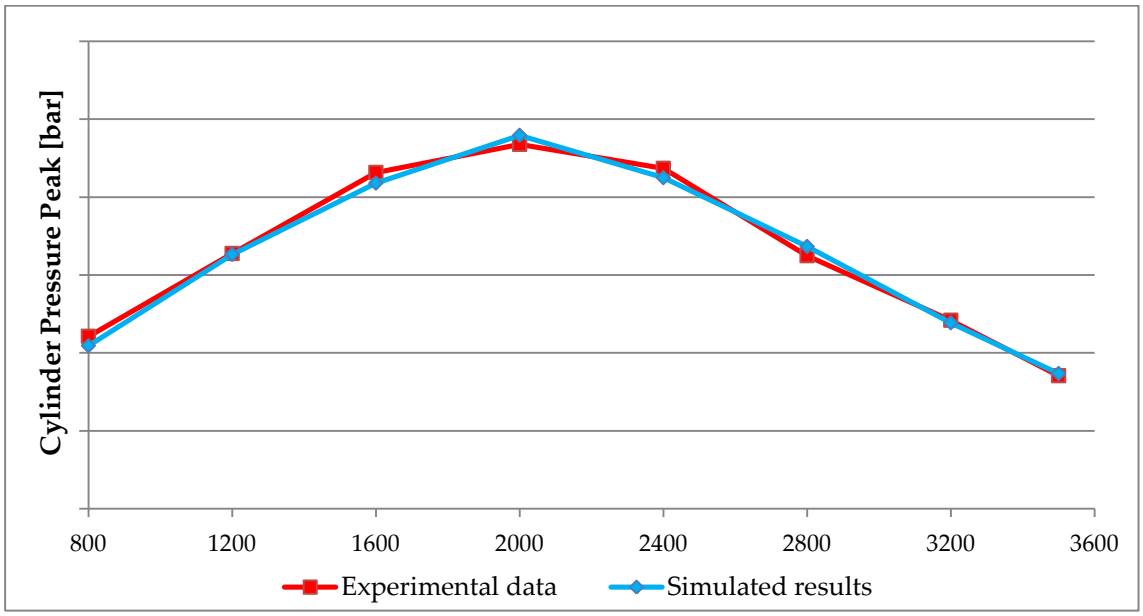

Figure 40: Measured vs Simulated Cylinder Pressure Peak

It is fundamental to check not only the pressure peak value, but also its position because a little delay or advance generates a significant change on the moment arm and so also on the torque generated. This can be easily calculated with a geometric analysis on the engine structure and in particular on that part which constitute the network between piston and crankshaft. Considering a uniform pressure field into the combustion chamber the forces generated and transmitted perpendicularly at the crankshaft is almost constant, but the arm strongly changes and so also the torque. There is an optimal angle which generates the maximum moment arm and the aim is to synchronize it with the pressure peak. Each engine has a proper optimal piston

position because it depends on the inner geometric measures of rod. So, if the simulated values are closed to the measured ones means that there is a global good approximation of the real combustion process, and it is a key target in order to validate all the others model parameters.

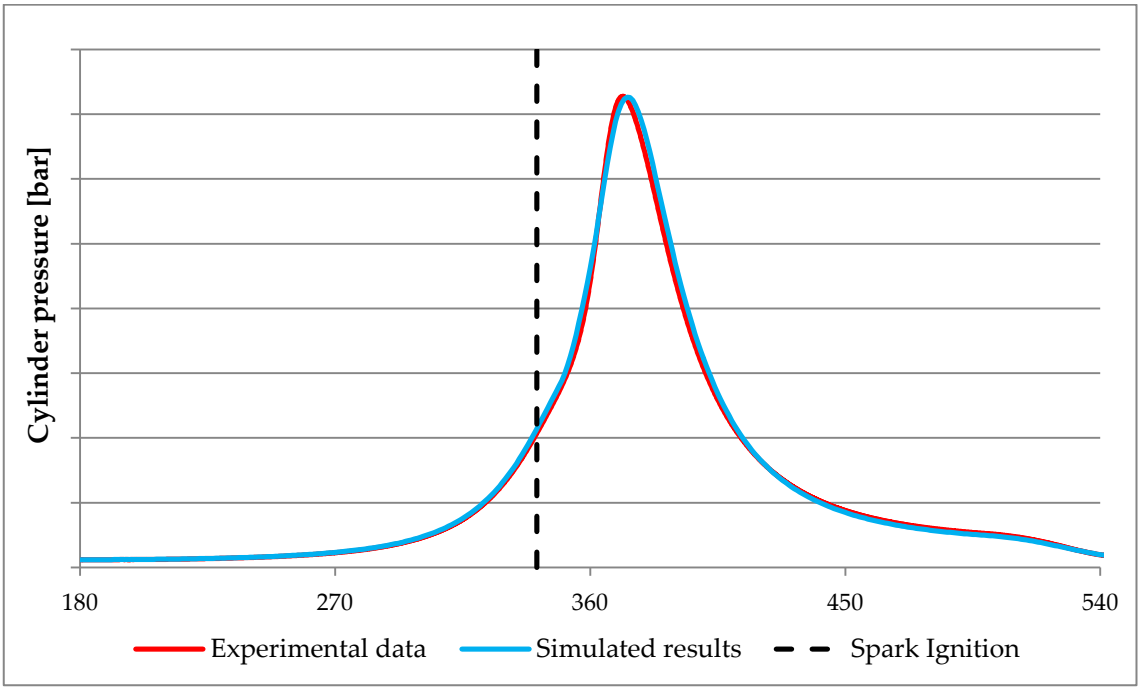

Figure 41: Measured vs Simulated Cylinder pressure at 1200 rpm

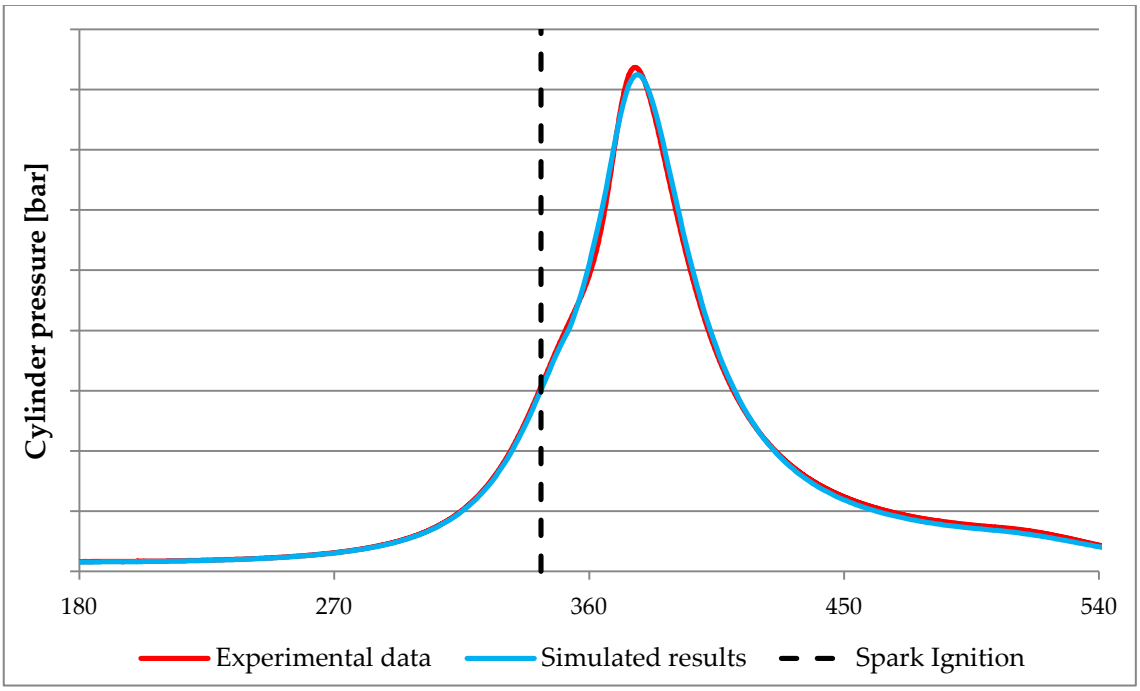

Figure 42: Measured vs Simulated Cylinder pressure at 2400 rpm

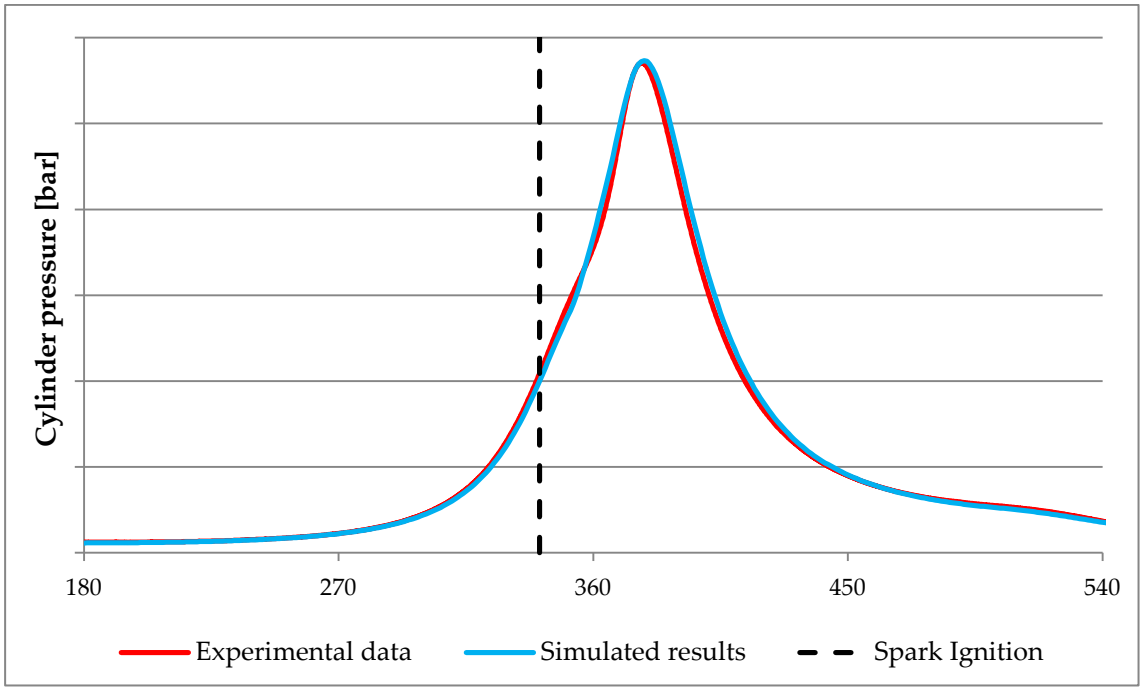

Figure 43: Measured vs Simulated Cylinder pressure at 3500 rpm

Observing the cylinder pressure curves plotted in the Figure 41, Figure 42 and Figure 43 it is possible to note that the combustion model works in a quite good way and sometimes it is also difficult to distinguish the measured and simulated data, even if further improvements could be achieved. The pressure peak value is reached at each engine regime, but a slight delay of about 3 ÷ 4 crank angle degrees is always present. It has to be allocated to the non-precise combustion parameters which are chosen with trial and error procedure starting from a reference combination.

The distance, in terms of crank angle degrees, between the ignition of the fresh charge and the combustion start, highlighted by a visible slope change in the pressure curve, is due to initial flame propagation (also improperly called the ignition delay). It depends on the physical and chemical properties of the combustible mixture. This period begins with the spark ignition impulse and ends at the point in which a clear slope change, due to the combustion, is visible in the pressure curve. This first phase has a different duration at different regimes, in terms of CAD, in relation to a slower or faster piston speed.

During the non-powering strokes the cylinder pressure behaviour has to be checked and a comparison with the measured data is represented in the Figure 44, Figure 45 and Figure 46. A quite good trend can be observed for the intake period at low regimes in which the average pressure level is reached even if some oscillations is always present. At higher engine velocities the difference increases, but the overall predicted

pressure trend doesn't change significantly and remain similar to the experimental one. On the other hand, in the exhaust one a significant difference is present, and it could be caused by an underestimation of the pressure losses in the exhaust manifold or by an inaccurate simulation of the valve opening timing.

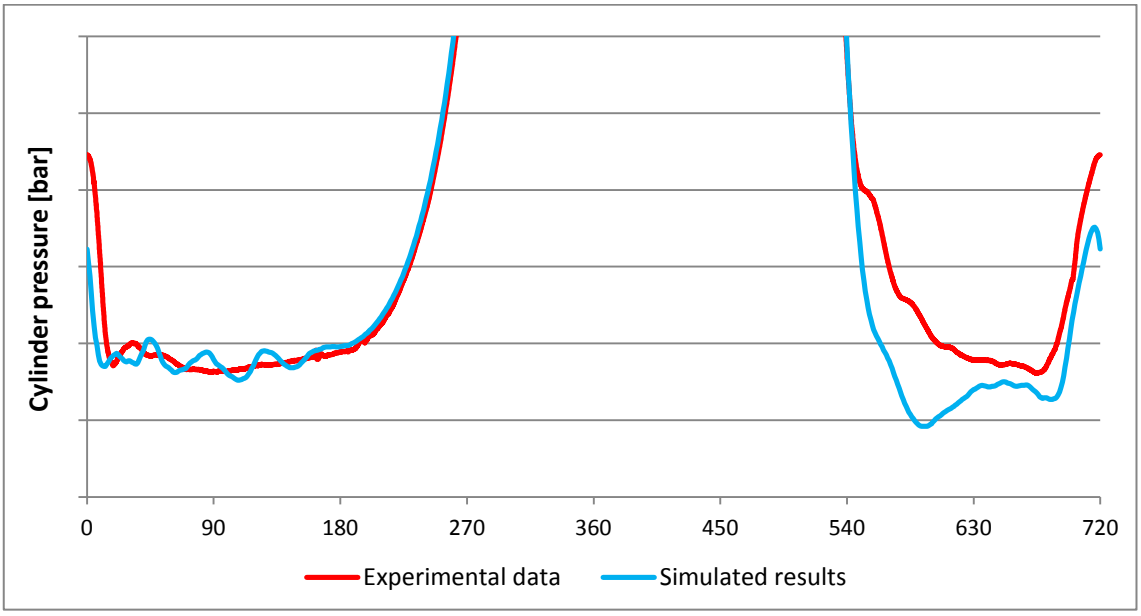

Figure 44: Measured and simulated cylinder pressure during the gas exchange process at 1200 rpm

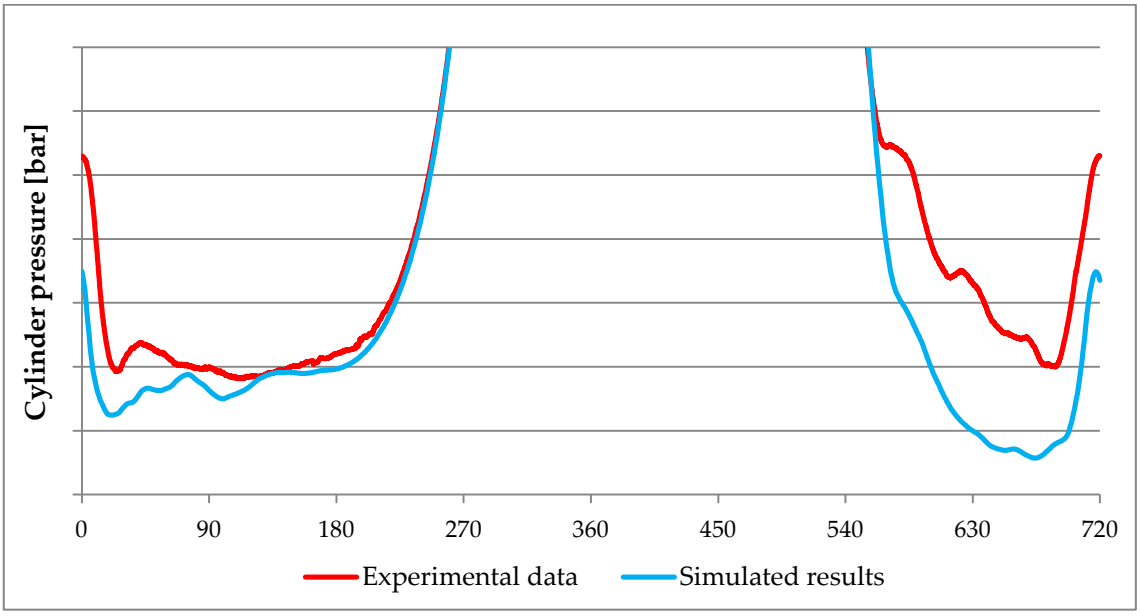

Figure 45: Measured vs Simulated Cylinder pressure during the gas exchange process at 2000 rpm

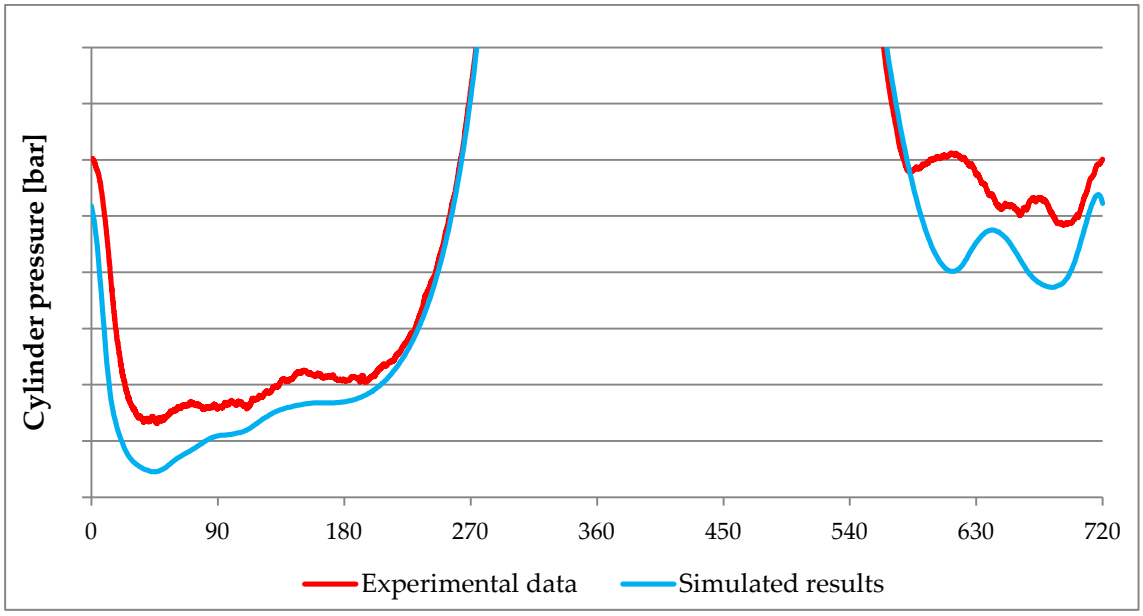

Figure 46: Measured vs Simulated Cylinder pressure during the gas exchange process at 3500 rpm

Looking at these graphs, which give us a complete analysis on the cylinder pressure through the whole cycle, it is possible to separate the compression, combustion and expansion strokes from the gas exchange period. The first group is characterized by a almost perfect prediction of the measured data, but when the valves open some problems comes out.

4.3.3 Injection check

In the Gasdyn code the injected mass of fuel is automatically regulated to reach the imposed A/F ratio as target. A mass balance on the injection region is made, to evaluate the amount of fuel injected, in each cylinder, in comparison to the imposed initial value and check how far the target it is.

The breathed air mass flow rate is a value which has to be kept under control, to be safe that the model represents, as much as possible, the real engine operating conditions. With a wrong amount of air, it would be quite difficult that the other parameters result right. This quantity is obviously regulated by the compressor boost pressure, but also by the pressure losses to which the air is subjected through the intake path. During the definition of the ducts geometry all the friction coefficients are required as Gasdyn input, but no available data are present and so they are estimated to reach fixed pressure levels at some reference points of the intake route. Measured values are referred to the regions closed to the compressor, intercooler and into the intake manifold. In the following graphs a comparison between measured and

simulated values is reported and a good fitting can be appreciated. Little discrepancies are present due to the finite number of the iteration cycles and due to a non-perfect estimation of the friction coefficients.

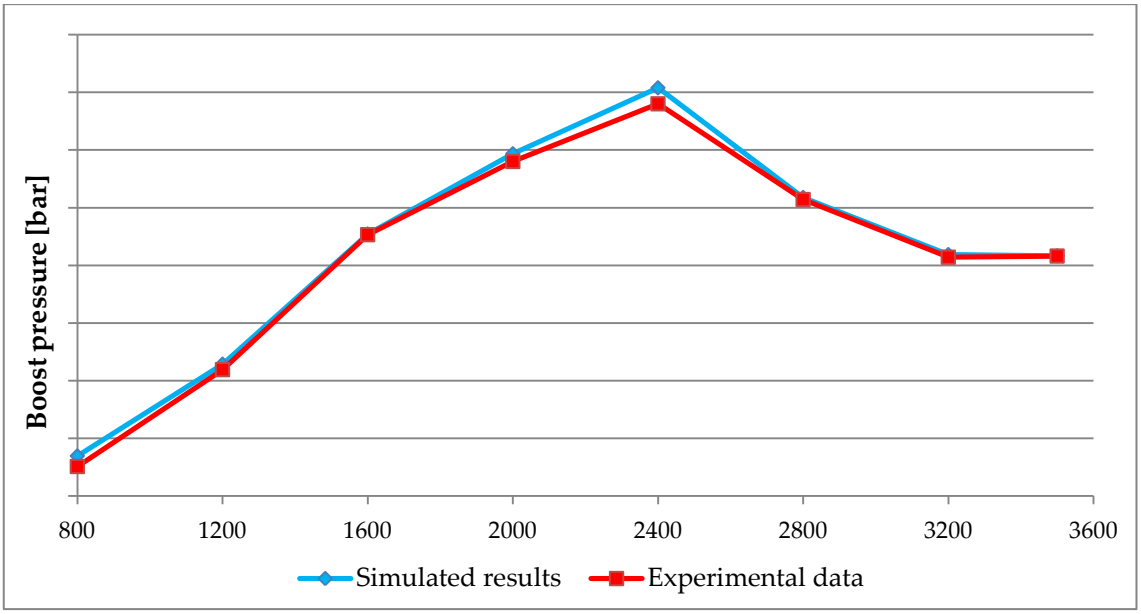

Figure 47: Target vs Reached Boost pressure

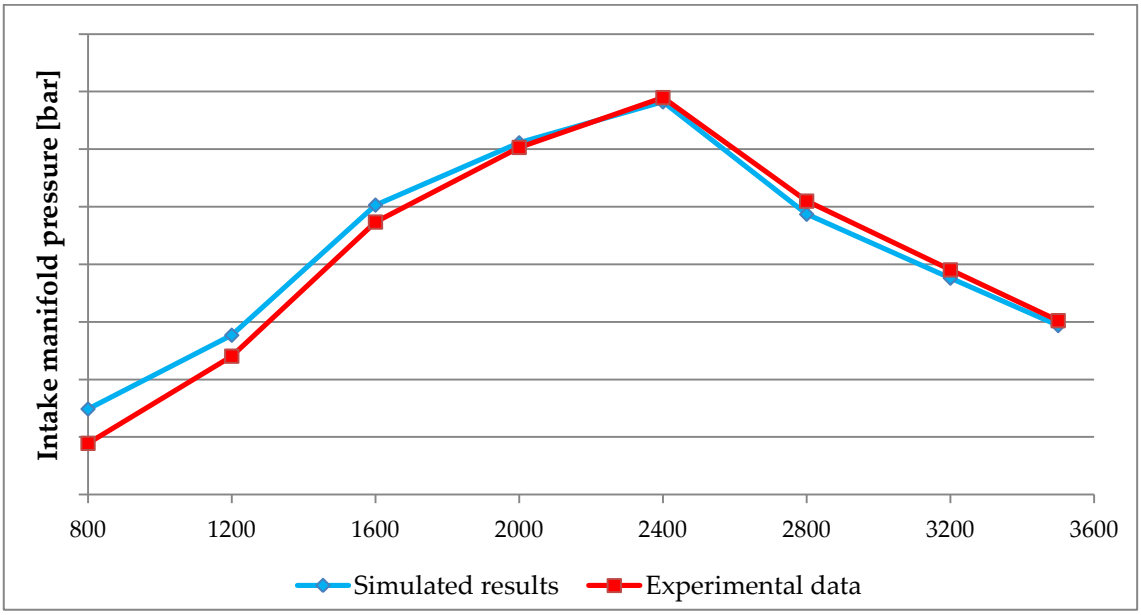

Figure 48: Measured vs Simulated pressure in the Intake manifold

Now that the pressure losses are calibrated with the real ones, it is possible to check the breathed air mass flow rate plotted in the Figure 49.

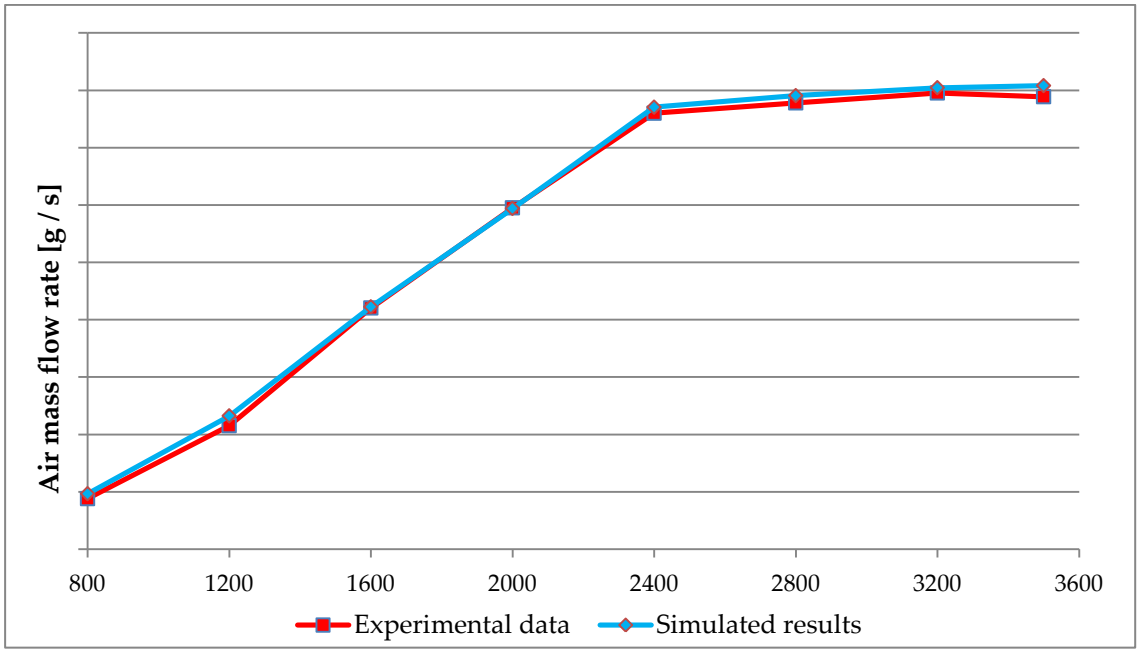

Figure 49: Measured vs Simulated Breathed air Mass flow rate

A little overestimation is presents both at 1200 rpm and this could be reconnected to a wrong turbocharger behaviour and also at the faster regimes. In this zone the curves trends are quite similar with a difference fixed around the 2% and this is a good sign because it means that the simulation error is equally distributed over the engine operating speed range and so could be also predicted and eliminated.

On the other hand, looking the fuel injected mass flow rate in the Figure 50 it is possible to say that good results are reached in the whole engine speed range.

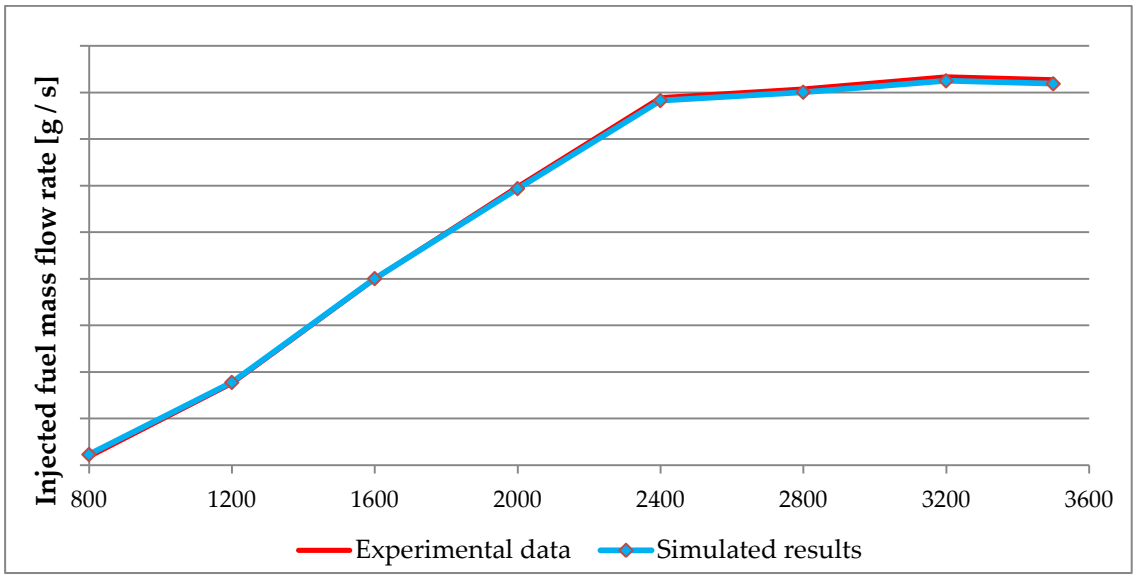

Figure 50: Measured vs Simulated Injected fuel mass flow rate

In conclusion we plot the calculated A/F ratio based on the simulated quantities of air and fuel flowing in the system in the Figure 51. At the beginning each cylinder has studied singularly with a control volume which contain 2 inlet pipes (one for the air and the other for the fuel) and 2 exhaust pipes.

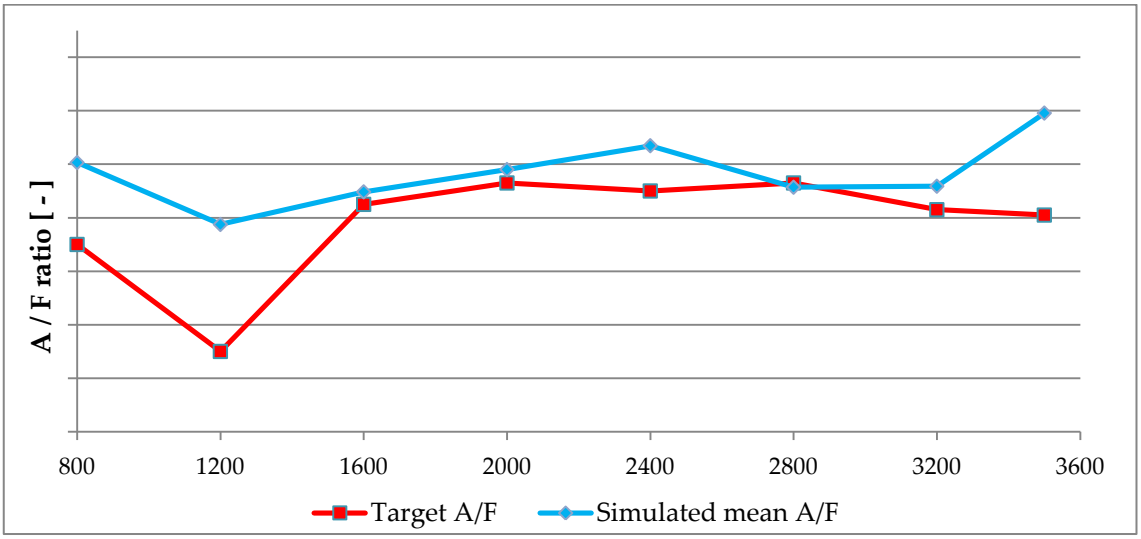

Figure 51: Target vs Simulated Mean A/F ratio

It is possible to note that in this case there is a general overestimation and this, according to me, is a problem which can be generated only by the numerical code because both the breathed air and the injected fuel coincide with the experimental data. It could be cause by a failure of the mass conservation equation in some critical points.

4.3.4 Turbocharger convergence criteria and shaft velocity

To obtain a good prediction of the engine operating parameters is fundamental to achieve the target boost pressure, but also the final turbocharger shaft speed is a key parameter which allow to understand if the turbine and compressor work as in the real condition. At the beginning, a first attempt velocity is chosen and during the simulation it is gradually changed by the software to obtain the target boost pressure searching a condition in which the shaft is balanced with the wastegate valve assistance.

After each simulation is strongly recommended to check if the turbocharger has reached the convergence condition with the chosen number of iterative cycle. If it doesn't occur means that the shaft is still changing velocity (speeding up or slowing down) and so also the boost pressure is not a stable value and obviously it will be different from the target one. Also the wastegate valve opening percentage will be wrong. So, if it happens a higher number of iterative cycle is needed.

In theFigure 52, Figure 53 and Figure 54 are represented the convergence Gasdyn output screenshots of the turbocharger referred to 3 reference regimes.

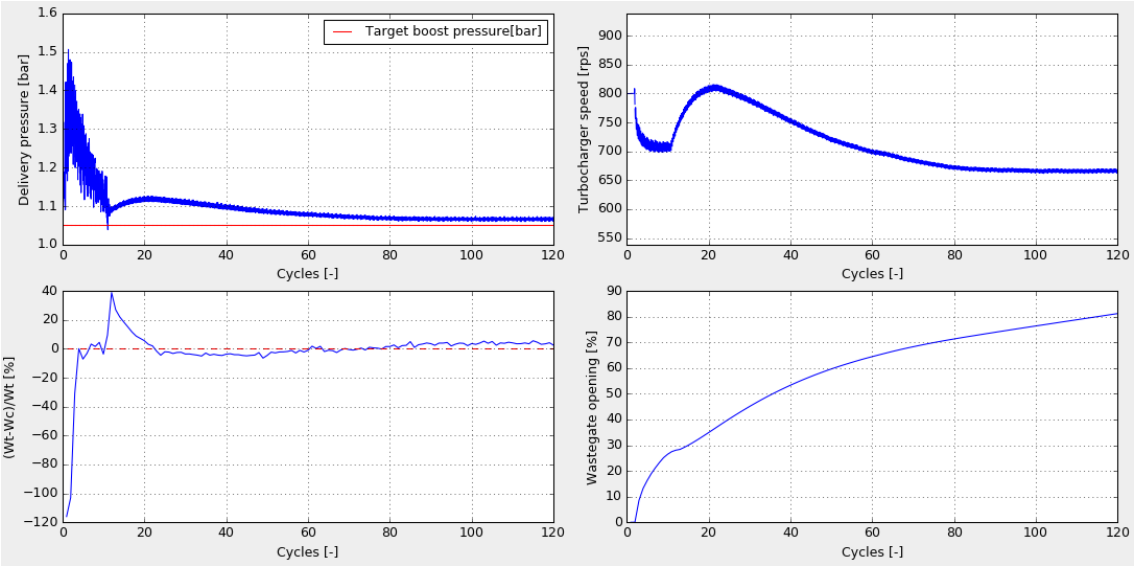

Figure 52: Convergence Gasdyn output screenshot at 800 rpm

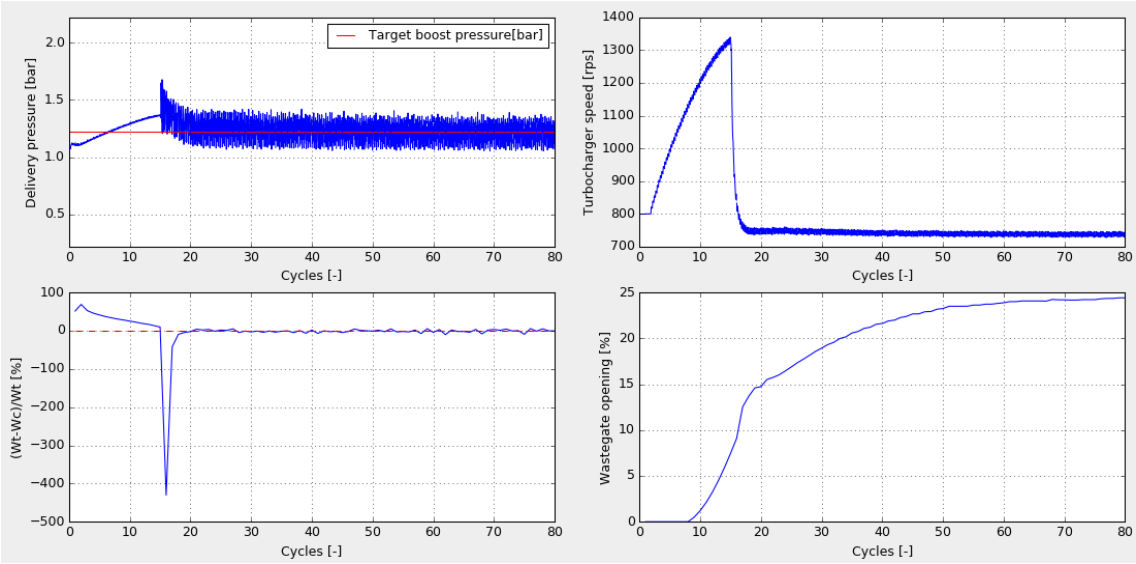

Figure 53: Convergence Gasdyn output screenshot at 1200 rpm

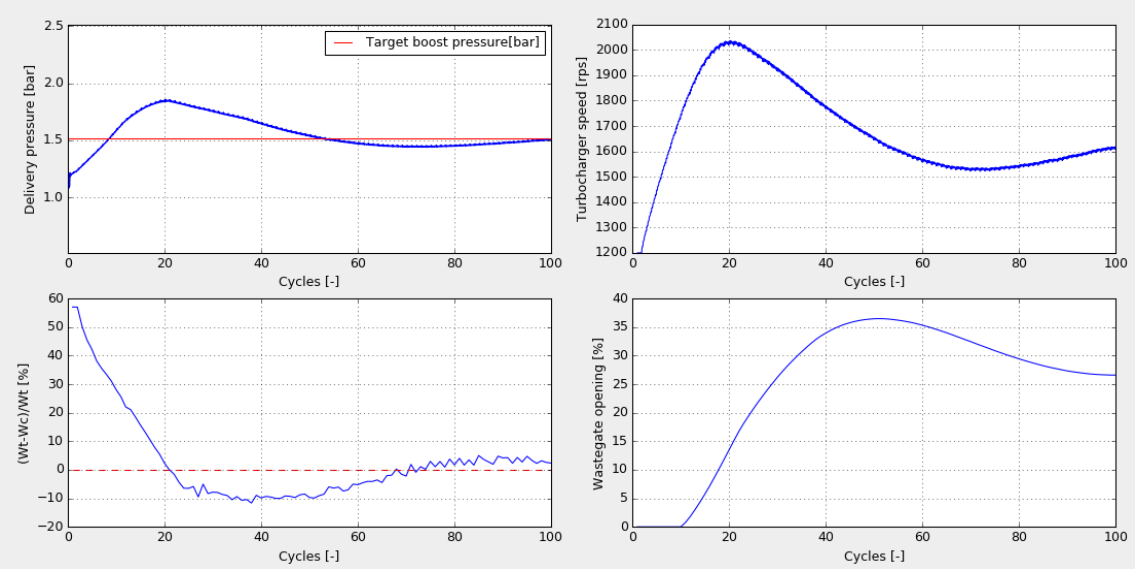

Figure 54: Convergence Gasdyn output screenshot at 2800 rpm

At low regimes some problems coming out due to some numerical problems in the computational code. At 800 rpm the compressor is not able to reach the boost pressure which has a too low value. Even if the wastegate valve is almost fully opened the shaft remain too fast. At this regime the new compressor curve has been used obtaining reasonable results. With the old non-extended compressor map we would have some numerical and mass conservation problems as at the previous regime.

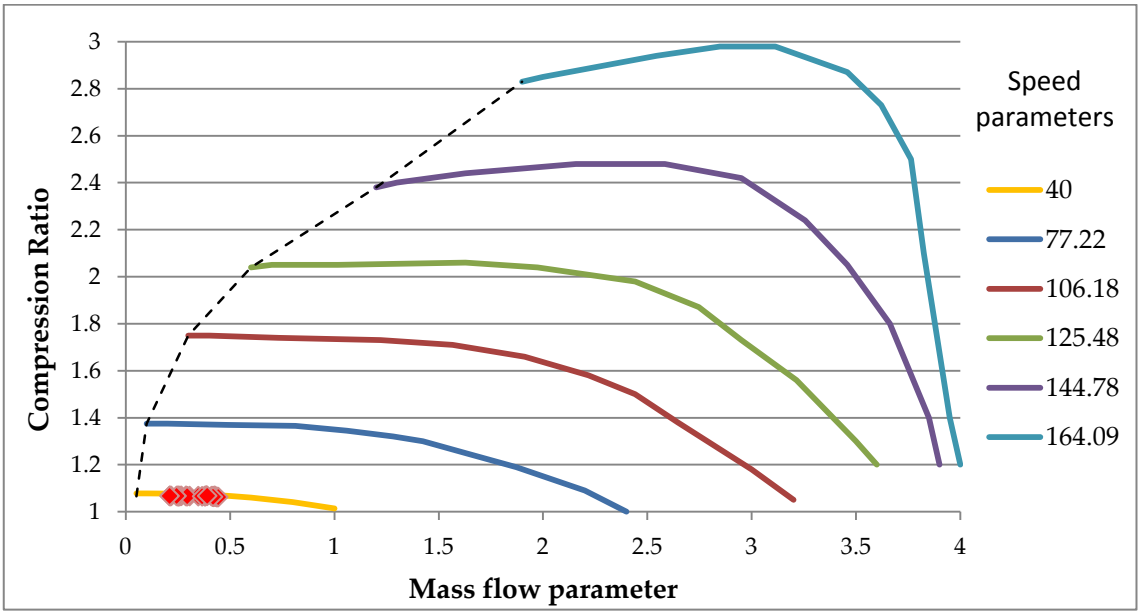

Figure 55: Compressor operating point at 800 rpm

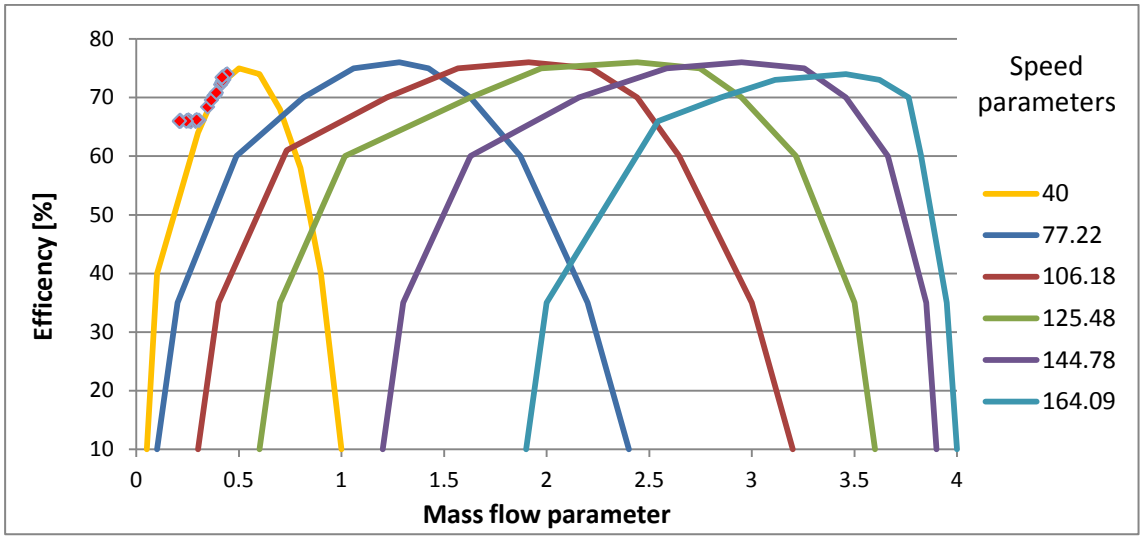

Figure 56: Compressor efficiency operating point at 800 rpm

For higher regimes there is no problems and the compressor goes to works in the map zone in which the curves are defined by the manufacturer and so with the certainty to use a right values. In the are plotted the operating points of a reference regimes which summarize the behaviour of all the others above 1600 rpm

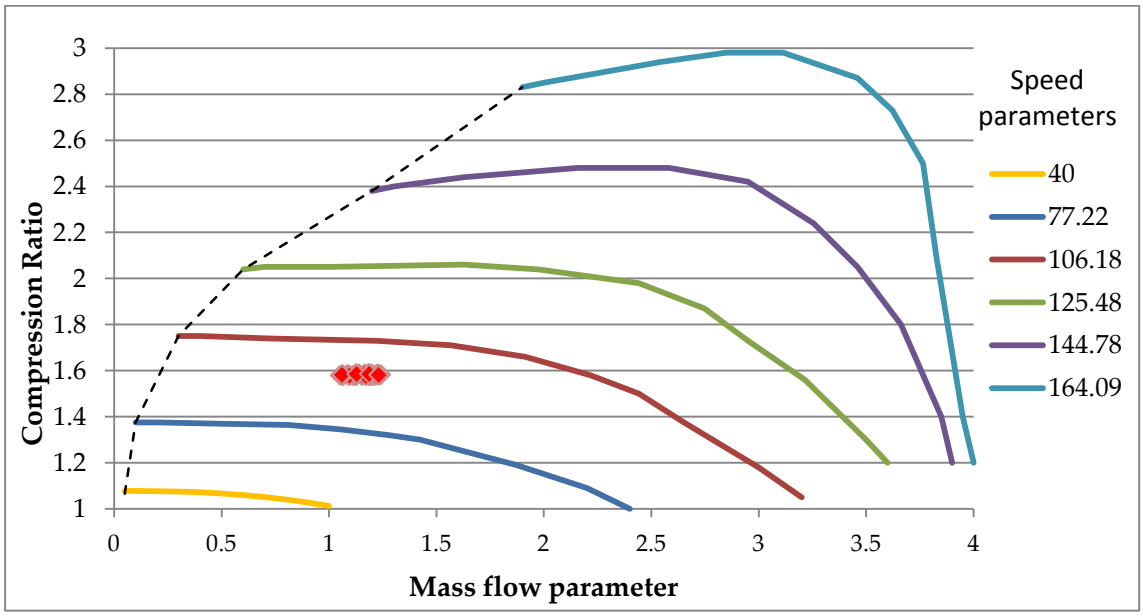

Figure 57: Compressor operating points at 2000 rpm

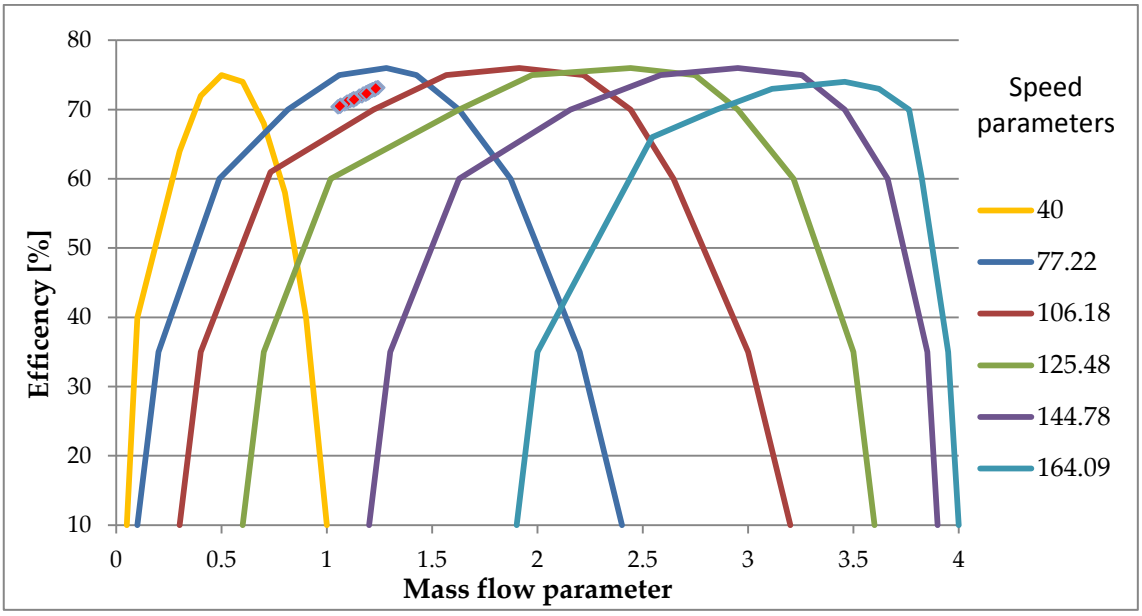

Figure 58: Compressor efficiency operating points at 2000 rpm

On the other hand, the turbine works well in the whole engine speed range. In the Figure 59 and Figure 60 are reported the operating points on the turbine maps referred to the lowest and highest regimes.

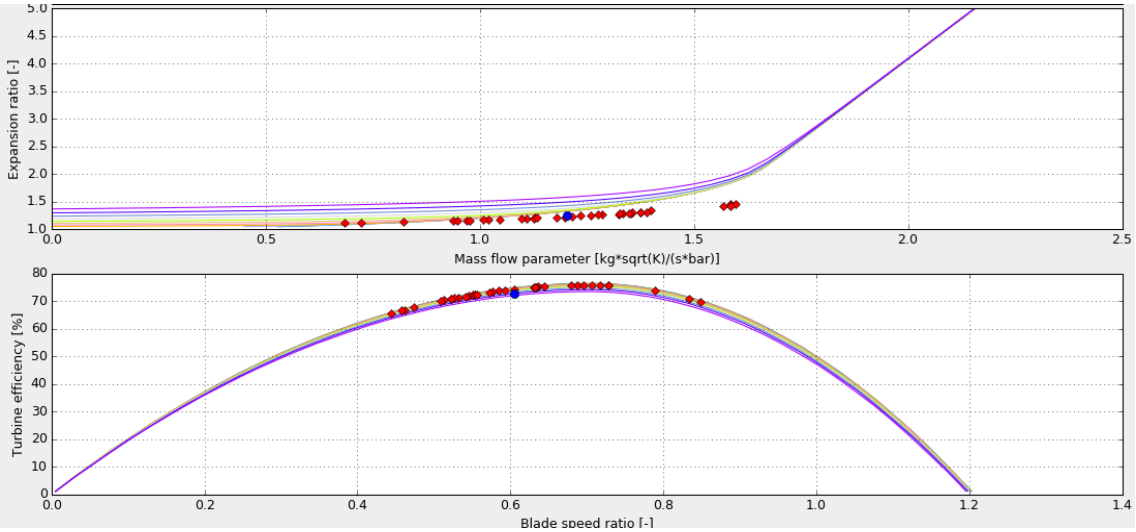

Figure 59: Turbine operating points on the characteristic curve at 3500 rpm

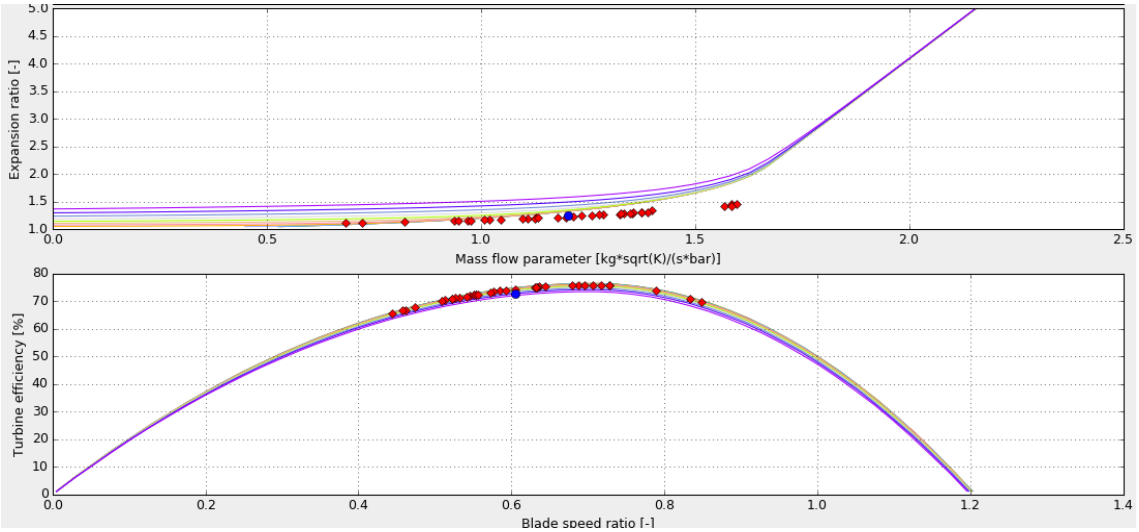

Figure 60: Turbine operating points on the characteristic curve at 3500 rpm

Concluding the turbocharger analysis is reasonable to check if the target boost pressure has been reached and if the predicted shaft velocity coincides with the measured value. The first one has already been studied previously in the sub-chapter 4.3.3, during the air mass flow analysis in relation to the pressure drops into the intake manifold. Anyway, it has been reached at each engine regimes, except for the lowest ones, and it is plotted it the Figure 47. Regarding the second check argument the situation is the same and the comparison between the simulated and measured turbocharger rotating speed is represented in the Figure 61.

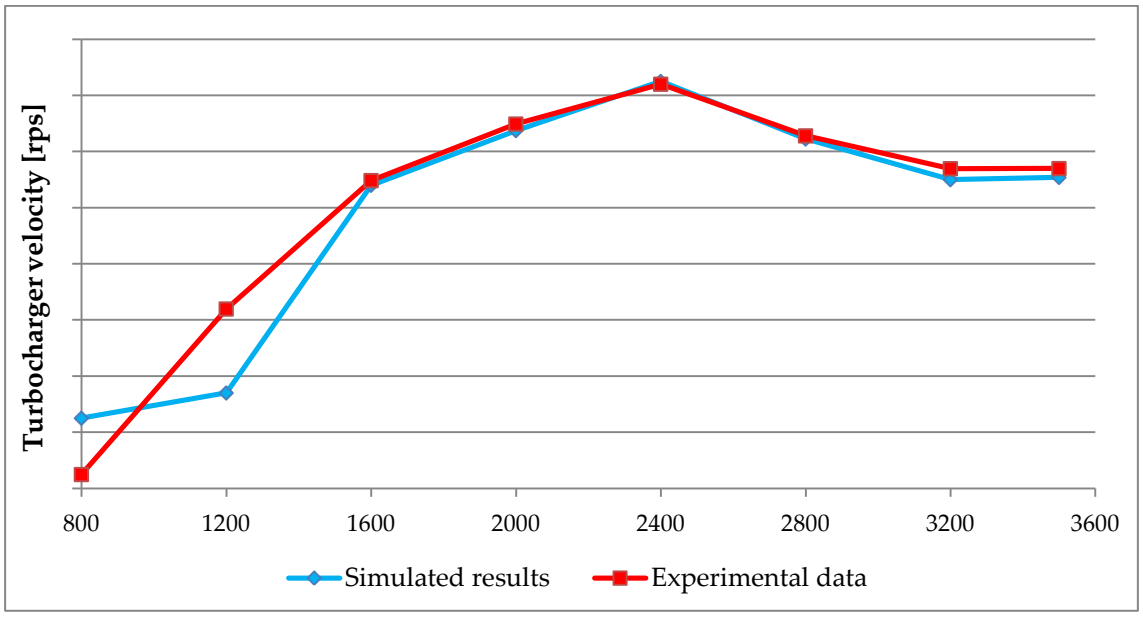

Figure 61: Measured vs Simulated Turbocharger shaft velocity

4.3.5 Intake pressure waves

The analysis of the instantaneous pressure in strategic places is a key part of the study of the waves effect, which strongly affect the amount of fresh charge and exhaust gases treated by each cylinder in a cycle. The purpose is to obtain a positive mass flow also at those crank angle degrees characterized by an opposite relative moving direction between gas flow and piston. For example, regarding the intake manifold, exploiting a positive pressure peak at the intake port, closed to the BDC, it is possible to keep the valves opened for some degrees, even during the compression stroke with a positive air mass flow rate and obtaining in this way a greater volumetric efficiency values. As consequence a lot of other parameters as torque, power, *bmep* and so on, are improved.

To well understand the nature of this phenomenon is fundamental to know how it works. When the intake valve open and piston goes down a pressure decrease occurs and a rarefaction wave is generated. It travels backward into the ducts up to when it finds a volume big enough which behaves like an open-end boundary condition and so characterized by a constant pressure level. At this point the rarefaction waves is converted into a pressure one and returns towards the intake ports. The aim is to find the right pipes lengths which allow to synchronise the positive pressure peak with the BDC in order to postpone the IVC.

This effect is obviously strongly related to the intake manifold geometry, because depends on the route which the pressure waves has to cover but depends also on other factors. A key aspect is the temperature of the gases in the ducts which define the moving velocity of the waves. The speed of sound in the intake manifold is usually around 340 ÷ 350 m/s, but some variations could occur in relation also to the intercooler discharge temperature.

So, from that has been said, a precise and deep analysis of the pressure level into the intake manifold with respect to the crank angle is a key point. At each regime a different situation take place, but we have decided to plot in the Figure 62 and Figure 63 those with the more significant trends.

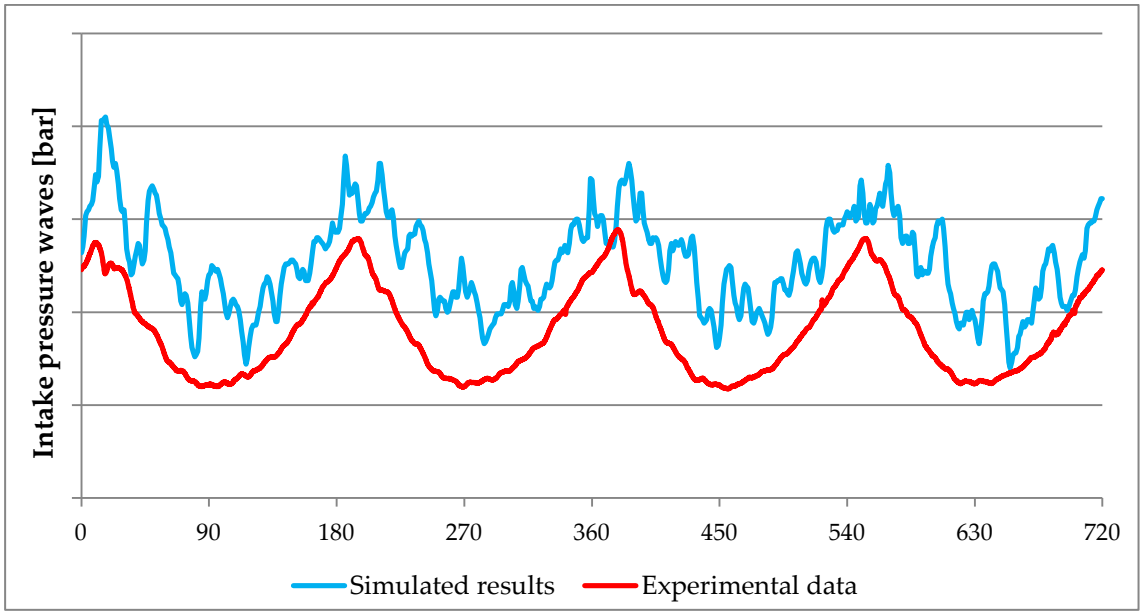

Figure 62: Measured vs Simulated pressure wave into intake manifold at 1200 rpm

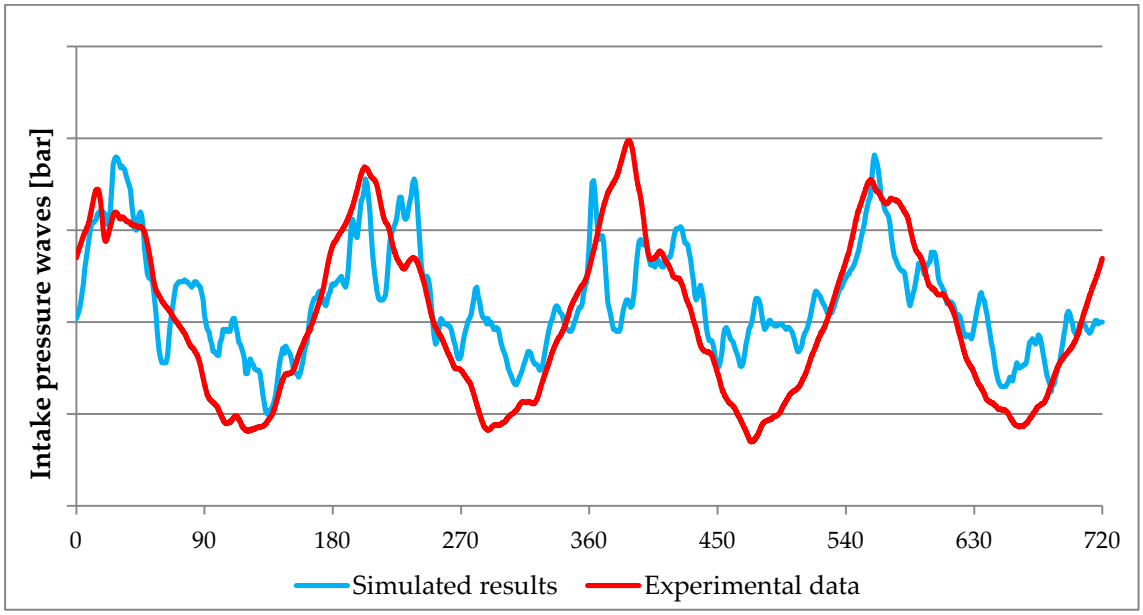

Figure 63: Measured vs Simulated pressure wave into intake manifold at 2000 rpm

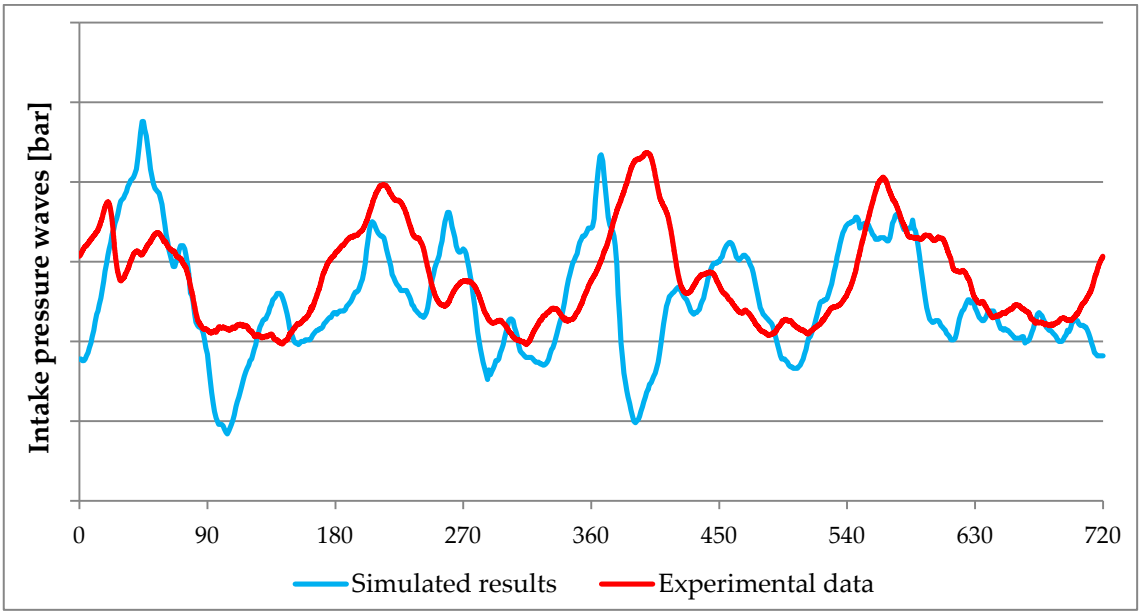

Figure 64: Measured vs Simulated pressure wave into intake manifold at 3200 rpm

The simulated pressure signals are much more disturbed and jagged with respect to the measured ones. The mean level is reached almost in the whole engine speed range, except for the lowest regimes, and it means a good turbocharger functioning and a correct prediction of the pressure drop through the intake manifold. Anyway, it is possible to find a certain similitude into the plotted waves between the measured and simulated results, in particular way in the left part of the graphs in which the pressure signal is directly affected by the intake stroke. The causes of these differences on the instantaneous value, according to me, could be searched in the numerical models which regulates the calculation of the pressure after a certain loss.

Anyway, looking the measured pressure trend, is possible to note the extreme cleaning of the pressure signal and so the use of a smoothing algorithm which eliminates oscillations cannot be excluded.

4.3.6 Exhaust pressure waves

In the exhaust manifold a quite similar phenomenon to the intake one take place and so the pressure waves analysis in a strategic point is recommended. With respect to the previous situation the exhaust gases are characterized by a much higher temperature and so, as consequence, the speed of sound is almost doubled (600 ÷ 700 m/s). A comparison of the predicted pressure values with the measured ones can be appreciated in the Figure 65, Figure 66 and Figure 67. The pressure waves at various regimes is characterized by a quite similar trend and so only 3 reference regimes results are plotted to avoid repetitions and to reduce the space.

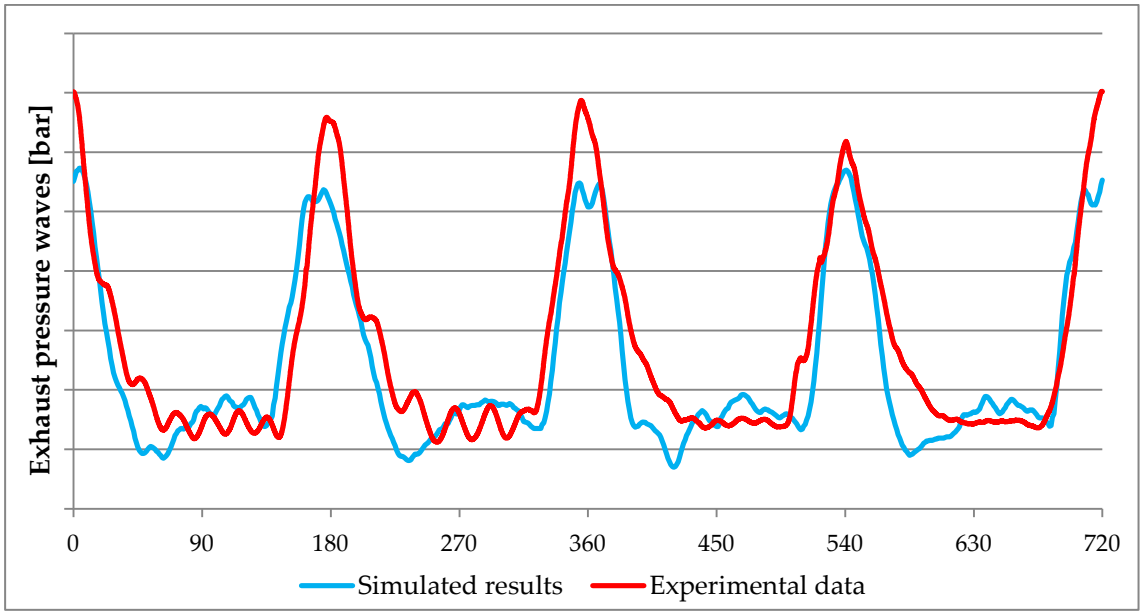

Figure 65: Measured vs Simulated pressure wave into exhaust manifold at 1200 rpm

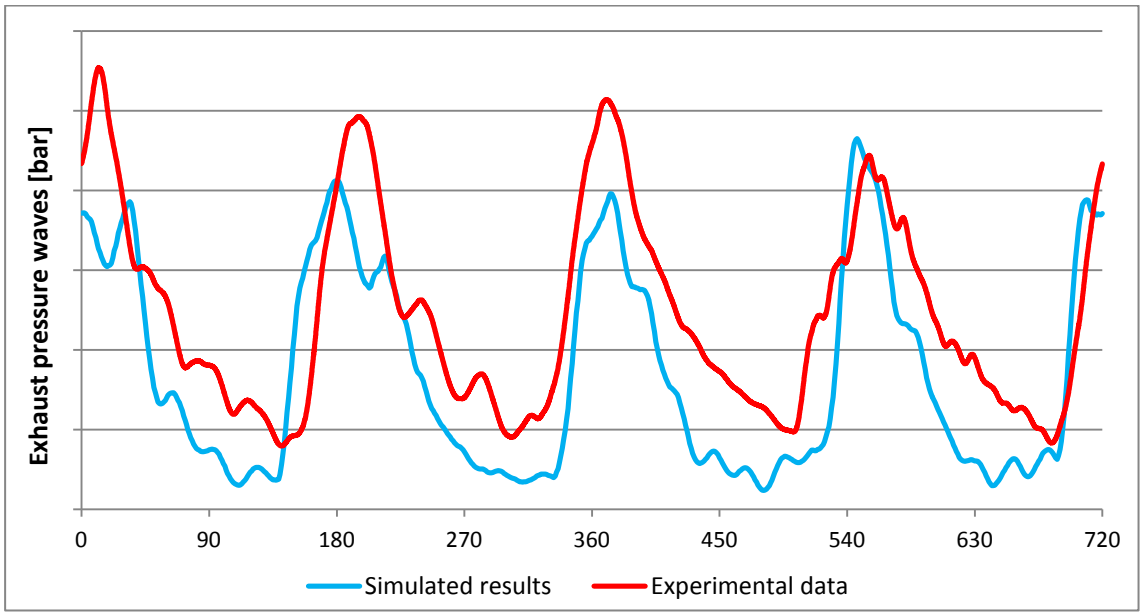

Figure 66: Measured vs Simulated pressure wave into exhaust manifold at 2000 rpm

Looking at the graphs it is possible to note that at low regimes there is a very good fitting both in terms of pressure peaks synchronisation and in terms of average values of the waves. On the other hand, the highest ones are affected by some errors and the pressure waves are characterized by a lower average value with respect to the experimental ones and with a non-synchronised trend.

Looking at the Figure 68 it is clear that the problem is not in terms of delay or advance of the pressure waves, but it is probably characterized by a different frequency of the system.

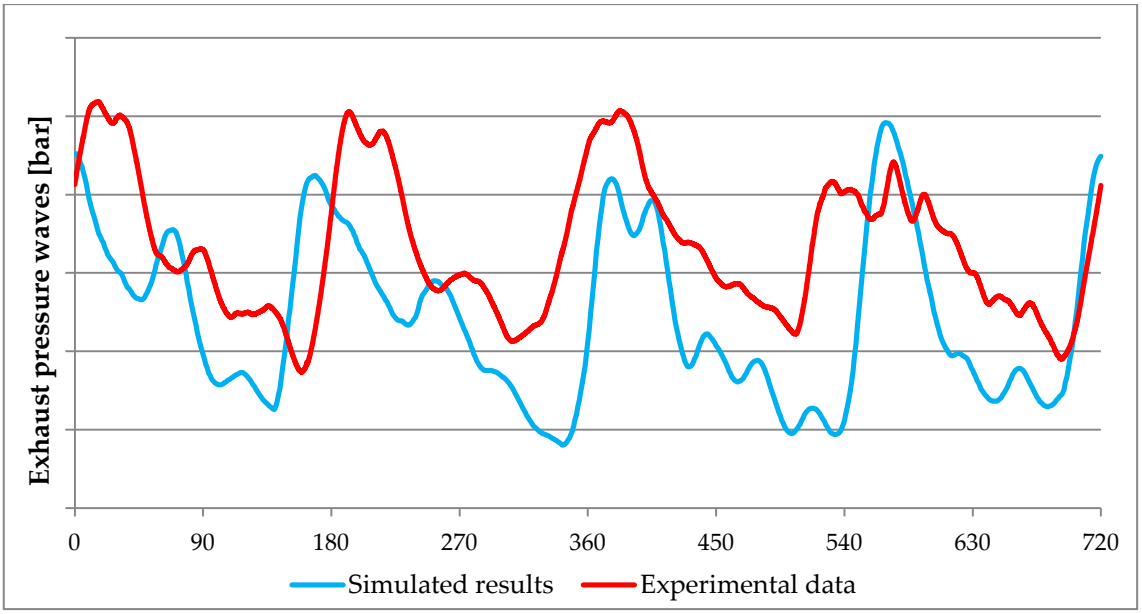

Figure 67: Measured vs Simulated pressure wave into exhaust manifold at 3200 rpm

In the exhaust manifold, the aim is to generate a phenomenon opposite to the intake one. During the opening of the exhaust valve the inside cylinder pressure is very high and the blowdown process occurs with a generation of a positive pressure waves. It travels in the exhaust pipes and with an accurate synchronisation, adjusting the exhaust manifold geometry, is possible to obtain a negative (relative) pressure peak which coincides with the closing of the exhaust valve. Moreover, it is also possible to manage the pressure waves also in those periods in which the valves are closed and so with a rigorous synchronisation is possible to sum at the negative pressure peak at the exhaust port during its closure, a further positive pressure peak at the intake valve when it opens. In this way the burned gases continue to exit from the combustion chamber also after the TDC when the piston begins to go down.

This sum of effects promotes the scavenging process during the overlap period, in which both the intake and the exhaust valves are simultaneously open. The combination of the negative and positive pressure peaks coupled with the big inertia of the exhaust gases promote a good exchange process between the burned gases, presents in the combustion chamber, and the fresh charge which enter into the cylinder.

4.3.7 Wave effect

As wave effects it means principally a couple of phenomena, one during the IVC and the other at the EVC. As previously explained they depends on the entity and on the synchronisation of the pressure waves with the valves opening and closing periods. In case of excellent job, the gain in terms of cylinder filling is significant, but on the other hand an overall decrease is also possible in case of wrong timing analysis. This problem cannot be always avoided because with a fixed ducts geometry, as in our situation, it is possible to design the engine system optimizing the waves effect only for a single velocity. It means that out from this value the synchronism is gradually lost and a opposite effect could be found at extreme (lowest or highest) engine speed.

The aim is to have a positive mass flow rate also at those crank angle degrees in which the valves should be closed theoretically. These cases can be described as moments in which the piston and the gas flow directions are opposite. It happens four times during a power cycle, but only at the exhaust valve closing and at the intake valve closing assume a relevant role. Sometimes also the waves behaviour during the period in which the intake valve remain closed is analysed in order to produce a positive pressure peak at the IVO. These phenomena are possible thanks to a positive or negative pressure peaks synchronised with the valves movements. They have been explained in detail in the previous sub-chapters 4.3.5 and 4.3.6.

To well analyse the behaviour and the efficiency of this effect a dedicated type of graph has been created using only values obtained from the simulations. Their comparison with the experimental ones has been already discussed. It contains the cylinder pressure curve and the instantaneous pressure obtained by the transducers placed, in the Gasdyn scheme, both at the intake and at the exhaust ports. For completeness are also indicated the opening and closing of the valves (EVO, IVO, EVC, IVC) and using the x-axis the piston position can be obtained knowing that the TDC is at 360 CAD.

Due to space reasons only 4 graphs are plotted and are referred to these regimes:

- 1200 rpm: Figure 68
- 2000 rpm: Figure 69
- 3200 rpm: Figure 70

These graphs are reported also in the same order in the appendix A with a greater dimension in order to facilitate the analysis of the critical period and the synchronism of the pressure waves.

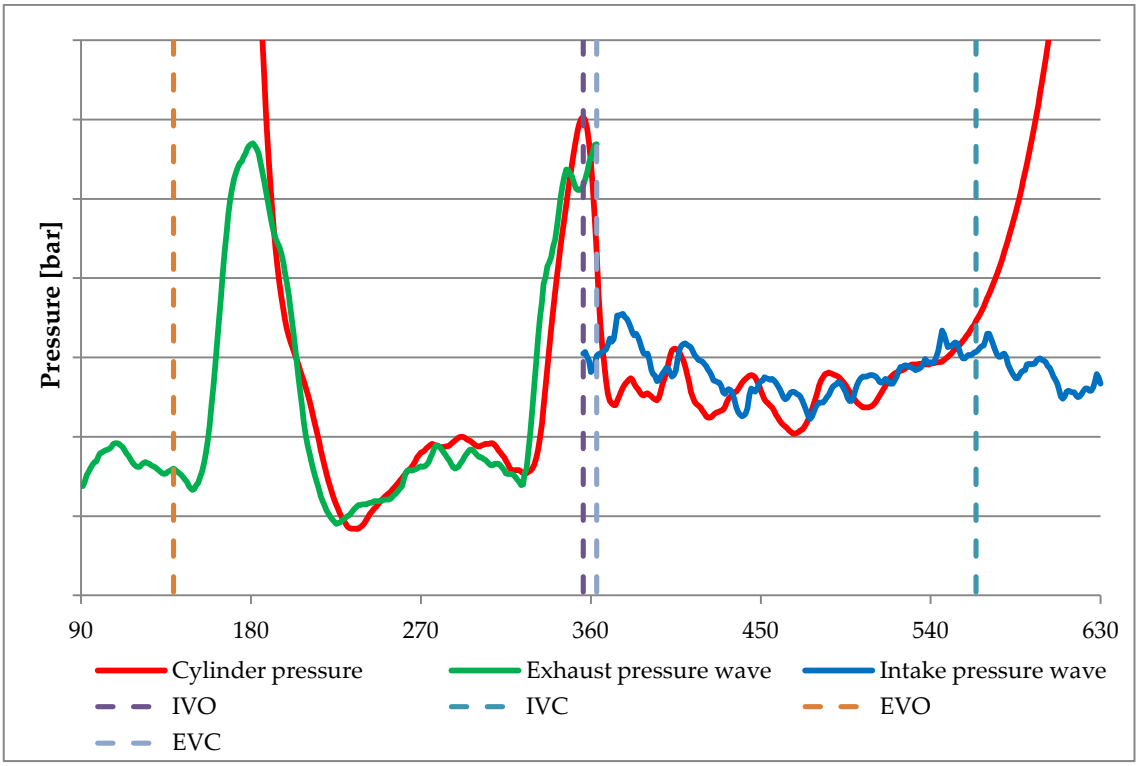

Figure 68: Pressure waves through the valve ports at 1200 rpm

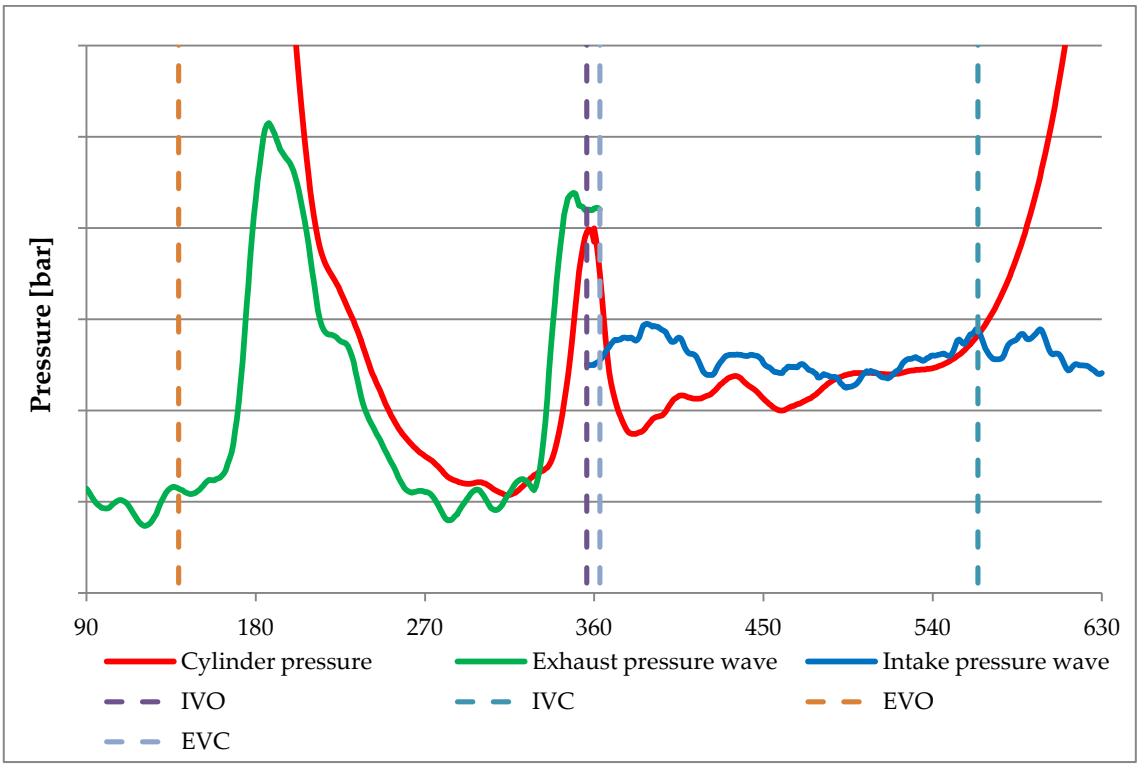

Figure 69: Pressure waves through the valve ports at 2000 rpm

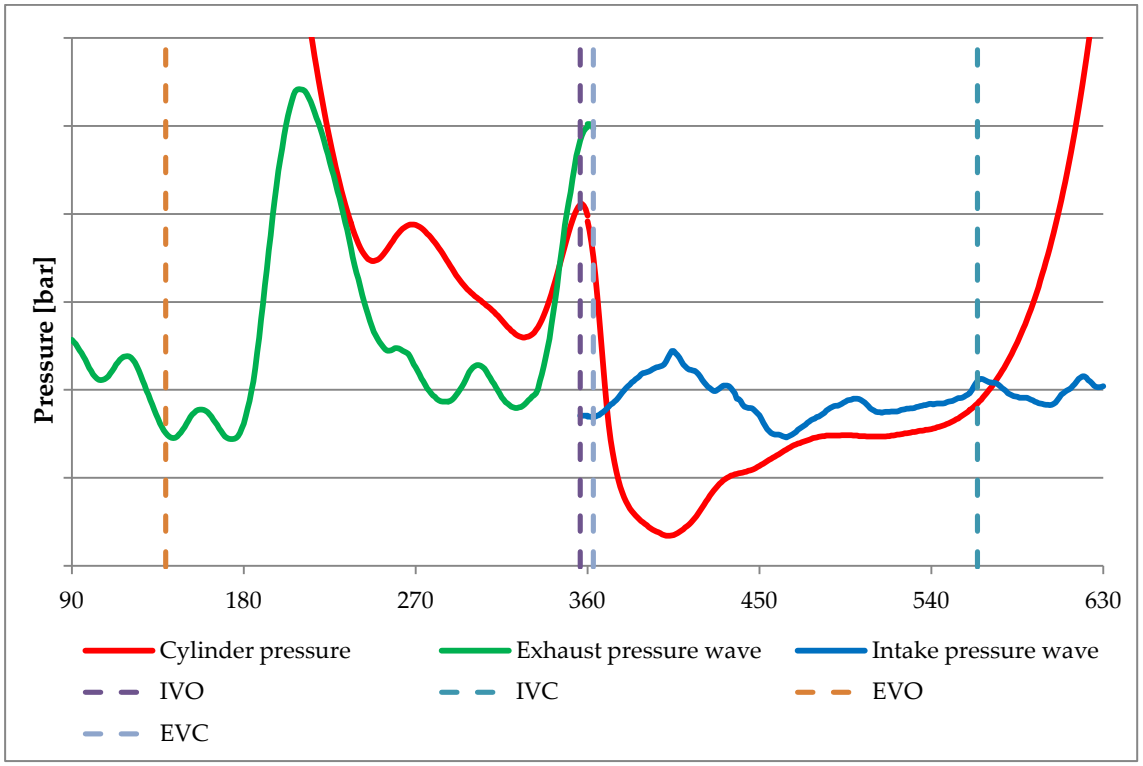

Figure 70: Pressure waves through the valve ports at 3200 rpm

IVC (Intake Valve Closing)

At the first view of the plotted results and relying on the comparison presented in the sub-chapter 4.3.5, is clear that the simulation of the pressure waves into the intake manifold has some problem. The pressure signal has a correct average value but presents a lot of oscillations which make difficult to identify the pressure waves where presents.

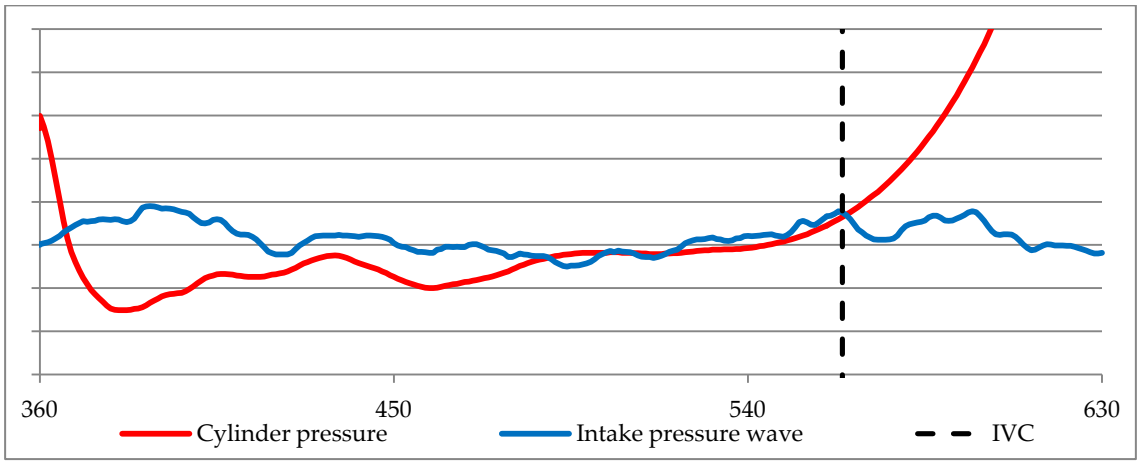

Figure 71: Zoomed IVC synchronisation with pressure waves at 2000 rpm

Focusing on the final part of the intake process, it is possible to note that the chosen IVC time is optimized for 2000 rpm. At this regime, Figure 71, is clearly visible that the positive pressure peak is perfectly synchronised with the valve closing moment in order to maximize the amount of fresh charge trapped into the cylinder. Obviously, it has some drawbacks out from the optimized operating point, characteristic of a system equipped with a fixed IVC degree.

At low regimes the valve remains open for a too long period after the BDC, Figure 72, and due to the lack of a significant positive pressure peak a backflow occurs. It can be also highlighted from the analysis of the mass flow rate through the intake port, plotted in the Figure 73 which represent a zoom of the instantaneous mass flow rate on the zone closed to the IVC moment. Looking at the values obtained from the simulations, its magnitude is not relevant with respect to the overall mass flow rate, but conceptually it represents the negative side of chosen a fixed closing time for the intake valve equal for the whole engine speed range.

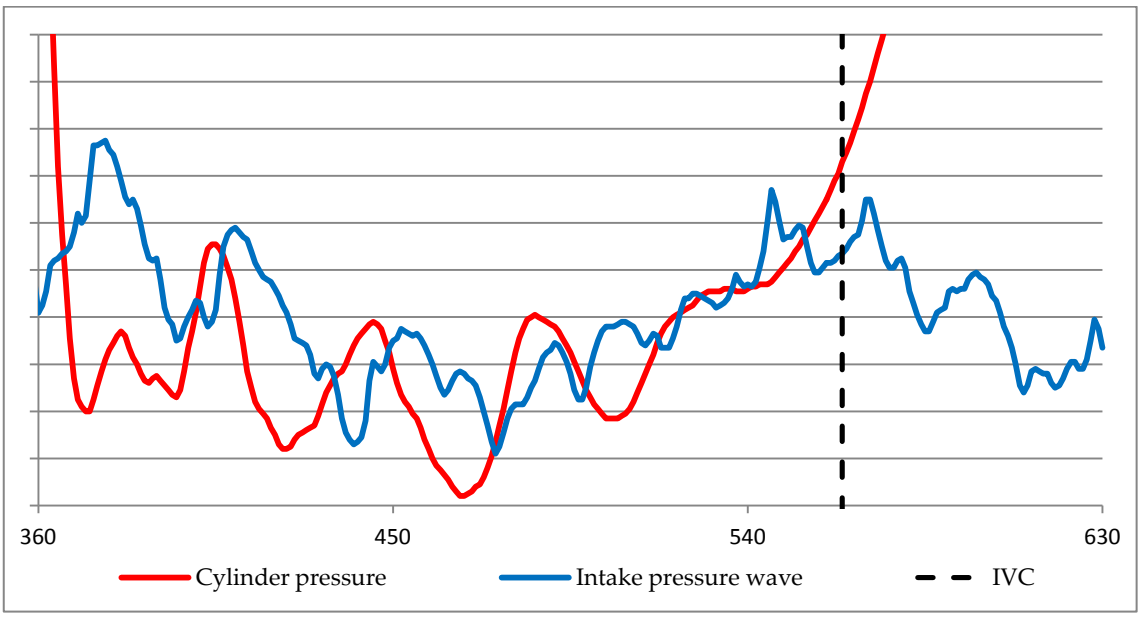

Figure 72: Zoomed IVC synchronisation with pressure waves at 1200 rpm

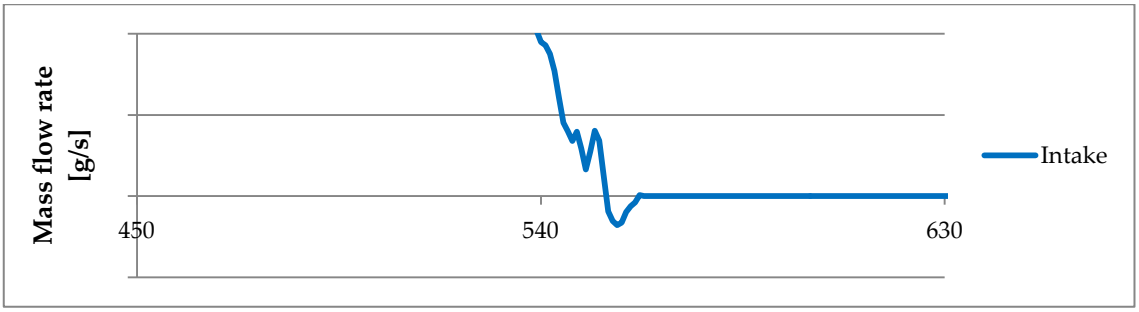

Figure 73: Zoomed Mass flow rate at the intake port closed to the IVC at 1200 rpm

On the other hand, at high regimes, Figure 74, the valve close too early wasting the big positive pressure peak which would be arrived few crank angle degrees after. Also in this case, looking at the simulation results, the mass flow rate percentage loss is negligible, and this is due to the small speed range (800 ÷ 3500 rpm) which characterise this engine.

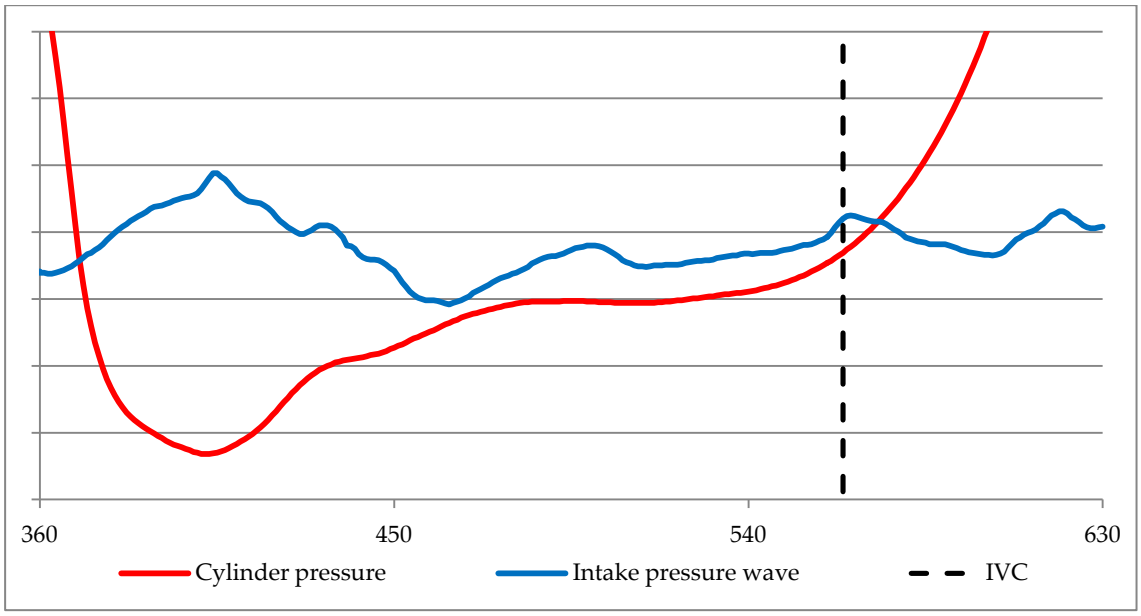

Figure 74: Zoomed IVC synchronisation with pressure waves at 3200 rpm

A possible solution could be to equip the engine with a Variable Valve Timing system (VVT) which regulates the IVC as function of the considered regime. In this case it is possible to work in the optimal condition at each engine speed, but obviously this solution leads to a significant increment of cost, which, according to me, in this type of engine is not convenient.

Another possible solution which allows to solve the problem of the IVC time is the adoption of a variable geometry intake manifold. It is composed of two ducts with different length which can be open or closed with a throttle valve, creating two configurations obviously characterized by two different optimal regimes. This type of solution is usually adopted in such engines characterized by a wide speed range and it is not our situation.

Overlap period

As previously said the overlap period is characterized by the opening of both the intake and exhaust valve and its aim is to promote the scavenging process eliminating the grater as possible amount of exhaust gas and substituting it with fresh charge. This effect is promoted by the burned gas inertia but also by the pressure peaks which occurs closed to the TDC. Obviously, we would have a positive pressure peak at the intake port and a negative pressure peak at the opposite port.

Starting from the graph which analyse the pressure waves timing in the cylinder relating to 3200 rpm, Figure 70, and zooming in the region around the TDC, closed to the overlap period, it is possible to note that the opposite phenomena occurs. The obtained graph, Figure 75, highlights the big positive pressure peak generated by the exhaust gases and also the complete lack of the pressure peak at the IVO.

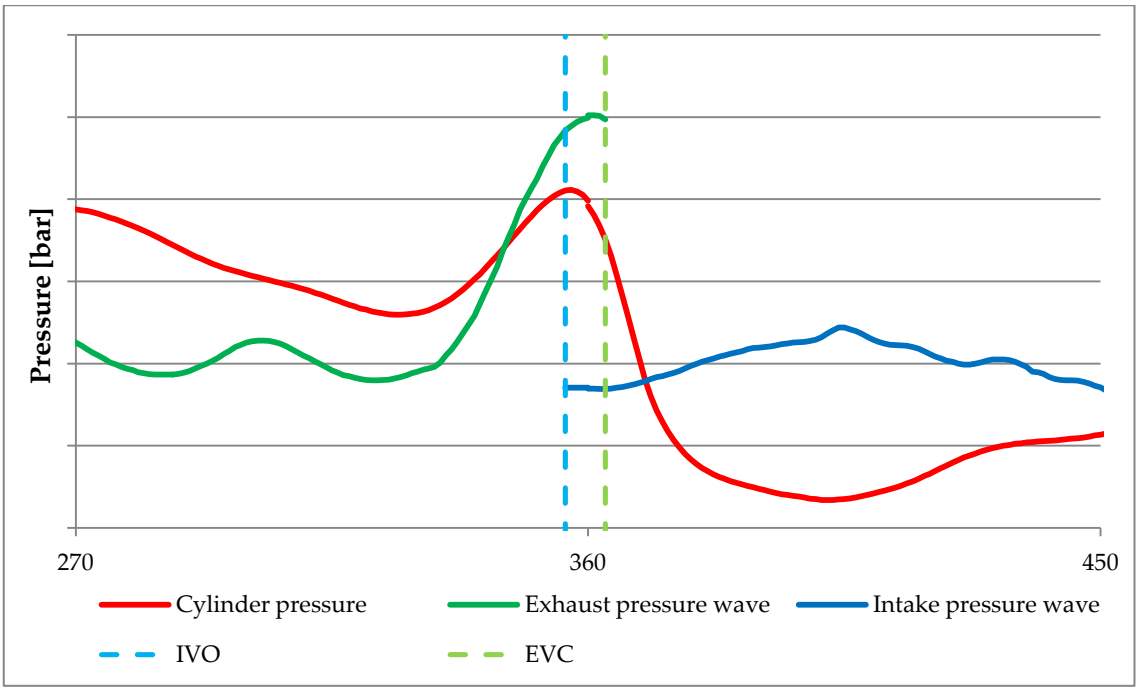

Figure 75: Pressure waves and cylinder pressure in the overlap period at 3200 rpm

This strongly affects the scavenging process and the whole gas exchange but has also a negative effect on the combustion development due to the presence of a relevant part of the burned gases, which remain into the combustion chamber and subtract a part of the cylinder available volume to the fresh charge. A further evidence of this problem can be highlighted with an analysis on the instantaneous mass flow rate at the valve seats (Figure 76). Focusing in the zone of the overlap period, and making a zoom, it is easy to note the negative value of the mass flow rate recorded at the intake valve opening, Figure 77. This amount of gases is obviously composed of combustion waste

which subsequently will be reintroduced into the combustion chamber removing space to the fresh charge.

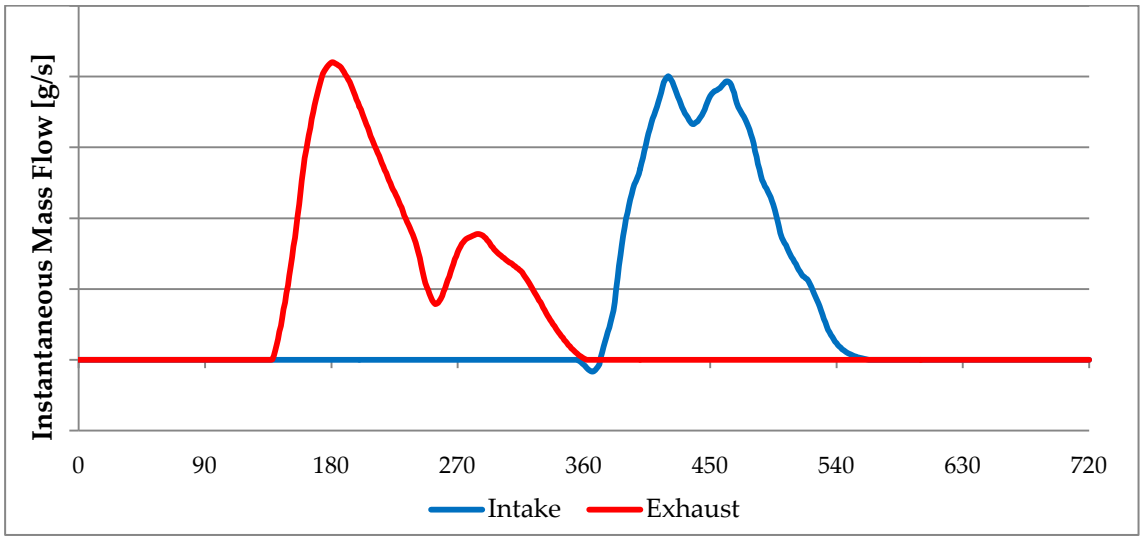

Figure 76: Mass flow rate analysis on the cylinder ports at 3200 rpm

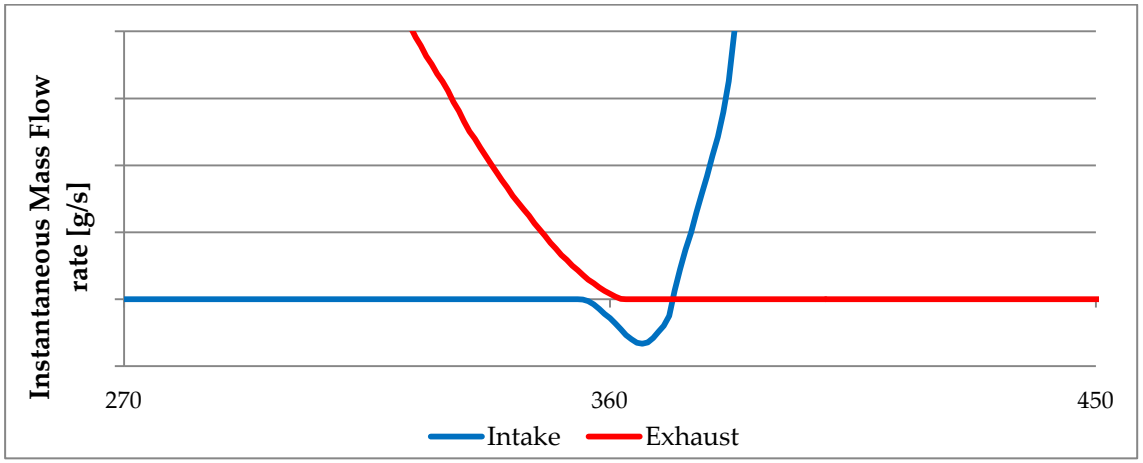

Figure 77: Zoomed mass flow rate analysis in the overlap period at 3200 rpm

The same situation is repeated also for all the other regimes and in particular to those two previously introduced (1200 and 2400 rpm). Due to the strong similarity with the one represented in the Figure 77, it is not necessary to plot all the other regimes.

According to me, a probable reason of this undesired phenomena could be identified into the pressure waves generated by the exhaust gases. It starts to travel when the blowdown occurs propagating into the exhaust manifold and after a certain period return at the port producing a positive pressure peak. The problem is that it happens too early and this can be caused by a shorter pipes or hotter gases.

The first one is improbable because all the geometric measures are provided directly by the constructor.

The second one contrariwise, must be analysed because a significant temperature difference is present in the exhaust gas flow. The measured value is characterized by a lower temperature with respect to the simulated ones which leads to a lower speed of sound. The comparison of the exhaust gas temperature is plotted in the **Errore. L'origine riferimento non è stata trovata.**.

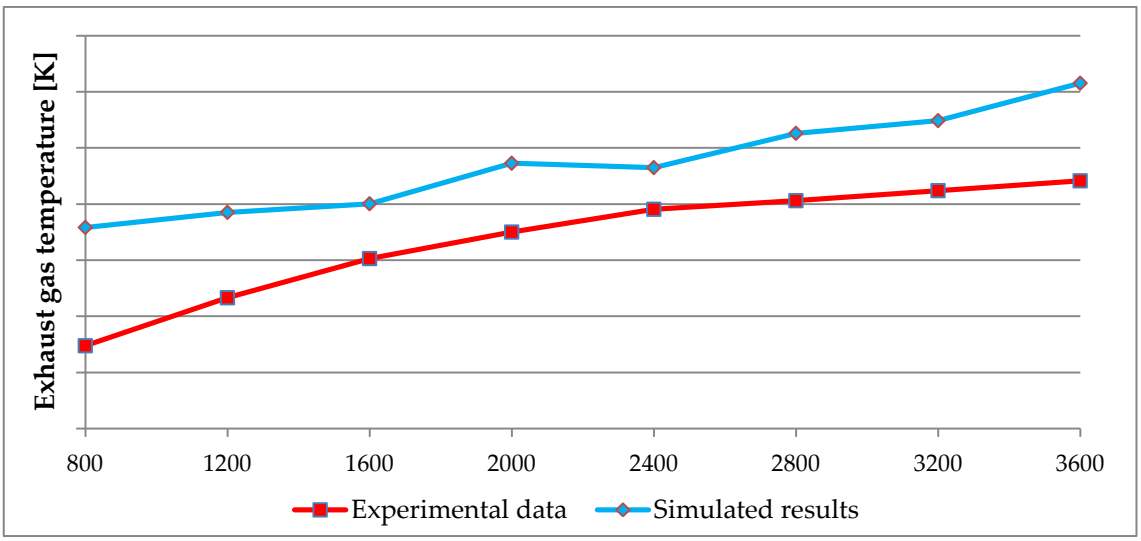

Figure 78: Measured vs Simulated exhaust gas temperature

To be sure that it is the real problem in the simulation, it is necessary to calculate the speed of sound in both the situations according the equation **Errore. L'origine riferimento non è stata trovata.** and the results are plotted in the **Errore. L'origine riferimento non è stata trovata.**. As it is possible to see, the difference in terms of speed of sound is not negligible, but the variation in the pressure peak position is in the order of few crank angle degrees and so doesn't solve the problem in the overlap period.

$$a = \sqrt[2]{\gamma \cdot \bar{R} \cdot T} \qquad \textbf{4.7}$$

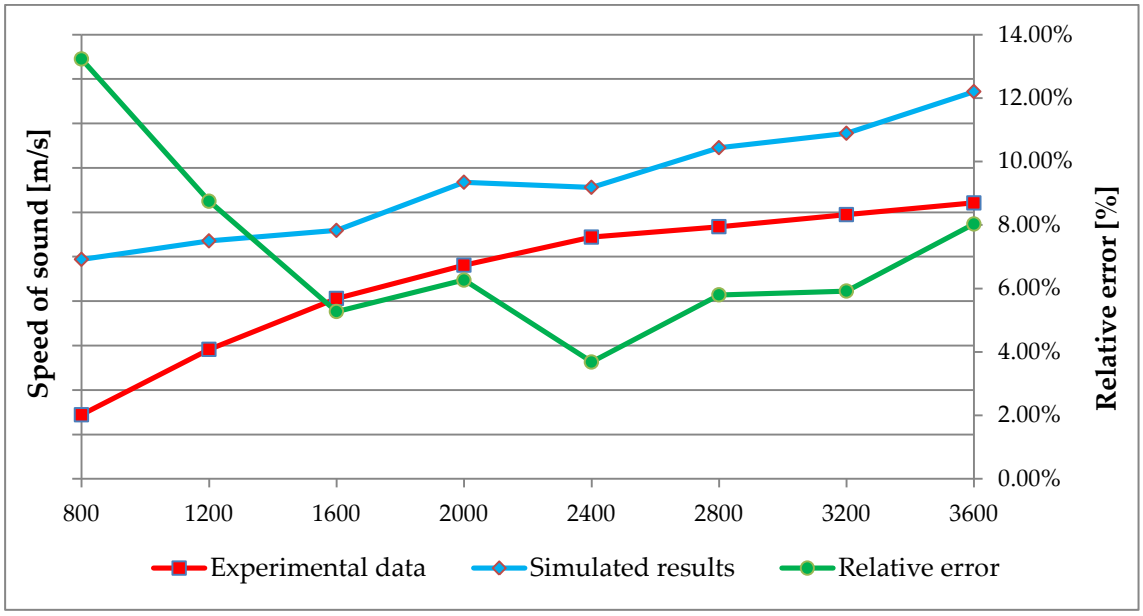

Figure 79: Measured vs Simulated Speed of Sound in the exhaust ducts with the indication of the relative error

4.3.8 Ram effect

It is an inertial effect which exploit the strong cyclicity of the cylinders which consequently affects also the gases, generating an important unsteady flow into the intake and exhaust channels. Thanks to this instability it is possible to have a final effect quite similar to the waves one. The purpose is to have a mass of air characterized by a high kinetic energy which arrives, for example, at the intake valves closed to the BDC when the piston begins to go up. So, it is possible to increase the amount of air which enters in to combustion chamber with the same advantages if the wave effect.

This is possible because the air already present into the cylinder act as a spring and all the system can be considered as a Helmholtz resonator. Its characteristic frequency is defined by the equation 4.8.

$$f_0 = \frac{\omega_0}{2\pi} = \frac{a}{2\pi}\sqrt{\frac{S}{L \cdot V_m}} \qquad \textbf{4.8}$$

Where: - a is the speed of sound.

- S is the section of the considered pipe.

- L pipe length.

- V_m is the mean cylinder volume.

After the calculation of the system characteristic frequency is possible to easily find the optimal regimes at which the ram effect is optimized exploiting the graph in the Figure 80. Usually it is chosen as optimal piston frequency the half of the resonator characteristic one. In our case, using the air properties referred to the condition inside the intake manifold, with some calculations, we have obtained an optimal regime at 1850 rpm. It is a reasonable value because the ram effect is usually optimized at very low engine velocity with respect to the waves one.

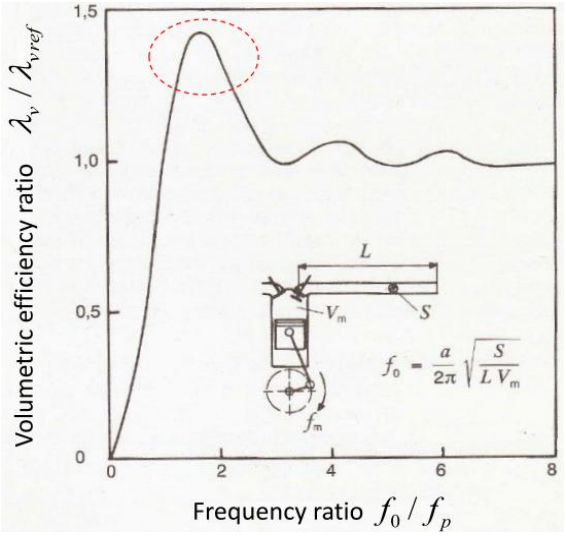

Figure 80: Helmholtz resonator optimum curve

It means that if our engine works closed to 1850 rpm is affected in positive way by the ram effects. Otherwise its advantage decreases gradually with the distance from the optimum regimes.

5 Conclusions

The aim of this thesis was to create an engine model for the software called Gasdyn which allows to predict as better as possible its behaviour under certain real operating conditions. Starting from a test bench and a GT-Power scheme an engine scheme has been created step by step with good results. High levels of accuracy are achieved in terms of air and fuel mass flow rate, but also in the combustion model which is able to fit in a quite precise way the cylinder pressure curves. Regarding the performances it is possible to further improve because actually they are overestimated. During the simulations some problems of various kind, regarding the used software, has been highlighted and solved promoting a constant development process of Gasdyn. Some others problems are still unsolved such as the non-convergence of the turbocharger at low engine regimes and the impossibility to exploit the multi-regime simulations.

With the analysis of the pressure waves at the cylinder head we have discover that the overlap period which should promote the scavenging process, in reality is characterized by a strong inefficient phenomena at all the engine regimes.

5.1 Future engine improvements

During the post-processing of the simulated results some negative points are highlighted. For example we have discovered that only at 2000 rpm the engine works with an optimized configuration in terms of gas exchange process. So it is possible to make some improvements and both a Variable Valve Timing (VVT) system and also a variable geometry intake manifold could by chosen. Obviously these improvements has a different effect, but also a different cost which have to be taken under consideration.

Moreover the dissipative wastegate valve could be substituted with a Variable Geometry Turbine (VGT), which has a higher cost but allow also to reduce the fuel consumption and increase the performances.

These are only some possible improvements, but also others could be chosen for different purposes.

5.2 Possible model developments

During this thesis period the engine model has been developed starting from a white sheet and only the full load condition has been analyzed due to lack of time caused by various factors.

In a following work could be a good idea to continue to study this engine under some other conditions such as at partial load. Otherwise could be interesting to analyse the pollution aspects with the introduction of the EGR and also the control of the emitted pollutants. This argument is a key point for a turbocharged engine feed of natural gas as the engine under analysis.

6 Appendix A

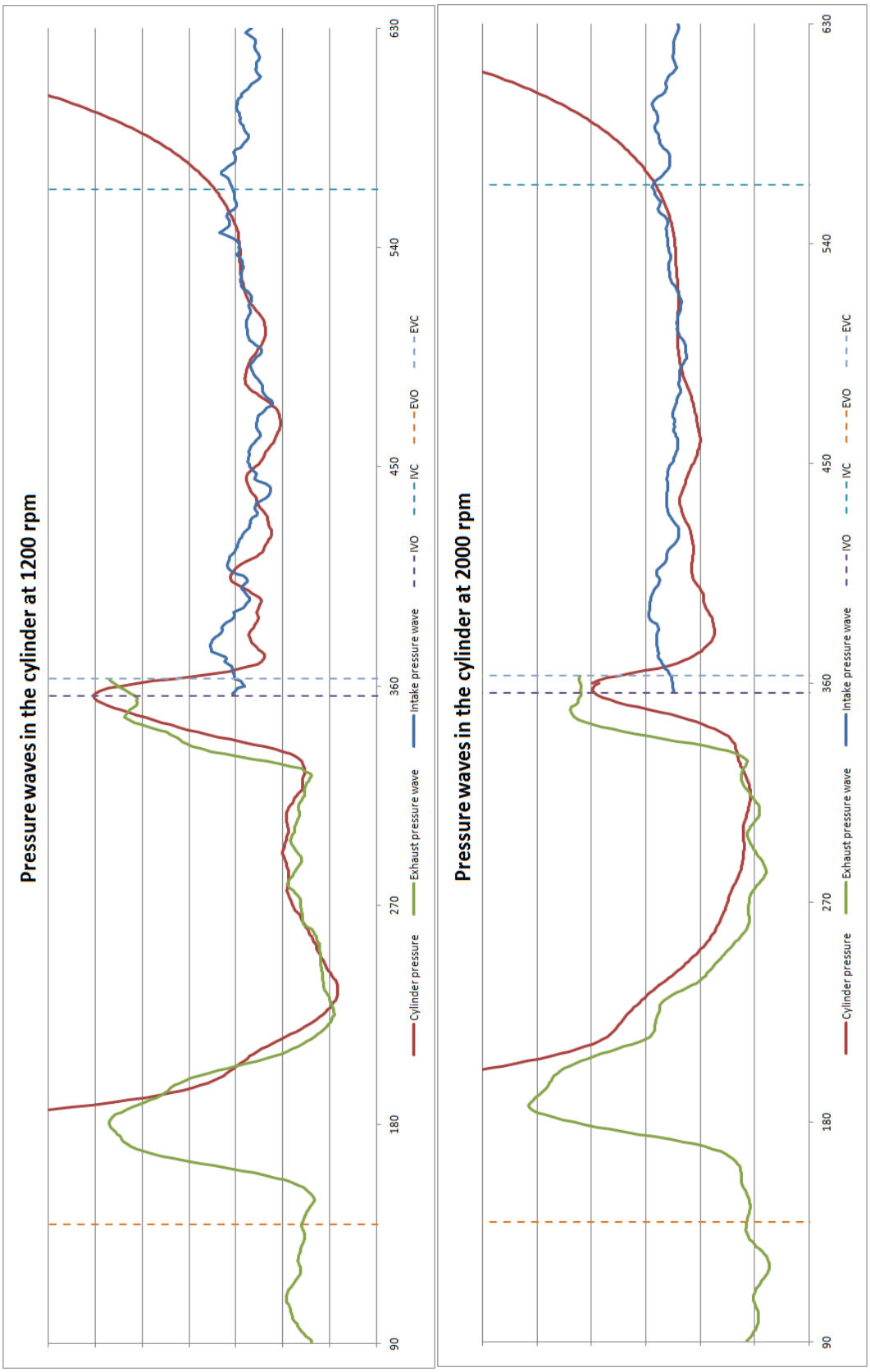
Pressure waves in the cylinder at 1200 rpm
90
180
270
360
450
540
630
Cylinder pressure
Exhaust pressure wave
Intake pressure wave
IVO
IVC
EVO
EVC
Pressure waves in the cylinder at 2000 rpm
90
180
270
360
450
540
630
Cylinder pressure
Exhaust pressure wave
Intake pressure wave
IVO
IVC
EVO
EVC

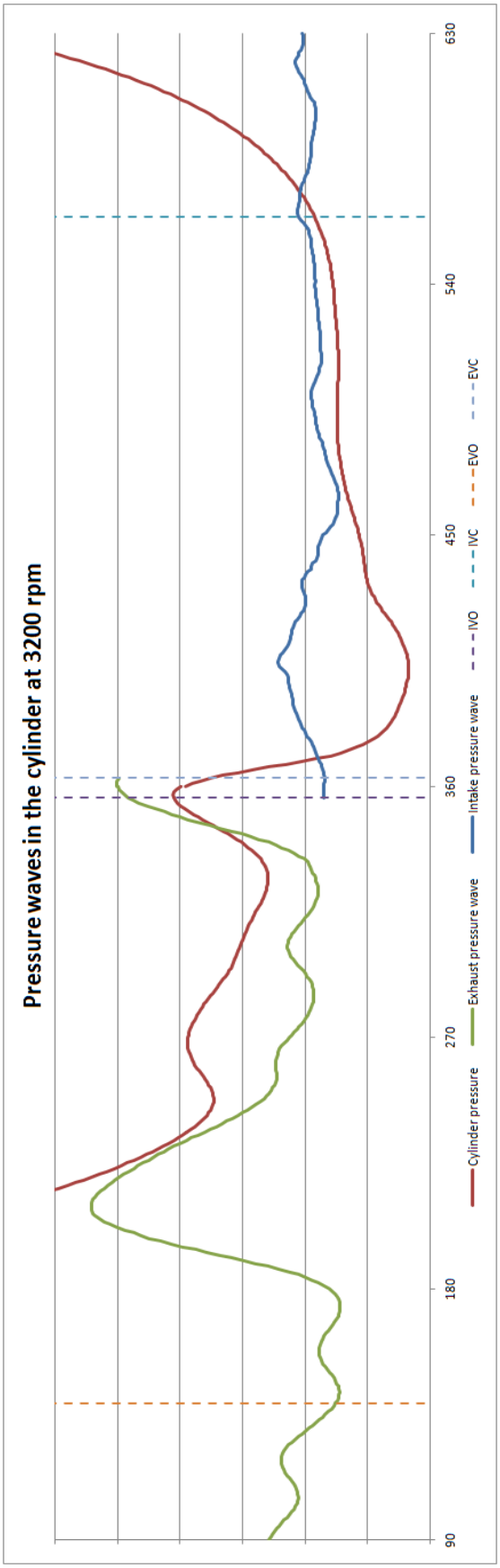
Pressure waves in the cylinder at 3200 rpm
630
540
450
360
270
180
90
Cylinder pressure
Exhaust pressure wave
Intake pressure wave
IVO
IVC
EVO
EVC

List of figures

List of tables

Bibliography

[1] G. Ferrari, *Internal Combustion Engines*, Esculapio, 2014

[2] D. E. Winterbone, R. J. Pearson, *Theory of Engine Manifold Design*, Professional Engineering Publishing, UK, 2000

[3] D. E. Winterbone, R. J. Pearson, *Design Technique for Engine Manifolds*, Professional Engineering Publishing, UK, 1999

[4] M. I. Sanfelice, T. Ripoldi, *1D thermo-fluid dynamic modeling of SI engines: performances, emissions and knock propensity*, Master graduation thesis, ITA, 2016

[5] G. F. M. Vismara, *1-D modelling of a turbocharged Diesel engine*, Master graduation thesis, ITA, 2016